Elements of Constitutive Modelling and Numerical Analysis of Frictional Soils

Jakobsen, Kim Parsberg

Elements of Constitutive Modelling and Numerical Analysis of Frictional Soils

Kim Parsberg Jakobsen

Geotechnical Engineering Group
Department of Civil Engineering
Aalborg University

2002

Elements of Constitutive Modelling and Numerical Analysis of Frictional Soils

Kim Parsberg Jakobsen

Geotechnical Engineering Group
Department of Civil Engineering
Aalborg University
2002

PREFACE

This thesis 'Elements of Constitutive Modelling and Numerical Analysis of Frictional Soils' is submitted as one of the requirements for obtaining the degree of Ph.D. according to the regulations put forward by The European Doctoral School of Technology and Science at Aalborg University.

The study was carried out in the period from August 1995 to July 1999 at Department of Civil Engineering, Aalborg University under the supervision of Associate Professor Lars Bo Ibsen and former Professor Jørgen S. Steenfelt.

The thesis consists of a collection of published scientific papers based on the studies. The relation between the key papers is explained and the more important conclusions are outlined. Some of the papers and reports are not included but can be acquired through the Department of Civil Engineering, Aalborg University.

Special gratitude goes to my former colleague Ulrik Praastrup for some quality discussions concerning the stress-strain behaviour of soils. Gratitude is also expressed to Professor Poul V. Lade for his inspiration, advice and continuous encouragement. Also thanks to the staff at the Geotechnical Engineering Laboratory for their help with the experimental work.

Aalborg, May 2002

Kim Parsberg Jakobsen

CONTENTS

FIGURES

ABSTRACT

This thesis deals with elements of elasto-plastic constitutive modelling and numerical analysis of frictional soils. The thesis is based on a number of scientific papers and reports in which central characteristics of soil behaviour and applied numerical techniques are considered.

The development of a constitutive model for soil is based on a profound knowledge of the soil behaviour upon loading. In the present study it is attempted to get a better understanding of the soil behaviour by performing a number of triaxial compression tests on sand. The stress-strain behaviour of sand depends strongly on the stress level and is generally difficult to describe by constitutive models. Thus, under drained conditions considerable irrecoverable volumetric strain is developed as the mean effective stress or the shear stress is increased. In the tests it is observed that the sand skeleton initially contracts and subsequently dilates during shear. The change in the volumetric behaviour of the soil skeleton is commonly referred to as the characteristic state. The stress ratio corresponding to the characteristic state is independent of the mean normal effective stress and the relative density, but depends on the stress path followed. However, theoretical considerations imply that the characteristic state obtained at a constant mean normal effective stress is similar to a state, known as the state of phase transformation, observed under undrained conditions. Under undrained conditions the phase transformation occurs as the mean normal effective stress reaches a minimum and the effective stress path has a 'knee'. The similarity in drained and undrained behaviour of the soil skeleton makes it possible to describe the change in volumetric behaviour by a single parameter, given as a characteristic friction angle.

The characteristic angle is considered to be an important parameter for calibration of elasto-plastic models to achieve a correct description of the irrecoverable volumetric strain. The classical models are generally too simple and more advanced models must be used to describe the soil behaviour accurately. Nevertheless, advanced constitutive models, are due to complexity and the computational costs, normally not available for use with commercial finite element programs used for numerical analyses. However, the computational costs can be reduced significantly by a proper selection of integration schemes. An example hereof is given by implementation of an advanced constitutive model for use with the finite element program ABAQUS. Different integration schemes have been applied and their effectiveness is investigated.

RESUME

Denne afhandling omhandler forskellige elementer af elasto-plastisk konstitutiv modellering og numerisk analyse af friktionsjord. Afhandlingen er bygget op omkring en række artikler og rapporter der berører en række vigtige materialemæssige egenskaber og anvendte numeriske teknikker.

Sammensætningen af en konstitutiv jordmodel bygger på en grundlæggende forståelse af jordens opførsel under belastning. Det er i det nærværende studie søgt at opnå en bedre jordforståelse gennem en række triaksiale trykforsøg udført på sand. Styrke- og deformationsegenskaberne for sand er stærkt afhængig af spændingniveauet og stiller generelt store krav til den konstitutive model. Således er sand under drænede forhold kendetegnet ved at undergå betragtelige irreversible volumentøjninger ved øget effektiv middelspænding og forskydningspåvirkning. I forsøgene observeres typisk en vis kontraktion af kornskelettet efterfulgt af en betragtelig dilatation ved øget forskydningspåvirking. Denne ændring af kornskelettets volumenmæssige egenskab fra kontraktion til dilatation benævnes ofte den karakteriske tilstand. Spændingsforholdet for hvilket den karakteristiske tilstand indtræder er uafhængig af den effektive middelspænding og den relative lejringstæthed, men findes iøvrigt at afhænge af spændingsvejen. Teoretiske overvejelser godtgør imidlertid at den karakteristiske tilstand opnået ved konstant effektiv middelspænding kan sidestilles med en lignende tilstand observeret under udrænede forhold. Under udrænede forhold indtræder tilstanden når den effektive middelspænding har opnået et minimum og den effektive spændingskurve har et knæk. Denne sammenhæng bevirker at ændringen i kornskelettets drænede og udrænede opførsel kan beskrives ved en enkelt tilstandsparameter udtrykt ved en karakteritiske friktionsvinkel.

Den karakteristiske friktionsvinkel betragtes som en væsentlig kalibrerings parameter, idet den kan anvendes til at fastlægge den elasto-plastiske models beskrivelse af irreversible volumentøjninger. Traditionelle modeller er generelt utilstrækkelige og mere avancerede modeller må anvendes. Sådanne modeller er på grund af deres kompleksitet og beregningsmæssige omkostninger normalt ikke tilgængelig for numerisk analyse ved brug af kommercielle element metode programmer. Et passende valg af integrationsskemaer kan dog nedbringe de beregningsmæssige omkostninger væsentligt. Som eksempel herpå er en avanceret elasto-plastisk konstitutiv jordmodel implementeret for brug med elementmetodeprogrammet ABAQUS. Forskellige integrationsskemaer og numeriske teknikker er bragt i anvendelse og deres effektivitet er undersøgt.

1 INTRODUCTION

The innovation of numerical techniques as the finite element method and the finite difference method as well as increased computer resources have during the last couple of decades changed the field of geotechnical engineering. The developments of these facilities have to a great extent motivated the geotechnical engineer to alter the basis of calculation from the two distinct conditions of linear elasticity and perfect plasticity (e.g. Ibsen & Jakobsen 1997, Ibsen & Jakobsen 1998) to a more complete description of the soil behaviour by use of elasto-plastic constitutive models.

The development and application of constitutive models used for description of soil behaviour typically require an experimental study to ensure that no essential phenomenons are disregarded. A robust model description may be based on the framework of elastic and plastic theory and an implementation of the model that enables the use with the finite element method.

The present study concerns some of the elements needed for development of constitutive models and techniques required for consistent and efficient implementation and numerical modelling of geotechnical structures. A comprehensive experimental study of the pre-failure deformation characteristics forms the basis for a discussion on model requirements, capabilities and testing of an existing advanced elasto-plastic constitutive model.

1.1 Historical Background

The development of elastic-plastic constitutive models, which more correctly describes the soil behaviour under different conditions, has been in progress since the 1950s, but only the recent removal of the computational obstacle has made these models useful to the practical engineer.

The investigation and development of constitutive models for engineering materials in general have been subjects of study for more than a hundred years. The first well-known models proposed by Tresca and von Mises were, however, developed for metals and can therefore not account for the special characteristics of soil. Consequently, various improvements have been proposed and used. The well-known Mohr-Coulomb (Shield 1955) and Drucker-Prager (Drucker & Prager 1952) models belong to this category and have been widely used. But the capabilities of these models are limited when it comes to special characteristics like stress path dependencies and volume changes. As a consequence a considerable amount of work has been done in the area of soil modelling. Many of the proposed models are based on the classical isotropic plastic hardening theory, and especially the concept of cap models pioneered by Drucker et al. (1955) and enlarged by Dimaggio & Sandler (1971), Lade (1977) and Nordal et al. (1989) has become popular, but also the critical state concept (Cam-Clay) initially proposed by Schofield & Wroth (1968) is widely used. Many of the models may capture the key characteristics under monotonic loading and moderate unloading quite well, but when it comes to the prediction of stress induced anisotropy and cyclic loading the capabilities of these models are inadequate. Similar limitations, however, apply to the otherwise promising isotropic hardening plasticity model proposed by Lade and Kim (Kim & Lade 1988, Lade & Kim 1988*a*, Lade & Kim 1988*b*).

Stress induced anisotropy occurs in many of the typical foundation problems, e.g. establishment of excavations, where the soil is subjected to large stress reversals and rotation of principal stresses or upon construction of structures, where the soil near the edges of the structure is subjected to reorientation of principal stress directions. The difficulties with prediction of soil under cyclic loading are mainly introduced in design of structures in seismic regions and in the marine environment, where the principal stresses are rotated and hysteretic effects occur. Most of the models that have been developed to take account of these different aspects are based on a combination of isotropic and kinematic plastic hardening rules, which can give

rise to a material description of considerable power and flexibility. The first to utilise the combined hardening rules were Mróz (1967) and Iwan (1967), who independently introduced the concept of nested yield surfaces in stress space, which makes it possible to present continuous yielding under arbitrary loading. Krieg (1975) and Dafailas & Herrmann (1982) simplified the concept to a two-surface formulation, termed the bounding surface theory. In the bounding surface concept the inner surface, called the yield or loading surface moves with the stress point inside the outermost surface referred to as the bounding surface. The response of the material is then correlated with the distance from the current state of stress to the bounding surface and a predefined mapping rule. Both concepts have their disadvantages: Large storage requirements for the nested yield surface concept and arbitrariness in the mapping rule for the bounding surface theory.

It is unlikely that these new models will replace the traditional methods for calculation of ultimate and serviceability limit states. However, the applicability and advantages of the numerical techniques are evident when it comes to boundary value problems, problems with complex geometry, layered soils or in cases where the working loads proceed beyond the elastic range and the material becomes plastic. The numerical analyses are therefore mainly applied in the design and construction of large structures, where the above-mentioned complications are most likely to occur.

1.2 Aims and Scope

Since the literature about new models and techniques are voluminous, an unproblematic application of these tools could be expected. Nevertheless, only a few of the basic models are available in commercial finite element programs like ABAQUS, DIANA and PLAXIS. These typically include variations of the Drucker-Prager, Mohr-Coulomb and Cam-Clay types of models. The finite element programs basically include the classical formulation of these models and have in different ways attempted to increase the functionality by introducing the non-normality concept or even using hyperbolic model formulations. The models may indeed be usable when it comes to modelling of normally consolidated cohesive materials, but are generally inadequate for modelling of frictional materials like sands.

The present study is therefore aimed at the implementation of an elasto-plastic model, usable for modelling of frictional materials, into a commercial finite element program. Ideally the model chosen for implementation should posses the following properties:

- The model should be founded on some physical interpretation of the frictional material response to changes in applied stresses or strains, i.e. key characteristics.
- It should be possible to identify the model parameters by means of a small number of standard material tests, e.g. drained triaxial tests.
- The model should be able to predict the behaviour for all stress and strain paths, and not merely restricted to the stress and strain path used for parameter fitting.

Although the aim is to use a model that describes the frictional materials behaviour accurately, it is vital that the model is 'simplified' so as to facilitate the application in engineering practice.

1.3 Thesis Outline

As mentioned above the ideal model should be able to capture the key characteristics of the frictional material derived from standard material tests. Frictional materials like sand have

been studied extensively in the past and a lot of information about general sand behaviour is available. Nevertheless, the present study contains an extensive testing program, including numerous drained and undrained triaxial tests.

The test program serves a two-fold purpose. Firstly, as a thorough investigation of the pre-failure deformation characteristics of dense sand for validation of the uniqueness of the characteristic state line and phase transformation line concepts. Hence, these concepts relate to the volumetric change of material, which plays a central role for the behaviour of sand and frictional materials in general. Secondly, the tests provide the background for determination of model parameters and serve as reference for comparisons and predictions made by model. The investigation of the triaxial behaviour of sand is described in Chapter 2. The chapter relates to the article about stress path dependency of the pre-failure deformation characteristics by Jakobsen et al. (1999) and to consistent analysis of triaxial tests by Praastrup et al. (1999).

The single hardening model (Kim & Lade 1988, Lade & Kim 1988*a*, Lade & Kim 1988*b*) posseses to a great extent the required properties given above and is chosen for implementation. The model's limitation to isotropic materials and monotonic loading and moderate unloading is found to be acceptable. Further, the use of models without these limitations is hardly usable in engineering practice as they imply large computational obstacles and requires non-standard material tests for calibration. The elasto-plastic framework of the single hardening model, implementation techniques and capabilities are discussed in Chapter 3. The chapter mainly relates to the papers by Lade & Jakobsen (2002) and Jakobsen & Lade (2002).

2 THE BEHAVIOUR OF SAND

When studying the behaviour of soils it is normal to distinguish between cohesionless and cohesive soils. Sand belongs to the first category, in which the interparticle forces have a negligible effect on the mechanical behaviour. The mechanical behaviour of sand solely depends on the friction between the grains, wherefore sand also is referred to as a frictional material. Sand is often characterised by the relative density or void ratio, the grain size distribution and the angularity of the grains.

In this chapter the general behaviour of sand will be described. The description deals primarily with drained, constant volume and undrained static triaxial compression tests. Both friction and dilation are important concepts for the understanding of failure in soil. For description of the soil deformation properties also the pre-failure characteristics become important. In this connection reference is often made to concepts like characteristic state or line and phase transformation line as these states indicate a change in the soil's stress and strain response. These states are considered to be important to the development and use af constitutive soil models as they seemingly divide the stress space into two regions with different deformation mechanisms. Hence, factors affecting these different states are discussed and illustrated by test results. The investigation is to the greatest possible extent based on the laboratory exeriments performed in connection to the project (Jakobsen & Praastrup 1998, Jakobsen 1998).

2.1 On the Analysis of Triaxial Tests

The study of the stress-strain behaviour of geomaterials is commonly accomplished by performing traditional triaxial compression tests and occasionally true triaxial tests. In both cases the Cauchy or true stress measure is adopted. This measure is physically easy to interpret, as it simply expresses the ratio between current force and current area. For porous materials in which the pores are interconnected the hydrostatic pressure of the fluid may affect the behaviour of the material greatly. As frictional materials deform and fail in response to effective stresses the pore pressure should be deducted from the total stresses.

Whereas the adoption of a suitable stress measure is straightforward, the choice of a measure that describes relative deformations, i.e. strains, is more difficult. Praastrup et al. (1999) demonstrated that the traditional method for analysis of triaxial tests is incorrect and proposed an alternative correct and consistent scheme. The proposed scheme adopts the finite natural/logarithmic strain measure that is valid for large strains. In triaxial tests where principal strain directions do not rotate the natural strain is simply defined as the natural logarithm of the current length relative to the initial length:

$$\varepsilon_i = -\ln\left(\frac{l_i^0 - u_i}{l_i^0}\right) = \ln\left(\frac{l_i^0}{l_i}\right); \qquad i = 1,2,3 \tag{2.1}$$

in which u_i is the directional displacement. For the natural strain measure the traditional relation between axial and volumetric strains holds:

$$\varepsilon_v = \sum_{i=1}^{3} \varepsilon_i = \ln\left(\frac{V^0}{V}\right) \tag{2.2}$$

The above definition of the total natural strain is only valid if the principal strain directions do not rotate. However, the principal directions generally change as the deformation takes place and it is seldom possible to calculate the total strain directly and the strain must be derived on an incremental form using basic continuum mechanics methods (see for example Malvern 1969).

The effect of strain measure may seem subtle, and for small deformations the effect is indeed hardly noticeable. However, for large deformations the choice of strain measure affects the determination of geotechnical strain dependent parameters significantly, e.g. a key geotechnical parameter like the angle of dilation may be overestimated (Praastrup et al. 1999). The effect of the different strain measures applied for analysis of a conventional drained triaxial test is shown in Figure 2.1.

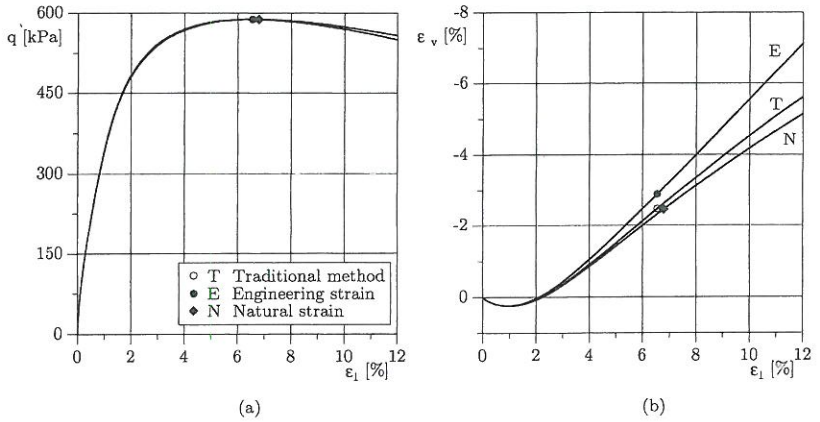

Figure 2.1: *Use of different strain measures for analysis of a triaxial test. (a) Stress strain curves. (b) Volumetric strain curves.*

The stress strain curve is slightly affected (Figure 2.1a) as the strain to failure is increased by the application of the natural strain measure (N). However, the volumetric strain is greatly affected by the applied strain measure. The effect is illustrated in Figure 2.1b were the volumetric strain is plotted versus both the axial engineering and natural strains. The three curves representing the consistent use of the engineering strain (E), the traditional analysis method mixing infinitesimal and finite strains (T) and the use of the natural strain (N) diverge significantly as the axial strain increases. The lowest rate of dilation (i.e. angle of dilation) is obtained by applying the natural strain measure, whereas the consistent use of the engineering strain measure overestimates the rate of dilation significantly.

The choice of strain measure may not only affect some of the traditional geotechnical parameters, but may also affect the calibration of parameters for numerical models. Thus it is mandatory that the strain measure on which the parameters are based is identical to the strain measure used by the analysis program. Hence, errors are incurred if model parameters based on the infinitesimal engineering strain measure are used in finite element programs like ABAQUS, which uses the finite natural strain measure. Consequently, the natural strain measure must be adopted.

2.2 Behaviour Under Drained Conditions

The stress-strain response and volumetric behaviour of sand are studied by performing drained triaxial tests on saturated reconstituted specimens. Several factors, which may be categorised

as either compositional or environmental, affect the material response. The compositional factors are related to the mineralogical properties and the state of packing of the grains. Thus, the basic friction angle between mineral grains affects the frictional capacity of the material (Rowe 1962). The state of packing of the grains, which can be expressed in terms of the void ratio or the relative density, has a large influence on the deformational behaviour and strength of sand. Dense sand has a higher stiffness and strength than loose sand and exhibits softening behaviour with a marked decrease in shear strength after peak failure. Whereas, loose sand is highly contractive and shows no dilative behaviour, the dense sand will initially contract and subsequently dilate. The degree of packing and the resulting friction or interlocking capacity is affected by the grain size distribution and shape. Depending on the deposition method the sand may further exhibit anisotropic or cross-anisotropic behaviour, as the grain orientation relative to the shearing plane becomes important (Oda 1972).

The environmental factors are related to the stress history of the sand deposit and the loading characteristics, i.e. pressure, stress path, overconsolidation and intermediate principal stress. The effect of these factors on the deformational behaviour and strength of sand has been thoroughly examined by several authors conducting triaxial and true triaxial tests (e.g. Lee & Seed 1967, Lade & Duncan 1973, Lade & Duncan 1976, Ladd et al. 1977). The description given in the following mainly focuses on the effect of stress path and pressure.

2.2.1 Friction and Dilation

Coulomb initially defined the shear strength of sand by the classic empirical failure criterion $\tau = \sigma' \tan \varphi$. This criterion, which assumes that the frictional resistance increases linearly with normal pressure, has formed the basis for evaluation of sands strength and indeed proved to be a valuable tool. However, experiments covering a wide range of confining pressures show that the strength of sand depends on the pressure in a non-linear way (e.g. Casagrande 1940, Lee & Seed 1967). Hence, the higher the confining pressure the smaller is the friction angle.

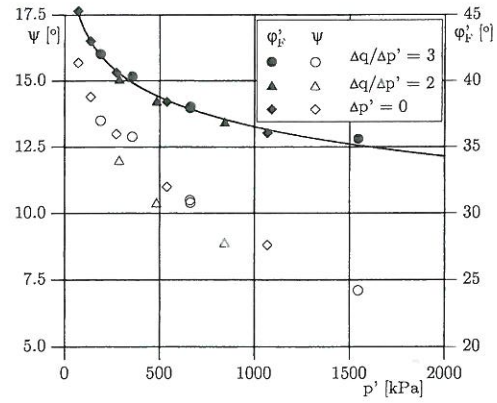

Figure 2.2: *Variation of angles of dilation, ψ and friction angles, φ for Eastern Scheldt sand with pressure and stress path.*

The pressure dependency of shear strength of sands is strongly related to the volume change that occurs during shear. Casagrande (1940) firstly demonstrated the effect of volume change

and showed that the friction angle increases as the rate of dilation or expansion increases. Thus, for a given void ratio the rate of dilation decreases with increasing confining pressure, resulting in a reduced friction angle. Taylor (1948), Bishop (1954), Rowe (1962) and others have suggested different approaches for deducting the shear resistance due to dilation. Whence, the shear strength is basically composed of two components, a frictional component given by the basic friction angle of the sand grains and a dilatancy component depending on pressure and void ratio. However, a third component accounting for rearrangement and crushing of grains must be taken into account for very loose sands or for sands at high pressures(Lee & Seed 1967).

The rate of dilation is occasionally expressed by the angle of dilation, ψ, defined by Hansen (1958). The angle of dilation is considered to be a characteristic parameter for description of soil behaviour, and it will, as the rate of dilation, decrease with increasing pressure.

The pressure dependencies of the friction angle and angle of dilation at the state of failure for dense Eastern Scheldt sand (Jakobsen & Praastrup 1998) are shown in Figure 2.2. Both the friction angle and angle of dilation at the state of failure show the anticipated pressure dependency and are seemingly independent of the stress paths followed. The latter is supported by the findings of Poorooshasb et al. (1966).

2.2.2 Characteristic Stress State

The concept of the characteristic state or the stress equivalent entitled the characteristic stress state plays an important role in understanding the stress-strain behaviour of sands. As described above dense sand will initially contract during shear and may continue to dilate with further straining. The transition from contraction to dilation defines the characteristic state at which the volumetric strain increment, $d\varepsilon_v$, is zero (Luong 1982). According to Luong (1982) the trace of the characteristic stress states, determined from several triaxial tests, defines a line in the plane, the characteristic line. The characteristic line divides the stress space into two regions with different deformation mechanisms. Stress combinations below the characteristic line lead to contraction, whereas stress combinations between the characteristic line and the failure envelop lead to dilation. The principle of the characteristic state is illustrated in Figure 2.3 by results from a number of conventional triaxial compression tests in which the confining pressure is held constant during shear.

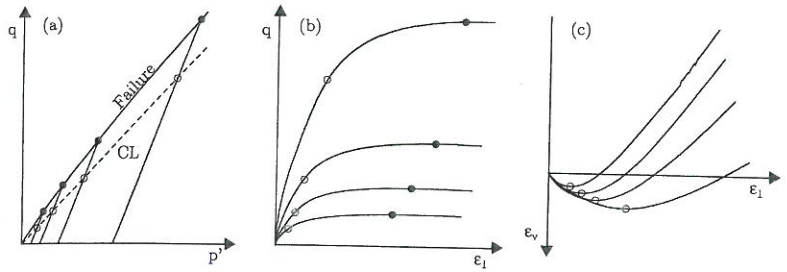

Figure 2.3: *Definition of the characteristic state from conventional triaxial compression test. (a) Characteristic line (CL) relative to failure in the $p'-q$ plane. (b) Stress-strain curves. (c) Volume change curves.*

A possible interpretation of these findings is to assume that the characteristic state corresponds to a quasi frictional component of the strength as stated by Kirkpatrick (1961). Hence, the definition of the characteristic friction angle, φ'_{CL}, becomes:

$$\sin\varphi'_{CL} = \frac{\sigma'_1 - \sigma'_3}{\sigma'_1 + \sigma'_3} \tag{2.3}$$

For conventional triaxial compression tests the characteristic angle is found to be independent of confining pressure or mean normal effective stress and void ratio (Ibsen & Lade 1998). Consequently, the trace of the characteristic stress states is indeed a line when tests are performed under such conditions.

Effect of Stress Path on the Characteristic Stress State

The characteristic line or angle should according to Luong (1982) moreover represent an intrinsic material parameter to be determined independently of the stress path. Experimental investigations performed by Jakobsen et al. (1999), however, invalidates this statement. A test program of several triaxial compression tests following different stress paths were conducted. All the tests emanated from the hydrostatic axis and passed through a characteristic stress state obtained from a conventional test. Hence, if the characteristic stress state is truly independent of the stress path, all of the tests should attain their characteristic state at the same state of stress, i.e. the characteristic stress state obtained from the conventional triaxial test. A complete description of the testing procedures can be found in Jakobsen & Praastrup (1998). The results of the tests are shown in Figure 2.4 where the characteristic stress states and failure states are marked by open and closed circles, respectively.

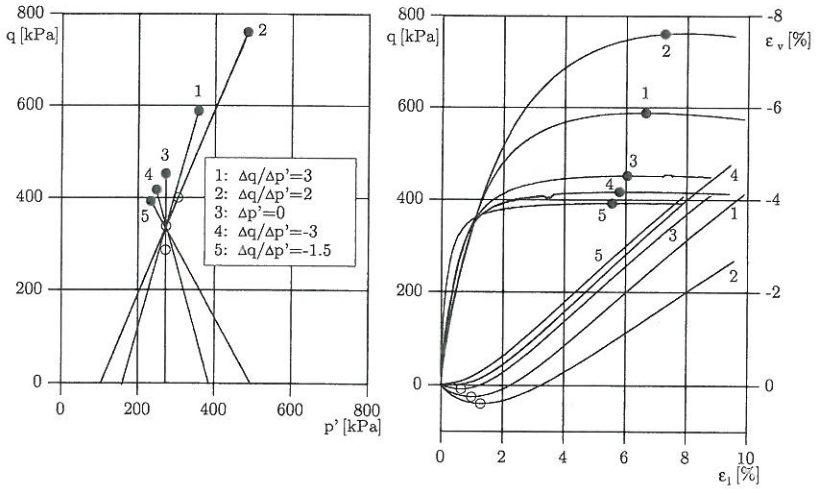

Figure 2.4: *Test results from five triaxial tests with different stress paths on dense Eastern Scheldt sand. (a) Stress paths in the $p'-q$ plane. (b) Stress-strain curves in combined $\varepsilon_1-q-\varepsilon_v$ diagram.*

As shown in the combined $\varepsilon_1 - q - \varepsilon_v$ and the $p' - q$ diagrams in Figure 2.4, it is only possible to determine a characteristic state for the tests with increasing and constant mean normal effective stress (denoted 1, 2 and 3). For tests with decreasing mean normal effective stress (4 and 5) it is impossible to determine a characteristic state, as the sand do not contract at all. The absence of contractive volumetric strain is due to the isotropic overconsolidation that occurs as the sand is sheared with decreasing mean normal effective stress. Thus, the sand is initially unloaded and recoverable volumetric expansion is greater than any potential irrecorverable contraction and the sand finally ends up dilating. The results show that the characteristic stress state is not an intrinsic parameter and indeed depends on the stress path. Hence the characteristic angle seemingly decreases as the slope of the stress path increases. This is supported by the observations made by Ibsen & Lade (1998).

Results from additional tests (Jakobsen & Praastrup 1998) support the observation above. Figure 2.5 show the effective friction angles corresponding to the measured characteristic stress states and failure states.

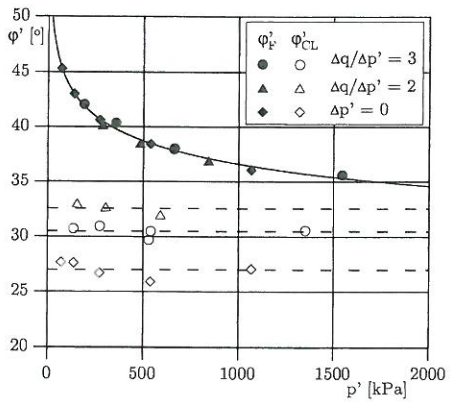

Figure 2.5: *Friction angles at characteristic stress states and failure states for various stress paths (Eastern Scheldt sand).*

The figure shows the expected effect of the stress path as the characteristic angle increases with decreasing slope of the stress path. The results show no effect of the mean normal effective stress. The characteristic state should be determined from tests performed with constant mean normal effective stress. Thus, for isotropic materials the recoverable volumetric strain is zero throughout the test and the characteristic state is obtained as the irrecoverable volumetric strain increment becomes zero. Poorooshasb et al. (1966) showed that the direction of the irrecoverable strain increment at a given state of stress is independent of the stress path. Hence, a definition of the characteristic state based on the irrecoverable volumetric strain increment becomes unique. Based on this definition the characteristic angle becomes an important parameter for development of constitutive models and calibration of model parameters (see Section 3.3).

2.3 Behaviour Under Undrained Conditions

The stress-strain and pore pressure response of sand is studied by performing undrained tests. The development of pore pressure in sand during shear is strongly related to the volumetric changes observed in drained tests, and the various compositional and environmental factors listed in the previous section will accordingly affect the potential for pore pressure development. Thus, under undrained conditions any tendency for dilation of the soil skeleton will lead to a decrease in pore pressure (generation of negative pore pressure), whereas a tendency for contraction will lead to an increase in pore pressure (generation of positive pore pressure). Consequently, any development in pore pressure will change the soils stiffness and strength. The drained failure envelope of the sand controls the occurrence of failure under undrained conditions, but the failure mode depends on the development in pore pressure.

1. For dilative sands the pore pressure decreases during shear leading to a strengthening of the sand. The pore pressure can, however, not drop below an absolute pressure of zero as at this pressure the pore water will cavitate. Hence, the tendency for dilation can no longer be prevented and the sand reaches a state of failure as prescribed by the drained failure envelope (Seed & Lee 1967).

2. For contractive sands the pore pressure increases during shear leading to a weakening of the sand. The generation of pore pressure will in turn lead to a shear strength which is substantially lower than the strength related to the initial state of stress. Hence, a minimum value is obtained and the condition of static liquefaction may eventually be reached (Alarcon-Guzman et al. 1988, Lade 1994, Verdugo & Ishihara 1996).

The effect of pressure, stress path and density on the development of pore pressure in sand is in the following illustrated by experimental results from traditional undrained and constant volume test. The two types of tests are differentiated in the way they are executed. Hence, in the undrained test, in which volume change is inhibited, a total stress path is followed and the corresponding pore pressure response is measured. In the constant volume test the confining pressure is continuously adjusted for maintenance of constant volume, i.e. the pore pressure is kept zero and the effective stress path is followed. The pore pressure is subsequently determined as the difference between initial and current confining pressure.

2.3.1 State of Phase Transformation

The drained and undrained responses of sand are, as already mentioned, closely related and whereas the drained response of dense sand is characterised by a change in volumetric behaviour, the undrained response is characterised by a change in the generation of pore pressure. Hence, the pore pressure initially increases and subsequently decreases due to the tendency for contraction and dilation of the sand skeleton, respectively. The transition from positive to negative generation of pore pressure in a conventional undrained or constant volume test is illustrated in Figure 2.6.

As shown in Figure 2.6a the stress path turn its direction in the $p' - q$ plane, i.e. the stress path has a 'knee' and the mean normal effective stress reaches a minimum value (marked by open circles). This stress state was denoted the state of phase transformation by Ishihara et al. (1975), and the trace of such states, determined from several undrained triaxial tests, defines a line, the phase transformation line. The name phase transformation is related to the sand response in cyclic undrained triaxial tests where Ishihara et al. observed that "it is necessary for a sample to go at least once through this critical value in order to be taken to a complete liquefied state". Hence, the stress state, or in particular, the friction angle corresponding to the state of phase transformation, φ'_{PL}, "may be considered as a threshold

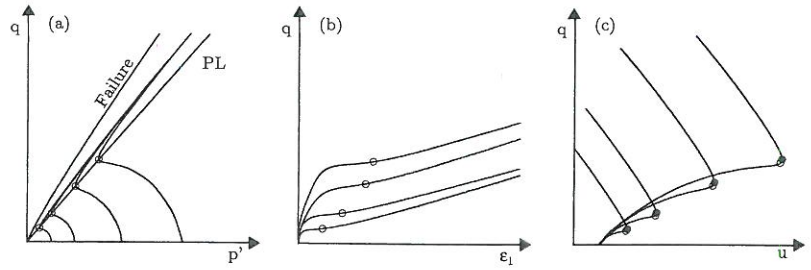

Figure 2.6: *Transition from positive to negative pore pressure generation in undrained and constant volume triaxial tests. (a) Definition of the state of phase transformation and the phase transformation line (PL) in the p' – q plane. (b) Stress-strain curves. (c) Curves for generated pore pressure.*

at which the behaviour of sand as a solid is lost and transformed into that of a liquefied state."

The state of phase transformation is not be confused with the stress state corresponding to the maximum generated pore pressure (marked by closed circles), which for constant volume tests and undrained tests with constant confining pressure occurs slightly later (see Figure 2.6c). The state of phase transformation is, as shown in Figure 2.8 and Figure 2.9, independent of initial mean normal effective stress and void ratio. Furthermore, the phase transformation line is independent of the total stress path as the effective stress path is unaffected by the change in confining pressure, i.e. the change in confining pressure is neutralised by a corresponding change in pore pressure (Skempton 1954).

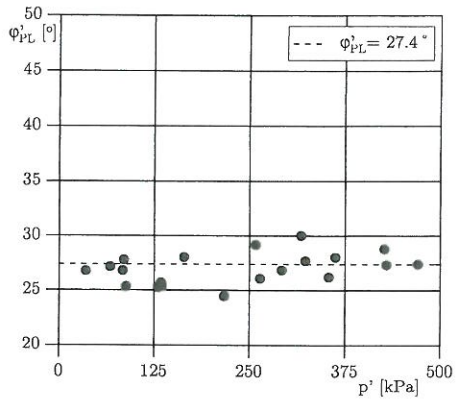

Figure 2.7: *Friction angles corresponding to the state of phase transformation for constant volume and undrained tests (Eastern Scheldt sand).*

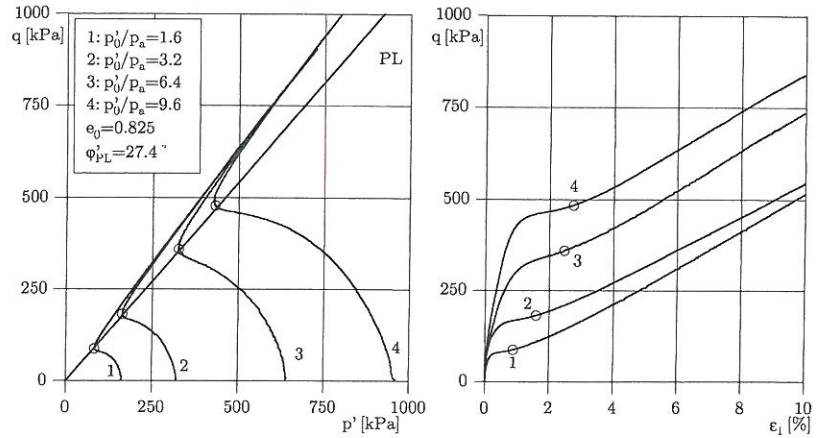

Figure 2.8: *Constant volume tests performed with different initial pressures on Eastern Scheldt sand. (a) Stress paths in the p' – q plane. (b) Stress-strain curves.*

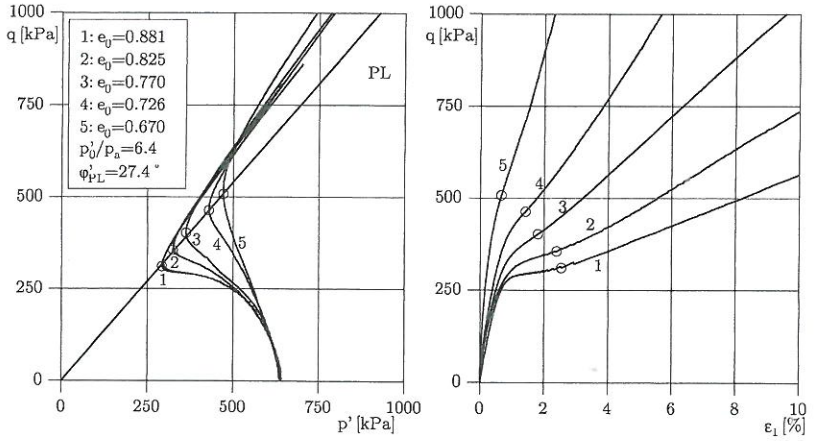

Figure 2.9: *Constant volume tests performed with different initial void ratios on Eastern Scheldt sand. (a) Stress paths in the p' – q plane. (b) Stress-strain curves.*

The friction angles, φ_{PL}, corresponding to the state of phase transformation are shown in Figure 2.7 for constant volume and undrained triaxial tests on Eastern Scheldt Sand (Jakobsen 1998). The friction angle is subjected to some scatter, but pressure and relative density do not affect the phase transformation line, which is seemingly unique for a given sand.

2.4 Comparison of Phase Transformation and Characteristic States

The present study of the drained and undrained behaviour of Eastern Scheldt sand has shown that the state of phase transformation is unique for a given sand, whereas the characteristic state is highly dependent on the effective stress path. However, as the states are mutually related some correlation between them should be expected. Thus, at the state of phase transformation the effective stress path in the $p' - q$ plane has a vertical tangent, i.e. zero increment in mean normal effective stress, corresponding to a transition from a tendency of contractive to dilative behaviour of the sand skeleton. Assuming isotropic material behaviour, the zero increment in mean normal effective stress may be interpreted as a state of zero recoverable and irrecoverable volumetric strain increments. For a drained test performed with constant effective mean stress the recoverable volumetric strain is zero throughout the test and the characteristic state is obtained as the irrecoverable strain increment becomes zero. Hence, the characteristic line determined from drained triaxial tests performed with constant mean normal effective stress should theoretically correspond to the phase transformation line.

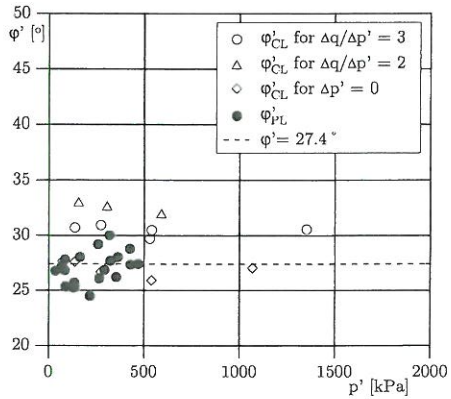

Figure 2.10: *Comparison of friction angles corresponding to the characteristic state (drained triaxial tests) and state of phase transformation (constant volume and undrained triaxial tests) for Eastern Scheldt sand.*

The friction angles for the state of phase transformation and characteristic states are compared in Figure 2.10. The friction angles corresponding to the characteristic states for drained triaxial tests performed with constant mean normal effective stress are located close to the phase transformation line (dashed line).

3 IMPLEMENTATION OF AN ELASTO-PLASTIC CONSTITUTIVE MODEL

The implementation strategy, techniques and suggestions for application of the single hardening model in connection with finite element calculations are presented. In order to explain the different aspects of the implementation of the single hardening model, a brief description of the components used in elasto-plastic constitutive models is given. The description is given in general terms and the set of formulae forming the single hardening model are not given, but can be found in Lade & Jakobsen (2002).

Some fundamental differences between the classic Mohr-Coulomb, Drucker-Prager and the single hardening models are discussed. It is shown that the single hardening model is able to capture the characteristic state or the state of phase transformation as defined previously for Eastern Scheldt sand.

The chapter is concluded with a few examples of simulations of drained triaxial tests verifying the capability of the single hardening model.

3.1 Components in Elasto-Plastic Constitutive Models

Constitutive models used for the description of soil behaviour in terms of stresses and strains can be composed of parts that account for aspects like elasticity, perfect-plasticity and hardening plasticity. The models may vary in complexity, and whereas refined models may include all the aspects of soil behaviour, simpler models can be formulated by adopting a combination of elasticity and perfect-plasticity.

Generally, the models use a separation of the deformations in recoverable (elastic) and irrecoverable (plastic) deformations. The occurrence of plastic deformations is controlled by a yield surface. The possible stress states are located within or on the yield surface, where stress paths within the surface results in purely elastic behaviour, and stress states on the surface results in perfectly-plastic or elasto-plastic behaviour of the soil. For hardening materials the yield surface changes during loading, creating a highly non-linear soil response. The changing of the yield surface is controlled by the so-called hardening rule that for isotropic hardening materials prescribes how the yield surface inflates and deflates during hardening and softening, respectively. The hardening rule depends on the plastic strain history, e.g. plastic strain or plastic work. The hardening of the soil is limited by a failure criterion ensuring that only stress states that the soil can withstand are obtained. For perfectly-plastic models the failure criterion and yield surface are identical. As soils cannot fail during isotropic loading the yield surface opens up along the hydrostatic axis. However, the opening of the yield surface along the hydrostatic axis neglects the plastic volumetric deformations that occur during isotropic compression. Drucker et al. (1955) among others solved this problem by introducing an additional cap yield surface.

On the occurrence of plastic deformations, a flow rule and a plastic potential surface define the relation between the plastic strain increment and the current state of stress. The flow rule and the plastic potential prescribes the magnitude and direction of the plastic strain increment by a plastic multiplier, which in some way depends on the elasto-plastic stiffness of the soil and the total strain increment, and by requiring that the increment is orthogonal the plastic potential. The plastic potential may coincide with the yield surface, in which case the flow rule is said to be associated. Some of the most popular models for soils, e.g. Cam-Clay, Mohr-Coulomb and Drucker-Prager, use associated flow and can be used to predict the stress-strain behaviour of normally consolidated clays. However, their ability to predict the stress strain

behaviour of dilative soils like sand is limited and it becomes necessary to use a non-associated flow rule in which the yield and plastic potential surfaces are defined separately. Basically a constitutive model must contain the following components:

- Elastic model
- Failure criterion
- Plastic potential surface and flow rule
- Yield surface and possibly hardening/softening law

Special comments are given below regarding the failure criterion and the plastic potential surface.

3.2 Failure Surface Approximations

The Coulomb criterion is the most well-know failure or yield criterion in soil mechanics. The criterion accounts linearly for the pressure dependency and can in terms of stress invariants be expressed as:

$$\frac{I_1}{3}\sin\varphi - \sqrt{\frac{J_2}{3}}\left((1+\sin\varphi)\cos\theta - (1-\sin\varphi)\cos\left(\theta+\frac{2}{3}\pi\right)\right) - c\cos\varphi = 0 \tag{3.1}$$

where I_1 is the first Cauchy stress invariant, J_2 is the second deviatoric stress invariant and θ is the Lode angle.

As shown in Figure 3.1a the Coulomb criterion forms an irregular hexagon in the octahedral plane taking into account that the soil strength is different in compression and extension, but neglects the effect of the intermediate principal stress on the soil strength. Despite the simplicity of the criterion it is due to its corners and singularities difficult to use in numerical analysis.

To avoid unstable numerical behaviour and complex corner formulations smoothed criteria can be used. The simplest mathematical and geometrical approximation is due to Drucker & Prager (1952):

$$\alpha I_1 - \sqrt{J_2} - k = 0 \tag{3.2}$$

where α and k are material parameters. The parameters can be related to the cohesion, c, and the friction angle, φ of the Mohr Coulomb model. The Drucker-Prager criterion forms a circle in the octahedral plane (see Figure 3.1a) and the material parameters must be adjusted to fit either the compressive or tensile strength of the soil. Hence, the problem is to determine a proper set of material parameters. If it is chosen to model the soil strength for triaxial compression the model overestimates the strength for all other cases. If associated plasticity is applied it further leads to excessive plastic dilatancy at failure.

Both the Mohr-Coulomb and the Drucker-Prager models are, due to the linear pressure dependency, limited to a narrow pressure range. The linear relation may, as shown in Figure 3.1b, lead to significant overestimation of the strength at high pressures. The failure criterion for the single hardening model shows good agreement with the experimental results. The failure criterion is given by:

$$\eta_1 = \left(\frac{I_1^3}{I_3} - 27\right)\left(\frac{I_1}{p_a}\right)^m \tag{3.3}$$

in which I_3 is the third Cauchy stress invariant, p_a is the atmospheric pressure and m and η_1 are material parameters. The failure criterion for the single hardening model is, as shown in Figure 3.1a, smooth and it circumscribes the Mohr-Coulomb criterion. The failure criterion of the single hardening model is numerical attractive and seemingly capable of prescribing the soil strength. Values of η_1 and m suitable for description of failure in dense Eastern Scheldt sand are listed in Table 3.1.

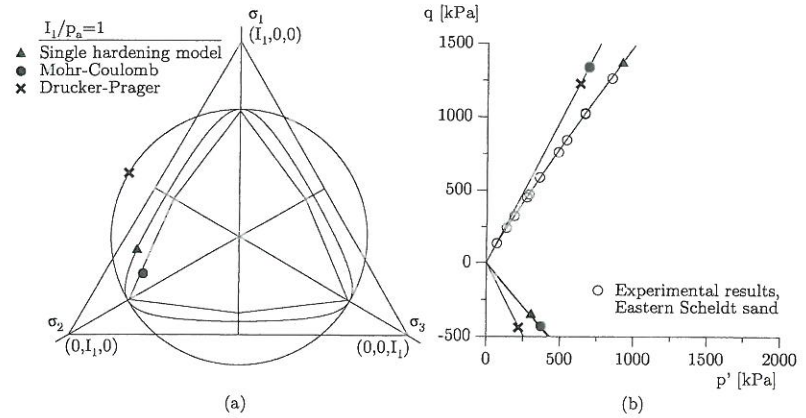

Figure 3.1: *Failure criterions for the Mohr-Coulomb, Drucker-Prager and single hardening model. (a) Octahedral plane. (b) $p' - q$ plane.*

3.3 Relation Between the Line of Phase Transformation and the Plastic Potential Surface

Under the assumption of isotropic material behaviour the study of the characteristic and phase transformation lines, revealed that the stress states located on this line corresponds to a material state at which the irrecoverable volumetric strain increment is zero. For elasto-plastic soil modelling this observation requires that the flow rule and plastic potential surface generate a zero volumetric plastic strain increment for stress states along the line of phase transformation. Hence, the plastic potential surface must at the state of phase transformation produce a plastic strain increment vector that is perpendicular to the hydrostatic axis.

This requirement cannot be fulfilled by the classical elastic perfectly-plastic models as they do not prescribe yielding and plastic deformations until the state of failure is reached. Hardening plasticity models may on the other hand be able to fulfil the requirement. For the single hardening model the plastic potential surface is given by:

$$g_p = \left(\psi_1\frac{I_1^3}{I_3} - \frac{I_1}{I_2} + \psi_2\right)\left(\frac{I_1}{p_a}\right)^\mu \tag{3.4}$$

where ψ_1 (depends on the material parameter m), ψ_2 and μ are material parameters. The material parameters have been determined from conventional drained triaxial tests performed on dense Eastern Scheldt sand and can be found in Table 3.1. The shape of the plastic potential surface in the octahedral plane is shown in Figure 3.2a for different function values.

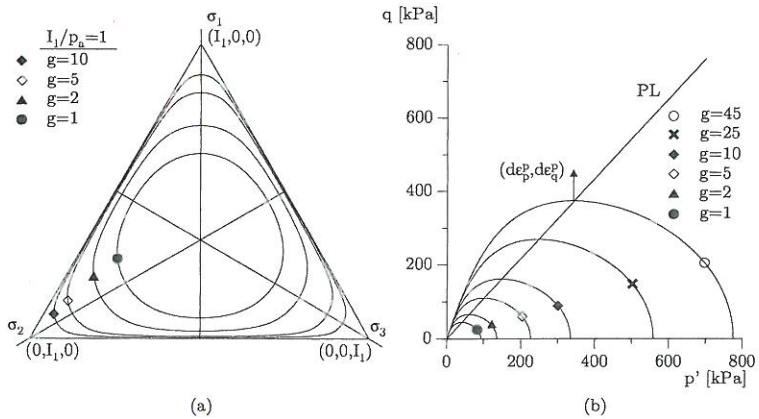

Figure 3.2: *Plastic potential surface of the single hardening model. (a) Octahedral plane. (b) $p' - q$ plane.*

The traces of the plastic potential surface in the $p' - q$ plane is shown in Figure 3.2b. The top points of the traces lie on the line of phase transformation (PL) for Eastern Scheldt sand. Consequently, the plastic strain increment is perpendicular to the hydrostatic and the volumetric plastic strain increment, $d\varepsilon_p^p$ is indeed zero. The material parameters ψ_2 and μ is normally determined by a technique that do not necessarily ensure that the top points of the traces of the plastic potential surface coincide with the line of phase transformation. However, this can be ensured by requiring that the derivative of the plastic potential surface with respect to the mean normal effective stress, p', is equal to zero along the line of phase transformation. The derivation leads to an irreducible seventh order polynomial in p' and q, which turns out to produce a straight line in the pressure octant of the stress space. By assuming a triaxial compression stress state the derivative can be rearranged for determination of the material parameter μ. The parameter μ is conveniently expressed by the angle of phase transformation and the parameters ψ_1 and ψ_2:

$$\mu = \frac{A^2\left(-9\psi_1 AB^2K + 2A^2K^2 - 6BK^2 + \psi_1 A^2B^3\right)}{3BK\left(A^2K + \psi_2 BK + \psi_1 A^3B\right)} \tag{3.5}$$

in which

$$\begin{aligned} A &= \frac{3 - \sin\varphi_{PL}}{1 - \sin\varphi_{PL}} \\ B &= \frac{3 + \sin\varphi_{PL}}{1 - \sin\varphi_{PL}} \\ K &= \frac{1 + \sin\varphi_{PL}}{1 - \sin\varphi_{PL}} \end{aligned} \tag{3.6}$$

The parameters μ and ψ_2 can, due to the condition of irreversibility, which requires that

the plastic work is positive (or zero), not be chosen arbitrarily (Kim & Lade 1988), but must further fulfil the requirements:

$$\mu > 0; \qquad \psi_2 > -27\psi_1 - 3 \tag{3.7}$$

Experience shows that the value of ψ_2 should be choosen close to the above limit. The plastic potential surface parameters for dense Eastern Scheldt sand given in Table 3.1 fulfil the requirements of (3.5) and (3.7).

3.4 Implementation Strategy and Techniques

The implementation of elasto-plastic constitutive models into finite element procedures requires that the models are derived on an inrecmental form, by which the stress increment is expressed in terms of the total strain incremement (e.g. Smith & Griffiths 1988, Chen & Mizuno 1990, Zienkiewicz & Taylor 1991):

$$d\boldsymbol{\sigma} = \mathbf{C}^{ep} d\boldsymbol{\varepsilon} = \left(\mathbf{C}^{e} - \mathbf{C}^{p}\right) d\boldsymbol{\varepsilon} \tag{3.8}$$

The incrementalizaton leads to the elasto-plastic stiffness matrix, $\mathbf{C}^{ep}$ of the soil at the current state of stress by combining the elastic, $\mathbf{C}^{e}$, and plastic, $\mathbf{C}^{p}$, soil stiffness contributions of the model. If the state of stress is within the elastic domain the plastic stiffeness vanishes and the elasto-plastic and elastic stiffnesses become identical. The incrementalization of the single hardening model is described by Lade & Jakobsen (2002).

Basically, the implementation must via the elasto-plastic soil stiffness provide an updated state of stress due to an imposed strain increment. As the stress-strain relation for hardening materials is highly non-linear and path dependent, special techniques for updating of the stresses accurately must be used. The updating is traditionally acomplished by use of backward Euler or explicit subincrementation integration schemes (Ortiz & Simo 1986, Sloan 1987, Abbo & Sloan 1993). The advantages and disadvantages of the schemes in connection with the implementation of the single hardening model are discussed in Jakobsen & Lade (2002). The present implementation of the single hardening model uses a number of different explicit subincrementation integration schemes for updating of the stresses.

The explicit schemes requires that the initial intersection of the yield surface must be computed if the state of the material changes from an elastic to an elasto-plastic state. Hence, the strain increment may initially be seperated in a truly elastic and an elasto-plastic part. From a state of stress located on the yield surface the explicit integration schemes use a finite incremental form of the constitutive model to predict the updated state of stress. Due to the non-linear soil behaviour, the explicit integration is only accurate for small strain increments, and it does not necessarily ensure that the updated stresses fulfill the consistency condition. This problem is solved by a two step procedure. Firstly, by subdividing the imposed strain increment into smaller increments and secondly by performing a correction for possible yield surface drift which would violate the consistency condition. The correction for yield surface drift, which tend to accumulate, must preserve the total strain increment, i.e. any change in elastic strain must be balanced by an equal and opposite change in plastic strain (Potts & Gens 1985).

The subdivision of the imposed strain increment can be performed in different ways. The simplest approach uses a forward Euler scheme with a fixed number of subincrements of equal size. The use of a fixed number of subincrements is computationally inefficient as the number of subincrements must be determined by trial-and-error so that the maximum experienced error is within some close stress tolerance. As alternatives a refined subincremental version of

the Euler scheme (Sloan 1987) and a Runge-Kutta scheme enhanced by Dormand & Prince (1980) are implemented. Both of the alternative schemes use active error control of the stresses by varying the size of the subincrement throughout the integration process. This ensures that only the necessary number of subdivisions are applied. Moreover, the procedure for correction of yield surface drift becomes redundant if the stress tolerance is selected properly.

Misuse of an explicit subincrementation scheme may lead to excessive computational costs that makes it inapplicable for practical use. However, a proper selection of the scheme can improve the efficiency dramatically without loss of accuracy. Hence, the investigation by Jakobsen & Lade (2002) of different explicit subincrementation schemes with the single hardening model, reveals that the use of the Runge-Kutta-Dormand-Prince scheme is superior to the traditional forward Euler scheme in terms of both computational efficiency and accuracy.

3.4.1 The ABAQUS interface

The finite element program ABAQUS provides an interface for employment of user defined material behaviour. The user matrial module (UMAT) is called by the program whenever a new estimate of stresses and soil stiffness is needed for establishment of the overall equilibrium of the finite element model. Hence, the UMAT must provide the updated stresses for evaluation of internal forces and a soil stiffness for establishment of the global stiffness of the finite element model. To keep track of the stress-strain history the UMAT also returns some so-called state variables, which basically contains information about the material hardening (maximum plastic work), stress level relative to failure, etc.

The single hardening model is implemented for use with ABAQUS using the implementation strategy given above. The material parameters and control parameters for the model used by the UMAT are defined in the ABAQUS input file. Subsequent calls from ABAQUS defines the inital state of stress, state variables and imposed strain increment. The interface for the single hardening model is described in detail by Jakobsen (2002).

3.5 Simulation of Drained Triaxial Tests

The efficiency of the implementation algorithm for the single hardening model has been investigated as described above and numerous tests have been performed to verify its ability to function, following different stress and strain paths (Jakobsen 2002).

The capacity of the model is well documented in the literature (Lade 1977, Kim & Lade 1988, Lade & Kim 1988*a*, Lade & Kim 1988*b*) and it is previously shown that the single hardening model is able to capture some of the key characteristics of sand. The capability of the model is further validated by comparison with experimental results from triaxial tests.

The model is calibrated against conventional triaxial tests on dense Eastern Scheldt sand following the procedure given in Kim & Lade (1988), Lade & Kim (1988*a*) and Lade & Kim (1988*b*). The material parameters of the model are listed in Table 3.1.

Table 3.1: *Material parameters determined for dense Eastern Scheldt sand.*

Model component	Parameter names	Parameter values		
Elastic properties	M, λ, ν	458.5	0.414	0.20
Failure criterion	a, m, η_1	0	0.288	70.2
Plastic potential surface	ψ_2, μ	-3.044	1.790	
Yield surface	h, α	0.590	0.386	
Hardening/Softening law	C, p, b	$8.281 \cdot 10^{-4}$	1.272	0.50

Simulations are performed for two conventional drained triaxial tests with $\Delta q/\Delta p' = 3$ (which have been used for calibration) and for two drained tests following stress paths of $\Delta p' = 0$ (constant mean normal effective stress) and $\Delta q/\Delta p' = 2$.

The simulations of the conventional tests are compared with experimental results in Figure 3.3a. Simulation and results are compared by stress-strain curves, $\varepsilon_1 - q$, and curves for the relative volume change, $\varepsilon_1 - \varepsilon_v$. As could be expected, there is a good agreement with the tests used for calibration. The deformation characteristics are described accurately and the model captures the transition from contractive to dilative behaviour of the sand. The material hardening close to failure is slightly underestimated, causing too high axial strains at failure.

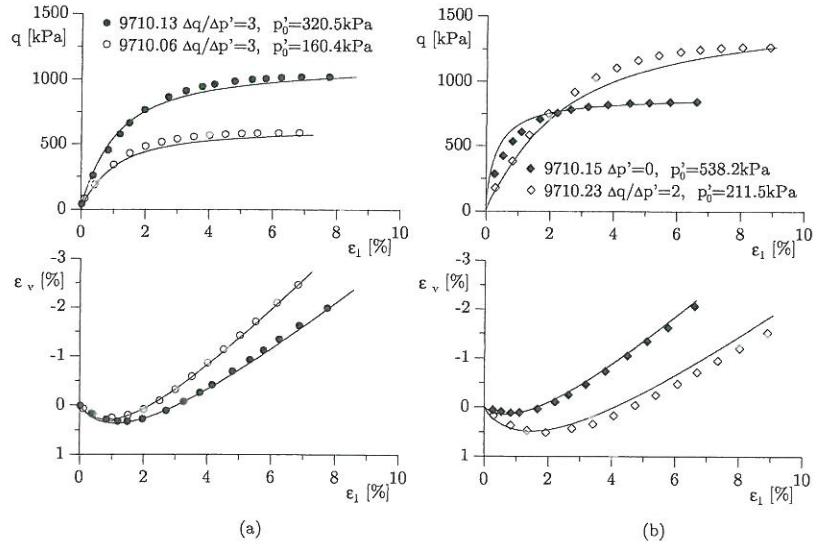

Figure 3.3: *Simulation of drained triaxial tests on Eastern Scheldt sand. (a) Conventional triaxial tests, $\Delta q/\Delta p' = 3$. (b) Triaxial tests with stress paths of $\Delta p' = 0$ (constant mean normal effective stress) and $\Delta q/\Delta p' = 2$.*

For the simulation of the test with a stress path of $\Delta q/\Delta p' = 2$ the material hardening is generally underestimated yielding a too high rate of dilation (see Figure 3.3b).

Figure 3.3b shows that the model reproduces the axial and volumetric strains accurately for the test performed with constant mean normal effective stress. From the stress-strain curve it appears that the model significantly overestimates the material stiffness. However, the model captures perfectly the characteristic stress state or state of phase transformation, as defined by the plastic potential surface in Section 3.3. The discrepancy between experimental and model results is expected, as the characteristic friction angle obtained from the experiment 9710.15 is lower than the friction angle determined in Section 2.4.

The model is seemingly capable of representing the experimental data. The model generally predicts the volumetric behaviour well, whereas the stress-strain response is slightly off.

4 CONCLUSION

Several elements related to the constitutive modelling and numerical analysis of soils have been studied and presented. Experimental investigations of the pre-failure stress-strain behaviour have been performed by drained and undrained triaxial testing (Jakobsen & Praastrup 1998, Jakobsen 1998). The tests, which were performed on dense Eastern Scheldt sand, have formed the basis for the evaluation of a single hardening constitutive model. During the analysis of the triaxial tests it was revealed that the traditional analysis method was based on an inconsistent use of strain measures. Two alternative methods of analysis were proposed by Praastrup et al. (1999). The methods uses the infinitesimal engineering strain measure and the finite natural strain measure consistently. The natural strain measure is generally applicable, whereas the use of the engineering strain measure only is applicable for small deformations. Thus, the natural strain measure has been adopted for analysis of the triaxial tests and calibration of constitutive model parameters. Moreover, the used strain measure comply with the strain measure commonly used in finite element programs like ABAQUS.

Jakobsen et al. (1999) investigated the effect of stress path on the characteristic stress state (characteristic line or characteristic angle) at which the soil starts to dilate during drained shear. The results from a series of drained triaxial tests showed that the characteristic angle depends on the stress path. The lowest characteristic angle was obtained for tests performed with constant mean effective normal stress and the angle increased as the slope of the stress path was decreased. A corresponding stress state, named the state of phase transformation, can be retrieved from undrained triaxial tests. The angle of phase transformation is shown to be unique for a given sand as it is independent of mean effective normal stress and density. Comparison of the angle of phase transformation and the characteristic angle obtained from tests with constant mean effective normal stress showed that the angles are identical for all practical purpose. This observation was supported by theoretical considerations based on elasto-plastic theory for isotropic materials. Hence, it has been shown that the phase transformation line is captured by the plastic potential surface of the implemented single hardening constitutive model.

Lade & Jakobsen (2002) derived the single hardening model on an incremental form, facilitating the implementation of the model into a finite element program. The implementation was initially based on a simple forward Euler integration scheme with a fixed number of subincrements for updating of stresses. However, the scheme was found to be computationally ineffective and the obtained stresses was drifting away form the yield surface, causing a violation of the consistency condition. The yield surface drift was eliminated by adopting an iterative procedure ensuring fulfilment of the consistency condition. However, to make the single hardening model applicable to engineering practice a reduction of the computational costs was needed. Two higher order explicit integration schemes with active error control and automatic adjustment of the subincrements were implemented and investigated by Jakobsen & Lade (2002). The schemes increased the computational efficiency dramatically, with the Runge-Kutta-Dormand-Prince scheme being superior in terms of both efficiency and accuracy. The use of the single hardening model together with the finite element program ABAQUS has been described in Jakobsen (2002).

The capability of the single hardening model was investigated by simulation of triaxial tests on Eastern Scheldt sand following different stress paths. The simulations showed that the model is capable of representing the experimental data.

The work with the implementation of the single hardening model has generally showed that it captures the key characteristics of dense sand and that prudence in the selection of the numerical techniques can make the model applicable to engineering practice. The implemented model can hopefully replace some of the classic constitutive models, yielding a more realistic response of sand.

REFERENCES

Abbo, A.J. & S.W. Sloan (1993), Backward Euler and subincrementation schemes in computational plasticity, *in* Valliappan, Pulmano & Tin-Loi, eds, 'Computational Plasticity', Balkema, Rotterdam, pp. 319–330.

Alarcon-Guzman, A., G. Leonards & J. Chameau (1988), 'Undrained monotonic and cyclic strength of sands', *Journal of Geotechnical Engineering* **114**(10), 1089–1109.

Bishop, A.W. (1954), 'Characteristics of saturated silt, measured in triaxial compression', *Geotechnique* **4**, 43–45.

Casagrande, A. (1940), *Characteristics of Cohesionless Soils Affecting the Stability of Slopes and Earth Fills*, Boston Society of Civil Engineers. (Contributions to Soil Mechanics, 1925-1940).

Chen, W.F. & E. Mizuno (1990), *Non-Linear Analysis in Soil Mechanics*, Elsevier, New York.

Dafailas, Y.F. & L.R. Herrmann (1982), Bounding surface formulation of soil plasticity, *in* Pande & Zienkiewicz, eds, 'Soils Mechanics - Transient and Cyclic Loads', Wiley, Chichester, U.K., pp. 253–282.

Dimaggio, F.L. & I.S. Sandler (1971), 'Material models for granular materials', *Journal of Engineering Mechanics Division* **97**(EM3), 935–950.

Dormand, J.R. & P.J. Prince (1980), 'A family of embedded Runge-Kutta formulae', *Journal of Computer Applied Mathematics* **6**, 19–26.

Drucker, D.C, R.E. Gibson & D.J. Henkel (1955), Soil mechanics and work-hardening theories of plasticity, *in* 'ASCE Annual Proceedings', Vol. 81, pp. 1–14.

Drucker, D.C & W. Prager (1952), 'Soil mechanics and plastic analysis or limit design', *Quaterly of Applied Mathematics* **10**, 157–165.

Hansen, B. (1958), Line ruptures regarded as narrow rupture zones, basic equations based on kinematic conditions, *in* 'Proceedings on Conference on Earth Pressure Problems', Vol. 1, Brussels, pp. 38–47.

Ibsen, L.B. & K.P. Jakobsen (1997), 'Dynamic bearing capacity of caisson breakwaters subjected to impulsive wave loading', MAST III PROVERBS Workshop.

Ibsen, L.B. & K.P. Jakobsen (1998), 'Limit state equations for stability and deformation', *AAU Geotechnical Engineering Papers* . ISSN 1398-6465 R9828.

Ibsen, L.B. & P.V. Lade (1998), The role of the characteristic line in static soil behaviour, *in* 'Proceedings on the 4th International Workshop on Localization and Bifurcation Theory for Soils and Rocks', Gifu, Japan.

Ishihara, K., F. Tatsuoka & S. Yasuda (1975), 'Undrained deformation and liquefaction of sand under cyclic stresses', *Soils and Foundations* **15**(1), 29–44.

Iwan, W.D. (1967), 'On a class of models for the yielding behaviour of continuous and composite systems', *Journal of Applied Mechanics* **34**, 612–617.

Jakobsen, K.P. (1998), 'Undrained triaxial tests on Eastern Scheldt sand', *AAU Geotechnical Engineering Papers* . ISSN 1398-6465 R9823.

Jakobsen, K.P. (2002), 'Application of the single hardening model in the finite element program ABAQUS', *AAU Geotechnical Engineering Papers* . ISSN 1398-6465 R0201.

Jakobsen, K.P. & P.V. Lade (2002), 'Implementation algorithm for a single hardening constitutive model for frictional materials', *International Journal for Numerical and Analytical Methods in Geomechanics* **26**, 661–681.

Jakobsen, K.P. & U. Praastrup (1998), 'Drained triaxial tests on Eastern Scheldt sand', *AAU Geotechnical Engineering Papers* . ISSN 1398-6465 R9822.

Jakobsen, K.P., U. Praastrup & L.B. Ibsen (1999), The influence of stress path on the characteristic stress state, *in* 'Procedings of the Second International Symposium on Pre-Failure Deformation Characteristics of Geomaterials', Balkema, Torino, Italy, pp. 659–666.

Kim, M.K & P.V. Lade (1988), 'Single hardening constitutive model for frictional materials, I. Plastic potential function', *Computer and Geotechnics* (5), 307–324.

Kirkpatrick, V.M. (1961), Discussion on soil properties and their measurement, *in* 'Proceedings on the 5th International Conference on Soil Mechanics and Foundation Engineering', Vol. III, Paris, France, pp. 131–133.

Krieg, R.D. (1975), 'A practical two surface plasticity theory', *Journal of Applied Mechanics* **42**, 641–646.

Ladd, C.C., R. Foot, K. Ishihara, F. Schlosser & H.G. Poulos (1977), Stress-deformation and strength characteristics, *in* 'Proceedings on the 9th International Conference on Soil Mechanics and Foundation Engineering', Vol. II, Tokyo, Japan, pp. 421–494.

Lade, P.V. (1977), 'Elasto-plastic stress-strain theory for cohesionless soils with curved yield surfaces', *International Journal of Solids and Structures* **13**, 1019–1035.

Lade, P.V. (1994), 'Instability and liquefaction of granular materials', *Computers and Geotechnics* (16), 123–151.

Lade, P.V. & J.M. Duncan (1973), 'Cubical triaxial tests on cohesionless soil', *Journal of the Soil Mechanics and Foundations Division* **99**(SM10), 793–812.

Lade, P.V. & J.M. Duncan (1976), 'Stress-path dependent behaviour of cohesionless soil', *Journal of the Geotechnical Engineering Division* **102**(GT1), 51–68.

Lade, P.V. & K.P. Jakobsen (2002), 'Incrementalization of a single hardening constitutive model for frictional materials', *International Journal for Numerical and Analytical Methods in Geomechanics* **26**, 647–659.

Lade, P.V & M.K Kim (1988*a*), 'Single hardening constitutive model for frictional materials II. Yield criterion and plastic work contours', *Computer and Geotechnics* (6), 13–29.

Lade, P.V & M.K Kim (1988*b*), 'Single hardening constitutive model for frictional materials III. Comparisons with experimental data', *Computer and Geotechnics* (6), 31–47.

Lee, K.L & H.B. Seed (1967), 'Drained strength characteristics of sands', *Journal of the Soil Mechanics and Foundations Division* **93**(SM6), 117–141.

Luong, M. (1982), Stress-strain aspects of cohesionless soil under cyclic and transient loading, *in* 'International Symposium on Soils under Cyclic and Transient Loading', Balkema, Swansea, U.K., pp. 315–324.

Malvern, L.E. (1969), *Introduction to the Mechanics of a Continuous Medium*, Prentice-Hall, Englewood Cliffs, N.J.

Mróz, Z. (1967), 'On the description of anisotropic workhardening', *Journal of Mechanics and Physics of Solids* **15**, 163–175.

Nordal, S., H.P. Jostad, A. Kavli & L. Grande (1989), A Coulombian soil model applied to an offshore platform, *in* 'Proceedings on the 12th International Conference on Soil Mechanics and Foundation Engineering', Vol. 1, Rio de Jameiro, pp. 471–474.

Oda, M. (1972), 'Initial fabrics and their relations to mechanical properties of granular material', *Soils and Foundations* **12**(1), 17–36.

Ortiz, M. & J.C. Simo (1986), 'An analysis of a new class of integration algorithms for elastoplastic constitutive relations', *Journal for Numerical Methods in Engineering* **24**, 893–911.

Poorooshasb, H.B., I. Houlbec & A.N. Sherbourne (1966), 'Yielding and flow of sand in triaxial compression: Part I', *Canadian Geotechnical Journal* **3**, 179–190.

Potts, D.M. & A. Gens (1985), 'A critical assessement of methods of correcting for drift from the yield surface in elasto-plastic finite element analysis', *International Journal for Numerical and Analytical Methods in Geomechanics* **9**, 149–159.

Praastrup, U., K.P. Jakobsen & L.B. Ibsen (1999), 'Two theoretically consistent methods for analysing triaxial tests', *Computers and Geotechnics* (25), 157–170.

Rowe, P.W. (1962), The stress dilatancy relations for static equlibrium of an assembly of particles in contact, *in* 'Proceedings Series', Vol. 269, Royal Society, London, pp. 500–527.

Schofield, A.N. & C.P. Wroth (1968), *Critical State Soil Mechanics*, McGraw-Hill, London.

Seed, H.B. & K.L. Lee (1967), 'Undrained strength characteristics of cohesionless soils', *Journal of the Soil Mechanics and Foundations Division* **93**(SM6), 333–360.

Shield, R.T. (1955), 'On Coulombs law of failure in soils', *Journal of Mechanics and Physics of Solids* **4**, 10–16.

Skempton, A.W. (1954), 'The pore pressure coefficients A and B', *Geotechnique* **4**, 143–147.

Sloan, S.W. (1987), 'Substepping schemes for the numerical integration of elastoplatic stress-strain relations', *International Journal for Numerical Methods in Engineering* **24**, 893–911.

Smith, I.M. & D.V. Griffiths (1988), *Programming the Finite Element Method*, 2nd edn, Wiley, New York, N.Y.

Taylor, D.W. (1948), *Fundamental of Soil Mechanics*, Wiley, New York, N.Y.

Verdugo, R. & K. Ishihara (1996), 'The steady state of sandy soils', *Soils and Foundations* **36**(2), 81–91.

Zienkiewicz, O.C. & R.L. Taylor (1991), *The Finite Element Method - Vol. 2: Solid and Fluid Dynamics and Non-Linearity*, McGraw-Hill, London, U.K.

LIST OF PUBLICATIONS

The experimental and numerical investigations performed in connection with the present study have lead to a number of papers and reports. Some of the reports are voluminious and only copies of the first four papers are included in the thesis.

PAPERS

Praastrup, U., K.P. Jakobsen & L.B. Ibsen (1999), 'Two theoretically consistent methods for analysing triaxial tests', *Computers and Geotechnics* (25), 157-170.

Jakobsen, K.P., U. Praastrup & L.B. Ibsen (1999), The influence of stress path on the characteristic stress state,*in* 'Procedings of the Second International Symposium on Pre-Failure Deformation Characteristics of Geomaterials', Balkema, Rotterdam, pp. 659-666.

Lade, P.V & K.P. Jakobsen (2002), 'Incrementalization of a single hardening constitutive model for frictional materials', *International Journal for Numerical and Analytical Methods in Geomechanics* **26**, 647-659.

Jakobsen, K.P & P.V. Lade (2002), 'Implementation algorithm for a single hardening constitutive model for frictional materials', *International Journal for Numerical and Analytical Methods in Geomechanics* **26**, 661-681.

Praastrup, U., K.P. Jakobsen & L.B. Ibsen (1998), 'On the choice of strain measures in geomechanics', 12th Young Geotechnical Engineers Conference, Tallin, Estonia.

Ibsen, L.B. & K.P. Jakobsen (1997), 'Dynamic bearing capacity of caisson breakwaters subjected to impulsive wave loading', MAST III PROVERBS Workshop, Las Palmas, Spain.

Ibsen, L.B. & K.P. Jakobsen (1998), 'Limit State Equations for Stability and Deformation', *AAU Geotechnical Engineering Papers*, ISSN 1398-6465 R9828.

DATA REPORTS

Jakobsen, K.P. & and U. Praastrup (1998), 'Drained triaxial tests on Eastern Scheldt sand', *AAU Geotechnical Engineering Papers*, ISSN 1398-6465 R9822.

Jakobsen, K.P (1998), 'Undrained triaxial tests on Eastern Scheldt sand', *AAU Geotechnical Engineering Papers*, ISSN 1398-6465 R9823.

Lund, W.P. & K.P. Jakobsen (1998), 'Permeability tests on Silkeborg sand no 0000', *AAU Geotechnical Engineering Papers*, ISSN 1398-6465 R9811.

Jakobsen, K.P (1998), 'Permeability tests on Eastern Scheldt sand', *AAU Geotechnical Engineering Papers*, ISSN 1398-6465 R9821.

Jakobsen, K.P (1998), 'Cyclic triaxial tests on Eastern Scheldt sand', *AAU Geotechnical Engineering Papers*, ISSN 1398-6465 R9824.

Steenfelt, J.S & K.P. Jakobsen (1998), 'Triaxial Tests on Heavy Sand, Namibia', *AAU Geotechnical Engineering Papers*, ISSN 1398-6465 R9808.

Jakobsen, K.P (1999), 'Cyclic triaxial tests on Eastern Scheldt sand with three different densities', *AAU Geotechnical Engineering Papers*, ISSN 1398-6465 R9915.

REPORTS

Jakobsen, K.P (1999), 'Application of the Single Hardening model in the finite element program ABAQUS', *AAU Geotechnical Engineering Papers*, ISSN 1398-6465 R0201.

MANUALS

Jakobsen, K.P (1998), 'Manual for udførelse af cycliske triaksialforsøg - Styring og måleprincipper samt forsøgsprocedurer' (Manual for cyclic triaxial testing - Control and measuring pricinples and testing procedures), *AAU Geotechnical Engineering Papers*, ISSN 1398-6465 R9825

Title:
Two theoretical consistent methods for analysing triaxial tests.

Authors:
Praastrup, U., K.P. Jakobsen & L.B. Ibsen.

Year of publication:
1999

Published in:
Computers & Geotechnics (25), 157-170.

ELSEVIER

COMPUTERS AND GEOTECHNICS

Computers and Geotechnics 25 (1999) 157–170

www.elsevier.com/locate/compgeo

Two theoretically consistent methods for analysing triaxial tests

Ulrik Praastrup, Kim P. Jakobsen, Lars Bo Ibsen*

Department of Civil Engineering, Aalborg University, Sohngaardsholmsvej 57, DK-9000 Aalborg, Denmark

Received 22 March 1999; received in revised form 11 June 1999; accepted 21 July 1999

Abstract

Constitutive models for geomaterials are frequently developed and calibrated on the basis of element tests. Prior to the analysis of element tests a suitable set of work-conjugated stress and strain measures has to be selected. The paper points out that the traditional analysis of triaxial tests is theoretically inconsistent as finite and infinite strain measures are mixed in the analysis. Therefore, two theoretically consistent methods are proposed and examined for the analysis of triaxial tests. These three methods affect strain-dependent material parameters differently. The effect is analysed using key geotechnical parameters and an advanced constitutive model.

Keywords: Strain measures; Triaxial tests; Constitutive modeling; Volume change

1. Introduction

Traditional triaxial tests, drained and undrained, are commonly used in the study of the stress–strain behaviour of geomaterials. Drained tests are solely considered here, but all observations presented in this paper apply to the undrained case as well. During drained triaxial tests simultaneous values of axial displacement, volume change, confining pressure and axial load are measured. Since all directional measurements coincide with the principal axes of stresses and strains, the analysis of the test data ought to be straightforward.

The stress and strain measures must, according to Malvern [1], be work-conjugated and, furthermore, refer to the same configuration (reference or current) when constitutive relations are investigated.

* Corresponding author. Fax: +45-98-142-555.
E-mail address: i5lbi@civil.auc.dk (L.B. Ibsen).

0266-352X/99/$ - see front matter
PII: S0266-352X(99)00021-X

From an engineering point of view, it is obvious to use the Cauchy, or true stress, as stress measure. The Cauchy stress can in simple terms be expressed as the ratio between current load and current area [2] and can with ease be calculated from the measurements carried out during a triaxial test. The Cauchy stress measure is adopted throughout this paper.

In cases where strains and displacements are assumed infinitesimal, the distinction between a description based on a reference or a current configuration becomes arbitrary as all stress and strain measures are work-conjugated in this case. Consequently, the engineering strain measure is work-conjugated with the Cauchy stress under this assumption. In situations where displacements or strains are large, another strain measure, a finite strain measure, must be introduced. This measure must be work-conjugated to the Cauchy stress measure. The natural strain increment, as stated in ABAQUS [3,4] and Crisfield [2], satisfies this requirement. Both strain measures, the natural strain (increment) and the engineering strain, are adopted in this paper.

In the traditional analysis of triaxial tests (denoted method T), the axial strain is calculated as the ratio between the measured axial displacement and the initial height of the specimen, i.e. the engineering strain measure or the infinitesimal strain measure is used. Products of displacement derivatives are neglected in the theory of infinitesimal deformations [5].

The volumetric strain is traditionally calculated as the ratio between measured volume change and the initial volume of the specimen. Squares and products of displacement derivatives are not neglected in this calculation [5]. Hence, a finite strain measure is adopted and an inconsistency arises in the assumptions as finite and infinite strain measures are mixed. The inconsistency can be eliminated by following one of two distinct methods, either by adopting the natural strain increment or simply by adopting the engineering strain consistently in the analysis. Using these two methods denoted N and E, respectively, requires a computation of an exact displacement field before the strains can be calculated. Both methods are in the following illustrated for the triaxial case and the results are compared with the traditional method T. The effect of the three methods on some key geotechnical parameters is investigated together with the effect on modelling the stress–strain behaviour using an advanced constitutive model.

2. Analysis of triaxial tests

During a drained triaxial test, simultaneous values of axial displacement, volume change, axial load and confining pressure are measured. On this basis, it is possible to obtain the radial displacement and true axial stress, thus yielding a complete stress–strain description of the soil specimen under axisymmetric conditions. The radial displacement can only be calculated under the assumption that the radial and tangential strains are equal which, as stated by Kirkpatrick and Belshaw [6], is the case for all practical purposes.

2.1. Analysis based on the exact displacement field

In a triaxial test the deformation of the soil specimen is characterised by the compression or elongation in the axial and radial directions.

The original size of a sample is fully described by the initial height, H_0, and the initial diameter, D_0, whereas the size in a deformed stage is fully described by its original size and the displacement components u_1, and u_3. Compression, as shown in Fig. 1, is considered positive. The current height, H, diameter, D, and cross-sectional area, A, are given by:

$$H = H_0 - u_1;\ D = D_0 - 2u_3 \tag{1}$$

$$A = \frac{\pi}{4}(D_0 - 2u_3)^2 = \frac{V_0 - \Delta V}{H_0 - u_1} \tag{2}$$

The current cross-sectional area is traditionally used in the calculation of the axial stress. Therefore, it follows that the axial stress is of the Cauchy type. The volume change, ΔV, is of great importance in geomechanics. In terms of the displacement components it may be expressed as:

$$\Delta V = \frac{\pi}{4}\left[H_0 D_0^2 - (H_0 - u_1)(D_0 - 2u_3)^2\right] \tag{3}$$

The radial displacement is traditionally not calculated in the analysis of a triaxial test, but this quantity is indispensable for a complete description of the displacement

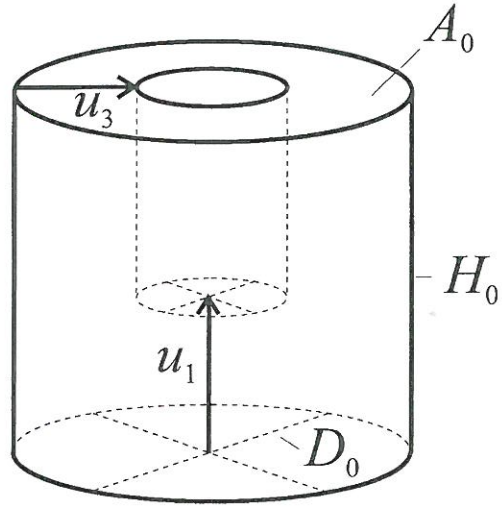

Fig. 1. Definition of geometric quantites.

field. As the axial displacement and the volume change are measured directly, the radial displacement can be expressed as:

$$u_3 = \frac{D_0}{2} - \sqrt{\frac{V_0 - \Delta V}{\pi(H_0 - u_1)}} \tag{4}$$

The radial stress or the confining pressure is measured directly as a Cauchy type of stress. Therefore, no intermediate calculations are required. An exact representation of the displacement and the Cauchy type of stress field has now been set-up.

The determination of geotechnical design parameters and the general study of material behaviour are commonly based on element tests, such as the triaxial test. As initial sample dimensions may vary from sample to sample and from apparatus to apparatus, the relevant parameters can obviously not be based on displacements. The parameters have to be based on relative deformations. As mentioned in the introduction there are two strain measures that are work-conjugated to the Cauchy type of stress measure. That is, as stated in [1], the engineering strain and the natural strain increment. Both strain measures are adopted in this paper.

2.2. Engineering strain versus natural strain

The linear engineering strain measure and the non-linear natural strain measure are briefly discussed in order to indicate their use and limitations. The simplest definition is the engineering strain, which is traditionally used in the theory of infinitesimal deformations:

$$\varepsilon_1^E = \frac{u_1}{H_0}; \varepsilon_3^E = 2\frac{u_3}{D_0} \tag{5}$$

The natural strain increment is often employed in the theory of finite deformations and/or in the theory of plasticity [4]. The natural strain increment is closely associated with the natural strain and based on the ratio between the initial height, H_0, and the initial diameter, D_o, and the current quantities, respectively:

$$\varepsilon_1^N = \ln\left(\frac{H_0}{H_0 - u_1}\right); \varepsilon_3^N = \ln\left(\frac{D_0}{D_0 - 2u_3}\right) \tag{6}$$

The natural strain measure makes no distinction between initial and final quantity and an interchange merely changes the sign. The difference between the natural and engineering strain measures in the one dimensional case is illustrated in Fig. 2. It is seen that $\varepsilon_1^E > \varepsilon_1^N$ and that the deviation is in the order of 4–5% for $|u_1/H_0| < 0.1$. The deviation is in general accepted and the assumption of infinitesimal deformations is commonly assumed to be valid. However, the difference becomes more pronounced when it comes to calculating the volumetric strain.

The volumetric strain is within the framework of the theory of infinitesimal deformations defined as the sum of the principal strains:

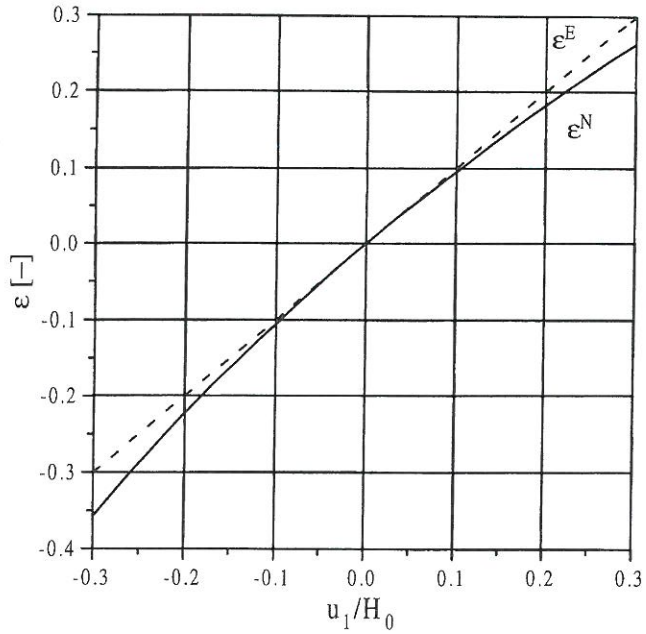

Fig. 2. The strain measures ε_1^E and ε_1^N for the one dimensional case.

$$\varepsilon_v^E = \varepsilon_1^E + 2\varepsilon_3^E \tag{7}$$

The volumetric strain is traditionally calculated as the ratio between the measured volume change and the initial volume of the specimen, i.e. a finite strain measure:

$$\varepsilon_v^T = \frac{\Delta V}{V_0} \tag{8}$$

Within the normal range of deformations, the disparity between the expressions in (7) and (8) may exceed 15–20%.

The volumetric strain, based on the natural strain definition, is found by addition of the principal strains:

$$\varepsilon_v^N = \varepsilon_1^N + 2\varepsilon_3^N = \ln\left(\frac{V_0}{V_0 - \Delta V}\right) \tag{9}$$

The disparity between the expressions in (7) and (9) may exceed 15–20% within the normal range of deformations.

Whether the engineering or the natural strain measure is chosen in the analysis of triaxial tests depends on whether finite or infinite deformations apply to the geotechnical

problem under investigation. The form of the constitutive relation must, moreover, be considered [4]. The volumetric strain measures are more thoroughly discussed in the succeeding section.

2.3. Analysis based on strains

The traditional analysis of triaxial tests, denoted method T, is strain wise performed by using the expressions in (5) and (8).

An analysis based solely on the theory of infinitesimal deformations (method E) is on the other hand performed by using the expressions in (5) and (7), whereas the method denoted N uses the expressions in (6) and (9). The traditional analysis of triaxial tests leads to an inconsistent use of the theory of infinitesimal deformations, as a finite strain measure (8) is mixed with an infinitesimal measure (5).

The two proposed methods, N and E, use their theoretical background consistently and could, therefore, both be used in the analysis of triaxial tests. However, method E has some limitations as significant errors are introduced under certain conditions. The error is investigated in the following and it is shown how the use of the natural strain measure leads to an exact description of the deformations.

2.3.1. Errors produced using E and T

The radial displacement component, u_3, can by using the expressions in (5), (7) and (8) be expressed as:

$$u_3^{T,E} = \frac{4\Delta V - \pi D_0^2 u_1}{4\pi D_0 H_0} \tag{10}$$

A comparison of (4) and (10) reveals the effect of the linear approximation. The error, e, on the radial displacement component is given by (11) and shown in Fig. 3.

$$e = u_3 - u_3^{T,E} = \frac{D_0}{2}\left(1 - \frac{4\Delta V - \pi D_0^2 u_1}{8V_0}\right) - \sqrt{\frac{V_0 - \Delta V}{\pi(H_0 - u_1)}} \tag{11}$$

Fig. 3 shows how e varies with respect to the two deformation measurements (most often) collected during triaxial tests. As expected the figure shows that the magnitude of e increases as the axial displacement increases. Moreover, the figure shows how the volume change influences e.

The use of method E can at moderate to high levels of deformation produce significant errors. So the method E should only be applied in cases where deformations are truly small.

2.3.2. Natural strain

If the natural strain definition is applied, the radial deformation can be determined on the basis of (6) and (9):

$$u_3^N = \frac{D_0}{2} - \sqrt{\frac{V_0 - \Delta V}{\pi(H_0 - u_1)}} \tag{12}$$

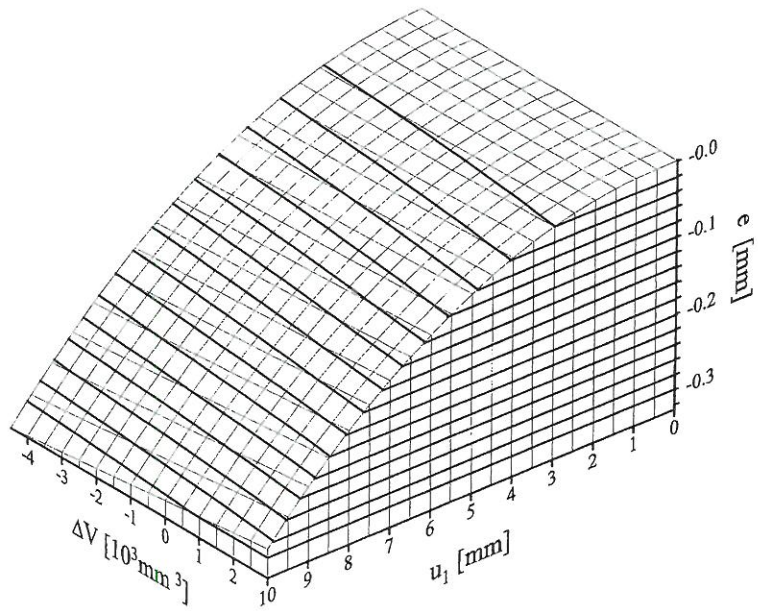

Fig. 3. Error due to the use of method E, $H_0 = D_0 = 70$ mm.

As this expression is seen to be identical to (4), it appears that the error e, and the inconsistency caused by mixed finite and infinite strain measures, can be eliminated by adopting the natural strain.

3. Effect on some key geotechnical parameters

As described in the preceding sections, precipitate analysis of triaxial tests can lead to erroneous results. The following reveals an investigation of how the strain measures affect the description of the behaviour of geomaterials, firstly by performing a simple analysis of a conventional triaxial compression test and secondly by calibrating a constitutive model which may be applied in more complex boundary value problems.

3.1. Analysis of a conventional triaxial compression test

The analysis of the conventional triaxial compression test is performed in two parts, firstly following an analysis based on the exact displacement field and secondly by the three methods (T, N and E). The conventional triaxial compression test is performed on Eastern Scheldt Sand deposit with a relative density of 72.5%. The

initial sample size was measured to $H_0 = 71.5$ mm and $D_0 = 69.5$ mm. More details concerning the sand and test procedures are found in Jakobsen and Praastrup [12]. The specimen was isotropically consolidated to an isotropic state of stress of 160 kPa and subsequently sheared at a constant confining pressure.

Fig. 4 shows the deviator stress $q = \sigma_1 - \sigma_3$ versus the directly measured axial displacement u_1.

The graph shows a typical stress–displacement curve for a medium dense sand, performed under the above-mentioned stress levels. The initial slope of the stress–displacement curve is steep and flattens out as the specimen hardens until failure and progresses into softening hereafter. The cross-sectional area of the specimen determines, indirectly, the axial stress applied onto the specimen during shear.

As the calculation of the cross-sectional area in each of the three methods is identical, the axial stress remains unaffected by the applied methods. The radial stress in triaxial tests is measured directly and is, therefore, unaffected by the methods. Geotechnical parameters that solely depend on stresses are hence unaffected by the three methods. Therefore, the two strain measures do not affect the geotechnical parameters that are determined solely on the basis of the stresses. The friction angle φ' is an important geotechnical parameter that is solely based on stresses. This parameter is unaffected by the strain measure. The secant friction angle for the test shown in Fig. 4 is $\varphi' = 40.3°$.

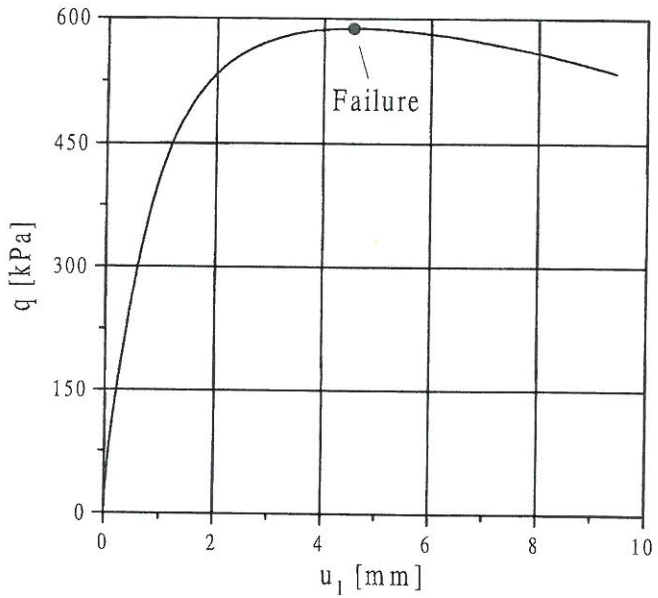

Fig. 4. Deviator stress versus axial displacement.

Geotechnical parameters that are based solely on strains, or both stresses and strains, will, however, be affected by the method and the strain measure used. Fig. 5 shows the measured volume change versus the measured axial displacement.

The figure shows that the specimen initially compresses and subsequently dilates. The effect on a particular strain-dependent parameter depends on how the parameter is determined and in particular on the strain level. Parameters determined at low strain levels are less affected by the chosen method than parameters determined at high strain levels. The initial tangent modulus of a stress–strain curve is for practical purposes unaffected as the parameter is determined in the beginning of the shearing process [7]. Geotechnical parameters such as the angle of dilation and strain to failure are affected more significantly. Parameters determined by strain increments will, however, be less affected than parameters determined by total strains.

In Section 2.1 it was mentioned that the volumetric behaviour is greatly influenced by the choice of strain measure. This effect is illustrated in Fig. 6, where the volumetric behaviour of the specimen is presented in terms of strains and plotted versus both the axial engineering and natural strains. The three curves representing each of the three methods diverge significantly as the axial strain increases. At failure the relative difference is as high as 18%. This difference affects the angle of dilation, which is an important parameter in the description of the volumetric behaviour of

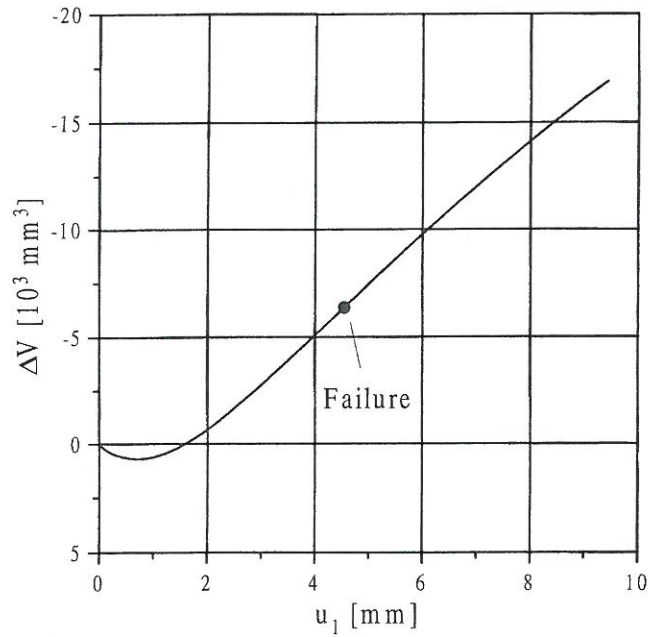

Fig. 5. Volume change versus axial displacement.

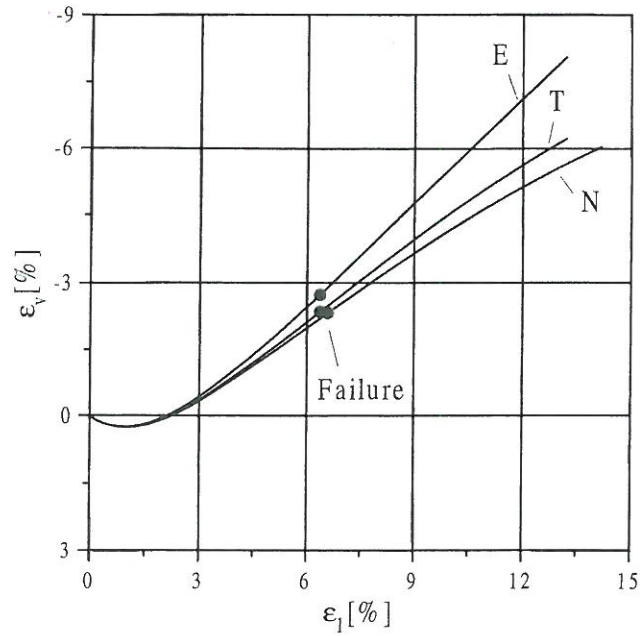

Fig. 6. Volumetric strain versus axial engineering and natural strain.

soils. The value of the angle of dilation is calculated to 12.7, 13.6 and 18.1° based on the methods N, T and E, respectively.

3.2. The single hardening model

In this section it is demonstrated how the three methods affect a particular constitutive relation, which is found important for the description of soil behaviour. The single hardening model is adopted for this purpose [8–11]. The single hardening model is an advanced constitutive model for frictional materials such as soils, concrete and rock. The single hardening model is an elasto-plastic constitutive model. The model consists, as do many other elasto-plastic models, of a failure criterion, a yield criterion, a plastic potential, a hypoelastic model and a hardening relation. The failure criterion determines the maximum load that a soil element can withstand. The yield criterion controls whether plastic deformations occur. The plastic potential controls the direction of the plastic strain increments and the elastic model determines the elastic behaviour of the material.

The single hardening model follows a non-associated flow rule because the yield criterion and the plastic potential are described by different functions. The model can in addition handle stress–strain behaviour in the softening regime, but cannot in

the form used herein handle large stress reversals. The model is, furthermore, restricted to model the stress–strain behaviour of isotropic materials. The single hardening model has as many as 12 material parameters, but they are all easily determined. For simplicity, it has been decided not to show any of the expressions involved in the model and just refer to the relevant articles and use an identical parameter representation.

The parameters listed in Table 1 are calibrated on the basis of the six conventional triaxial compression tests performed on the sand mentioned in the previous section and deposited with the same relative density. The specimens were sheared under constant confining pressures ranging from 80 to 800 kPa [12].

Material parameters fitted solely on the basis of stresses are independent of the three methods as explained above. Poisson's ratio ν is set to a constant value of 0.2 due to significant scatter in the test results [11]. The variation among the parameters associated with the elastic behaviour of the material is small. The parameters for T and E are identical. A minor change in the elastic parameters can barely be observed on a monotonic stress–strain curve as the elastic contribution is small compared to the plastic contribution for a normally consolidated sand as none of the specimens has been presheared. Minor changes among the parameters included in the plastic potential and the yield function have a more pronounced effect on the overall stress–strain behaviour. The effect is illustrated by a prediction of the test described in the previous section. The prediction has been limited to show the relationship between volume change and the axial displacement as the effect of the three methods is most pronounced for the volume change. However, it should be mentioned that the three

Table 1
Material parameters

Parameter	Method T	Method E	Method N
Elastic behaviour			
ν	0.20	0.20	0.20
M	477.65	477.65	458.45
λ	0.4142	0.4142	0.4081
Failure criterion			
a^a	0.00	0.00	0.00
m^a	0.2879	0.2879	0.2879
$\eta_1{}^a$	70.19	70.19	70.19
Plastic potential			
$\psi_1{}^a$	0.00754	0.00754	0.00754
ψ_2	−3.1375	−3.1118	−3.1540
μ	1.9862	1.7814	2.0611
Yield function			
$10^{-4}C$	1.3101	1.3101	1.2748
p	1.6188	1.6188	1.6078
h	0.6416	0.6476	0.6166
α	0.5613	0.5726	0.5525

[a] Strain-independent parameters.

predicted deviator–displacement curves all capture the deviator–displacement curve shown in Fig. 4 quite accurately. Fig. 7 shows that the choice of the strain calculation method has considerable impact on the prediction relationship between the volume change and the axial displacement. It is, moreover, observed that none of the predictions captures the compressive portion of the measured soil response. This may be a shortcoming of the single hardening model itself and has nothing to do with the three methods.

Fig. 7 shows further that the difference between the three methods at small levels of axial displacement is insignificant. It is also observed that method E fails in predicting the soil response at moderate to high displacements levels. This is a consequence of limitations associated with this method.

Methods N and T capture the soil response equally well. As method N is theoretically consistent and method T is theoretically inconsistent, the correct choice is to use method N in the analysis of triaxial tests.

A comparison of the graphs in Figs. 6 and 7 reveals that the single hardening model is very robust and that it can be used independently of the two strain measures. So the variation among the parameters in Table 1 reflects the difference between the three methods, thus allowing the model to capture the soil response using different strain measures.

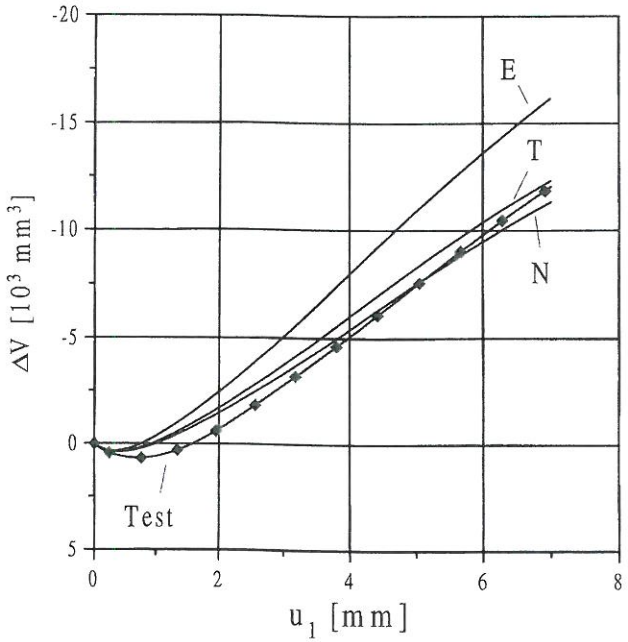

Fig. 7. Predicted and measured volume change versus axial displacement.

4. Conclusion

Within the scope of this work, which concerns the choice of strain measures in geomechanics, the conclusion that can be drawn from the results presented in this paper is that the chosen strain measure has a considerable effect on the volumetric strain. The effect on the volumetric strain affects strain-dependent geotechnical parameters, while parameters solely determined on the basic of stresses are unaffected. The traditional analysis of triaxial tests, denoted method T, has been found to be theoretically inconsistent as an infinitesimal strain measure is mixed with a finite strain measure. Therefore, two theoretically consistent methods, denoted N and E, were proposed and examined. Method N is based on the natural strain measure, whereas method E is based on the engineering strain measure. Method E has been found to produce erroneous results within the normal range of deformations in triaxial tests. Therefore, the authors suggest that method N is used in the analysis of triaxial tests. Method E could, however, apply in situations where deformations are reasonably small and where the material with reasonable justification could be modelled as a purely elastic material. The recommended procedure for analysing triaxial tests is outlined below:

- Establish the exact displacement field using both measured volume change and axial displacement.
- Establish all Cauchy stress components using the current cross-sectional area.
- Establish all strain components using the natural strain measure, i.e. method N.
- Finally display the results using the same diagrams as used in method T.

It has been shown that the traditional method of analysing triaxial tests has severe shortcomings and may result in erroneous calculations of soil parameters that depend on strains, whereas employment of natural strains results in correct calculation of strain-dependent soil parameters.

References

[1] Malvern LE. Introduction to the mechanics of a continuous medium. New Jersey: Prentice Hall, 1969.
[2] Crisfield MA. Non-linear finite element analysis of solids and structures, vol. 1: essentials. Chichester: Wiley, 1991.
[3] ABAQUS — standard user's manual, ver. 5.5. Hibbit, Karlson & Sorensen, Inc., Providence, 1995.
[4] ABAQUS — theory manual, ver. 5.5. Hibbit, Karlson and Sorensen, Inc., Providence, 1995.
[5] Spencer AJM. Continuum mechanics. UK: Longman Mathematical Texts, 1980.
[6] Kirkpatrick WM, Belshaw DJ. On the interpretation of the triaxial test. Geotechnique 1968;18:336–50.
[7] Janbu N. Soil compressibility as determined by oedometer and triaxial tests. Proceedings of the European conference on soil mechanics and foundation engineering, vol. 1, Wiesbaden, 1963. p. 19–25.
[8] Kim MK, Lade PV. Single hardening constitutive model for frictional materials, I: plastic potential function. Computers and Geotechnics 1988;5:307–24.
[9] Lade PV, Kim MK. Single hardening constitutive model for frictional materials, II: yield criterion and plastic work contours. Computers and Geotechnics 1988;6:13–29.

[10] Lade PV, Kim MK. Single hardening constitutive model for frictional materials, III: comparison with experimental data. Computers and Geotechnics 1988;6:31–47.
[11] Lade PV, Nelson RB. Modelling the elastic behaviour of granular materials. International Journal for Numerical and Analytical Methods in Geomechanics 1987;11:521–42.
[12] Jakobsen KP, Praastrup U. Drained triaxial tests on Eastern Scheldt Sand. AAU Geotechnical Engineering Papers, AGEP R9822, Aalborg, 1998.

Title:
The influence of stress path on the characteristic stress state.

Authors:
Jakobsen, K.P., U. Praastrup & L.B. Ibsen.

Year of publication:
1999

Published in:
Procedings of the Second International Symposium on Pre-Failure Deformation Characteristics of Geomaterials, Balkema, Rotterdam, pp. 659-666.

The influence of the stress path on the characteristic stress state

K.P. Jakobsen
Aalborg University, Aalborg, Denmark

U. Praastrup
Aalborg University, Aalborg, Denmark

L.B. Ibsen
Aalborg University, Aalborg, Denmark

ABSTRACT: Volume change is the core phenomenon in understanding the behaviour of frictional materials, such as sands. In conventional drained triaxial compression tests the transition from contraction to dilatation occurs along a well-defined line in triaxial stress space, the characteristic line. However, little information exists about the effect of stress path on the characteristic line. A test program has been carried out to scrutinise this effect. The tests were designed to emanate from the hydrostatic axis and pass through a characteristic stress state obtained from a conventional triaxial test. In case of stress path independency all tests should start to dilate at the same state of stress. The results show an indubitable dependency of the stress path and that the characteristic friction angle is constant for a given type of stress path. It is further examined how these findings comply with the theory of plasticity.

1 INTRODUCTION

The core to understanding the stress-strain behaviour of frictional materials, such as sands, lies in understanding the effect of volume change and in particular the various factors that influences the volume change. Experimental observations show that factors influencing the volume change are relative density, stress level, stress path, drainage conditions and properties of the test material.

Element tests, such as triaxial tests, are performed in order to provide the understanding of the stress-strain behaviour of frictional materials and to support the development of constitutive models. Only tests performed under drained conditions are considered in this paper, but the findings may apply to undrained tests as well.

Volume changes can be either compressive or expansive in nature. The analysis of several triaxial tests reveals that expansive or dilative volume changes are most pronounced for dense specimens sheared at low confining pressures. Conventional triaxial compression tests performed on dense specimens at low pressures demonstrate that the specimens initially contract and subsequently dilate. This state where the transition from contraction to dilation occurs is entitled the characteristic state (Luong 1982).

This paper focuses on the characteristic state and in particular the stress equivalent entitled the characteristic stress state. In the view of developing more accurate constitutive models it is important to consider how the characteristic state is captured. It is important because this state significantly influences the progress of the volumetric strain. A constitutive model that is not able to capture this state cannot predict the stress-strain behaviour of frictional materials correctly.

One of the components in an elasto-plastic constitutive model is the plastic potential surface, which is closely related to the characteristic stress state. The state of stress on the plastic potential surface farthest off the hydrostatic axis controls the plastic transition from contraction to dilation. This corresponds to the characteristic stress state except for an elastic contribution.

Due to this relation, it is important to be familiar with the factors that influence the location of the characteristic stress state. The factor or issue investigated here is whether the stress path in triaxial tests has any effect on the location of the characteristic stress state. The effect of stress path on the state is studied experimentally by carrying out two series of triaxial tests.

2 BASIC IDEA

The basic idea behind this paper is to investigate whether the characteristic stress state is stress path independent as claimed by Luong (1982). The first series of tests is especially designed to verify or

invalidate this statement. A state of stress is expressed in terms of the mean normal effective stress p' and the deviator stress q:

$$p' = \sigma'_1 + 2\sigma'_3; \quad q = \sigma_1 - \sigma_3 \tag{1}$$

The total axial and radial stresses are given by σ_1 and σ_3, respectively. Primes denote effective stresses.

The characteristic state is in this paper defined as the point on a volume curve where the volumetric strain increment, $d\varepsilon_v$, is zero (Luong 1982). The characteristic stress state is defined by the state of stress at the characteristic state.

According to Luong (1982) the trace of characteristic stress states, determined from several triaxial tests, defines a line in the $p' - q$ plane, the characteristic line. This line divides the stress space into two regions with different deformation mechanisms. Stress combinations below the characteristic line lead to contraction, whereas stress combinations between the characteristic line and the failure envelope lead to dilation. A possible interpretation of these findings is to assume that the characteristic state corresponds to a quasi frictional component of the strength as stated by Kirkpatrick (1961). Hence, the definition of the characteristic friction angle, φ'_{cl}, becomes:

$$\sin\varphi'_{cl} = (\sigma'_1 - \sigma'_3)/(\sigma'_1 + \sigma'_3) \tag{2}$$

Results from conventional triaxial compression tests, where the confining pressure is held constant during shear, show that the characteristic angle is independent of confining pressure, effective mean stress and void ratio when performed on specimens with height equal to diameter and with lubricated end plates (Ibsen & Lade 1998). This means that the trace of the characteristic stress states is indeed a line when tests are performed under such conditions. However, the trace of the characteristic stress states may be non-linear when other stress paths are followed. This could potentially blur the test results and it is, therefore, necessary to design a test program where non-linearities are hindered. Thus, the variation in mean effective stress should be diminished when investigating for stress path dependencies. A test program complying herewith has been set-up and is outlined for a single stress point in Figure 1.

The figure shows five distinct stress paths passing through a fixed state of stress. The fixed state of stress corresponds to the characteristic stress state obtained from a conventional triaxial compression test (CTC-test). This test is carried out and analysed prior to performing the tests with other stress paths. The remaining tests are planned in such a way that the stress "quantities" indicated on the figure can be held constant during shear. In all the tests the deviatoric stress ratio, q/p', increases and compression tests are solely considered.

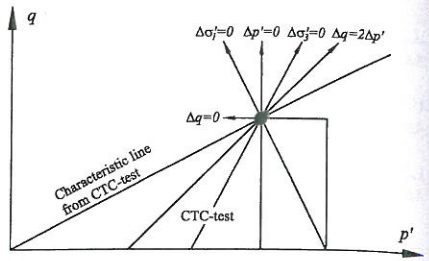

Figure 1. Outline of test program for examination of stress path dependencies of the characteristic stress state.

The idea behind the test program is as follows. If the characteristic stress state is truly independent of the stress path all of the tests should attain their characteristic stress state at the same state of stress, i.e. the characteristic stress state determined from the conventional triaxial compression test. If the stress state on the other hand is stress path dependent it cannot be viewed as intrinsic as stated by Luong (1982).

The second series of tests are performed for investigation of non-linearities of the trace of the characteristic stress states. These tests are performed with various monotonous stress paths covering a wide range of stress levels.

3 SOIL TESTED AND TEST PROCEDURES

All tests are performed on reconstituted specimens of Eastern Scheldt Sand, which is a well-sorted line shore quartz sand composed of subrounded to rounded grains. The classification properties of the sand are summarised in Table 1.

Table 1. Classification properties for Eastern Scheldt Sand.

Property	Value
Specific gravity, G_s	2.65
Maximum void ratio, e_{max}	0.886
Minimum void ratio, e_{min}	0.591
Maximum grain size, d_{100}	0.500 mm
Mean grain size, d_{50}	0.166 mm
Fines content	1.3 %
Uniformity coefficient	1.52
Curvature coefficient	0.99

The tests are performed in a renewed version of the Danish triaxial apparatus. The working principles of the apparatus were developed in the late sixties by Jacobsen (1970). The newly developed version uses similar working principles, but the data acquisition has been completely modified and enhanced together with automatic load control. Measurements of axial load, cell pressure, pore pressure, volume change and axial displacement are automatically and electronically collected and transmitted to a computer for storage and processing. Any stress path within the failure envelope can be followed automatically and very precisely.

3.1 Specimen preparation and testing procedure

In order to facilitate the present study a combination of relative density and stress level that enhances the size of the contraction zone and still features dilation is chosen. For that reason the tests are performed on medium dense specimens sheared at moderate confining pressures.

The specimens are prepared in a cylindrical split mould by air pluviation with an initial void ratio of 0.672, tolerating a deviation of ± 0.001.

Since all measurements merely represent average quantities, it must be required that the stress and strain state inside the specimen are homogeneous throughout the test. This requirement is met by using lubricated end plates and preparing the specimen with a height and diameter of approximately 70 mm (see for example Ibsen 1993).

In the triaxial apparatus the specimen is saturated using a combination of the vacuum and water percolation method (Jakobsen & Praastrup 1998). Subsequently the specimens are isotropically consolidated at a maximum loading rate of 5 kPa per minute and afterwards sheared at a constant axial strain rate of 3.0% per hour. The specimens are all sheared into the softening regime and terminated at an axial strain of approximately 10%.

3.2 Analysis of triaxial tests

The results are presented in terms of Cauchy or true stresses and non-linear logarithmic strains. This approach leads to a consistent set of formulas as it is based on an exact representation of the displacement field and uses a finite strain measure for both axial and volumetric strains. It also has the advantage that the stress and strain measures are work conjugated (Praastrup et al. 1998).

4 STRESS PATH DEPENDENCY

A series of tests are performed in accordance with the principles outlined in Section 2 in order to investigate the stress path dependency of the characteristic stress state. The test program shown in Figure 1 is carried out at two different stress levels. Consequently, two conventional triaxial compression tests are initially performed as their characteristic stress states determine the initial isotropic stress state for the remaining tests. The results of the two conventional tests are listed in Table 2.

Table 2. Characteristic stress states for conventional triaxial compression tests.

Test no.	σ'_3 [kPa]	p'_{cl} [kPa]	q_{cl} [kPa]	φ'_{cl} [°]
971005	320.0	539.7	659.3	30.5
971006	160.0	272.9	338.6	30.9

There is according to Figure 1 only one type of the tests that follows a non-monotonous stress path. In this test the mean effective stress and subsequently the deviator stress is held constant. The soil can according to the elasto-plastic theory exhibit either elastic or elasto-plastic behaviour. The non-monetonous test and in the test where the axial effective stress is held constant the specimens are sheared into the elastic region. These two tests make it possible to examine some elastic effects on the characteristic stress state (see Section 4.2). In the other three types of tests the specimens are plastically sheared throughout the test.

The test results are shown in Figure 2. The different stress paths are shown in $p' - q$ diagrams whereas the measured strains are shown in combined $\varepsilon_1 - q - \varepsilon_v$ diagrams. The characteristic stress states and failure states are marked by open and closed circles, respectively.

4.1 Evaluation of characteristic stress states

The stress-strain curves in Figure 2 reveal that the characteristic stress state can only be determined in the tests with increasing and constant mean effective stress (4, 5, 6, 15, 22 and 23). The figure also reveals that the location of the characteristic stress state differs significantly. The characteristic angles for the specimens sheared under constant mean effective stress (tests 4 and 15) are lower than the angles observed in the two conventional tests. The deviation in the angle between test 5 and 15 is 15.1%, whereas the deviation between test 4 and 6 is 13.6%. The characteristic angles for specimens sheared with a slope of 2 in the $p' - q$ plane are higher that the angles observed in the two conventional tests. The deviations are found to 4.9% and 5.8%. The deviations between the highest and the lowest angle is as high as 26.3%. The magnitude of these deviations leads to the conclusion that the characteristic stress state is indeed dependent on the stress path. On the other hand, it is observed that the characteristic

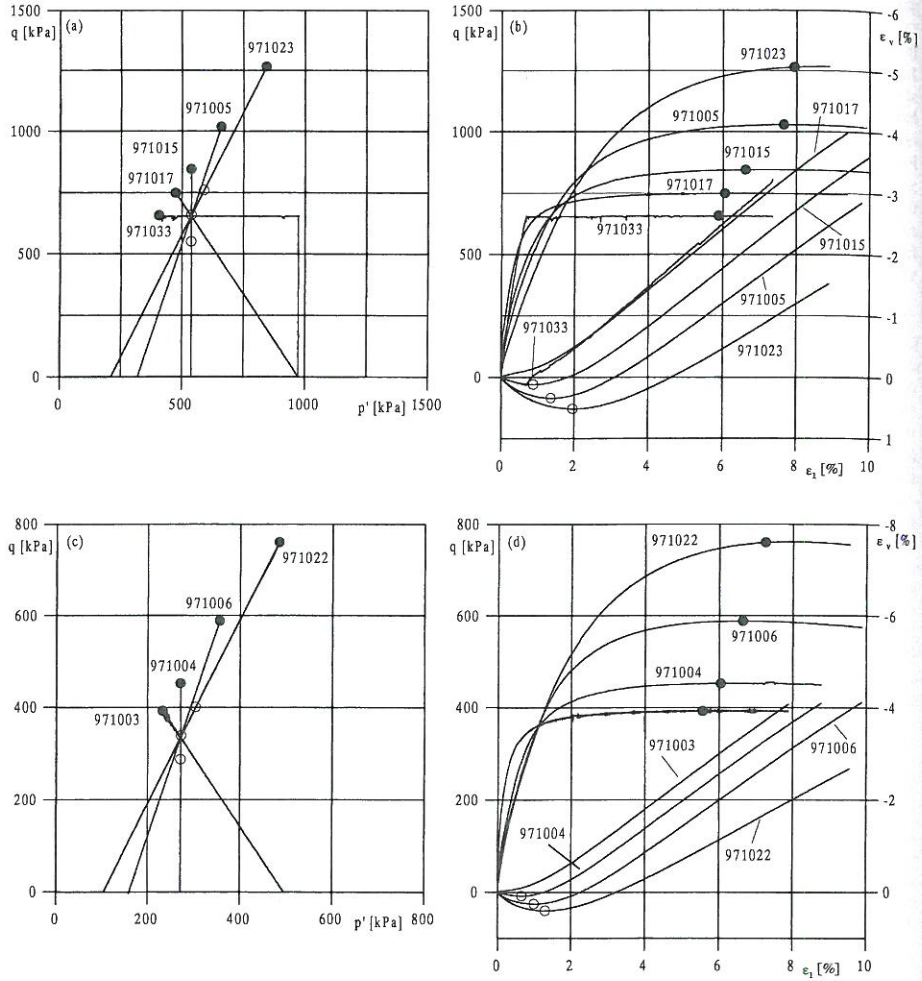

Figure 2. Test results from nine triaxial tests. The tests are grouped according to the characteristic stress states determined from the two conventional triaxial tests (971006 and 971005). (a) and (c) Stress paths in $p' - q$ diagrams, (b) and (d) $\varepsilon_1 - q - \varepsilon_v$ curves.

angles for specimens sheared with the same slope in the $p' - q$ plane are very similar. Between such tests the highest deviation is 3.1% which is an order of magnitude lower than the other deviations and may be ascribed to the scatter in the tests results.

Another interesting observation is that the characteristic angle seemingly decreases as the slope of the stress path, dq/dp', increases. Thus, the lowest characteristic angle (25.9°) is observed for test 15, which is performed with constant mean effective stress. The highest angle (32.7°) is observed for test 22, where the slope of the stress path is two. This is supported by the observations made by Ibsen & Lade (1998). The key results for the tests are summarised in Tables 2 and 3.

Table 3. Results of triaxial tests.

Test no.	σ'_3 [kPa]	p'_{cl} [kPa]	q_{cl} [kPa]	φ'_{cl} [°]
971004	176.0	271.7	287.1	26.7
971015	354.8	538.3	550.5	25.9
971022	170.6	304.0	400.1	32.7
971023	337.1	590.1	759.1	32.0

Surprisingly, it is impossible to determine the characteristic stress states for the tests with constant axial effective stress and constant deviator stress (3, 17 and 33). The specimens sheared at constant axial effective stress tests do not contract at all, whereas both contraction and dilation occur in the test with constant deviator stress (Figure 2b). However, the transition from contraction to dilation is caused entirely by the sudden change of stress path. Such a transition is not in accordance with the definition of the characteristic state.

4.2 Numerical analysis of tests 17 and 33

The stress-strain behaviour of soils can be modelled by use of elasto-plastic constitutive models. In order to investigate the behaviour in tests 17 and 33 the single hardening model has been employed. The single hardening model is an advanced elasto-plastic constitutive model for frictional material such as soils, concrete and rock (Kim & Lade 1988; Lade & Kim 1988a,b Lade & Nelson 1987). A hypoelastic model describes the elastic behaviour, whereas the framework for plastic behaviour consists of a failure criterion, a yield criterion and a non-associated flow rule.

The failure criterion bounds a domain of possible stress states and simply determines the maximum load that a soil element can withstand. As the plastic deformations, within the domain of possible stress states, follow a non-associated flow rule the yield criterion and the plastic potential surface are described by different functions. The yield criterion controls whether plastic deformations occur. The plastic potential surface controls the direction of the plastic strain increments. At the top point of the plastic potential surface, in the $p' - q$ plane, the plastic strain increment vector is perpendicular to the hydrostatic axis corresponding to a zero increment in plastic volumetric strain (Wood 1994). The plastic strain increment vector will, depending on the current state of stress, point in the inward or outward direction of the hydrostatic axis, indicating plastic dilation or contraction, respectively.

Consequently, the characteristic state and the top point of the plastic potential surface are closely related. The relation between the two is due to the fact that the plastic volumetric strain increment is zero on the top of the plastic potential surface, whereas the characteristic state occurs where the "total" volumetric strain increment is zero. The trace of the top point of the plastic potential surface in the $p' - q$ plane should, therefore, except for an elastic contribution, reflect the trace of the characteristic stress states.

The single hardening model has been employed to draw the curves in Figures 3 and 4. The figures show two sets of yield and plastic potential surfaces labelled "Y" and "P", respectively. Y_A-curves correspond to the yield surfaces prior to elastic shearing and the P_A-curves to the plastic potential surfaces which are activated when the soil starts to yield again. Y_B and P_B refer to the yield and plastic potential surfaces that passes through the characteristic stress state found in the conventional triaxial tests (5 and 6). The characteristic states for these tests are marked with open circles, whereas the failure points for the investigated tests are marked with closed circles.

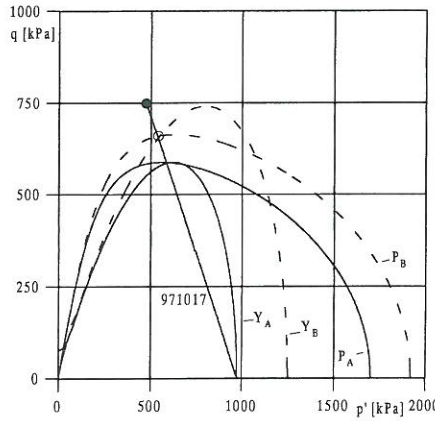

Figure 3. Yield and plastic potential surfaces. Test 971017.

A comparison of Figures 2b and 3 reveals that the yield criterion of the single hardening model captures the first yield point very well. Both figures show that the soil behaves purely elastic until a deviator stress of approximately 580 kPa. Subsequently, the soil starts and continues to yield throughout the test. The most interesting portion of the stress path is between the point of first yield and the characteristic stress state observed for the conventional triaxial test. The shape of the two plastic potential surfaces indicates that the top of the plastic potential surface is passed somewhere between P_A and P_B along the stress path shown in the figure.

This is a fact even though a characteristic state is not observed at all. As the mean effective stress decreases during shear the elastic volumetric strains become negative and therefore expansive. The contours of P_A and P_B illustrate that the plastic volumetric strain merely enhances the elastic expansion (Figure 3) as the plastic deformations are not activated prior to the point of first yield. Moreover, it is seen that the portion where plastic contraction occurs is small and too small to establish a characteristic state.

The findings can be summarised as follows: A characteristic state is not observed as the elastic expansion outplays the small portion of plastic contraction, which occurs right after the first yield point.

It would appear that a definition of the characteristic state on the basis of the plastic volumetric strain increment instead of the total strain increment could result in a stress path independent definition of the characteristic stress state. However, such a definition requires knowledge of the elastic properties as the elastic strains produced during shear should be subtracted.

If the soil behaves isotropically and a hypoelastic model is found to be suitable, tests can with advantage be performed with constant mean effective stress. Under these circumstances no elastic volumetric strain will be produced (Ibsen & Lade 1998, Wood 1994).

The yield and plastic potential surfaces (Figure 4) show that the above findings also apply to test 33 except that plastic contraction cannot be detected at all as the top point of the plastic potential surface is passed prior to the point of first yield.

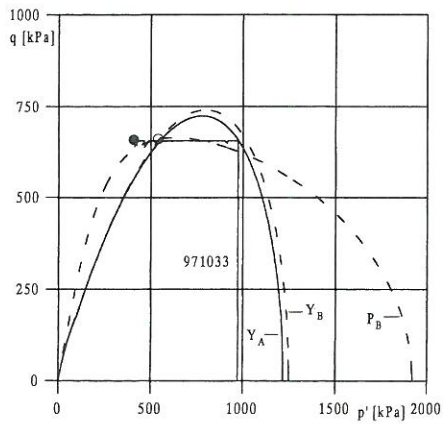

Figure 4. Yield and plastic potential surfaces (Plastic potential surface P_A is not included as it is almost identical to P_B). Test 971033.

The absence of characteristic states in the tests performed with decreasing mean effective stress is ascribed to the followed stress paths, stress level and specimen properties. These parameters will essentially prescribe the location and succeeding development of yield and plastic potential surfaces and hereby also the development of plastic volumetric strains.

The characteristic state will occur for other stress paths with decreasing mean effective stress. Thus, as the slope of the stress path decreases and approaches the stress path for a test performed with constant mean effective stress, the plastic contractive volumetric strain increases and a characteristic state could be observed.

4.3 Perspectives

Several conclusions can be drawn from the evaluation of the above mentioned tests. The characteristic state, angle and line as defined by Loung (1982) are stress path dependent. The characteristic angle decreases as the slope of the stress path increases. The stress state does not even exist for some of the stress paths examined in this paper. It was moreover observed that the deviation on the characteristic angle is small when tests are performed at different stress levels but with the same slope. Consequently, the trace of the characteristic stress states for tests performed at different pressure levels, but following stress paths with identical slopes may turn out to be linear.

5 STRESS LEVEL DEPENDENCY

As observed in the previous section there is a significant difference between the characteristic stress states obtained from tests performed using different stress paths. Tests performed at different initial stress levels, but with the same slope in the $p' - q$ plane showed little deviations among the characteristic stress states. Therefore, it could be argued that the deviations are due to scatter in the test results and not an indication of stress level dependency. This issue is investigated by performing an additional series of tests. The tests are performed with constant confining pressure, constant mean effective stress and with a slope of the stress path in the $p' - q$ plane equal to two.

The test results are summarised in Figure 5 where the different stress paths are shown in $p' - q$ diagrams whereas the measured strains are shown in a combined $\varepsilon_1 - q - \varepsilon_v$ diagram. The characteristic stress states and failure states are marked by open and closed circles, respectively.

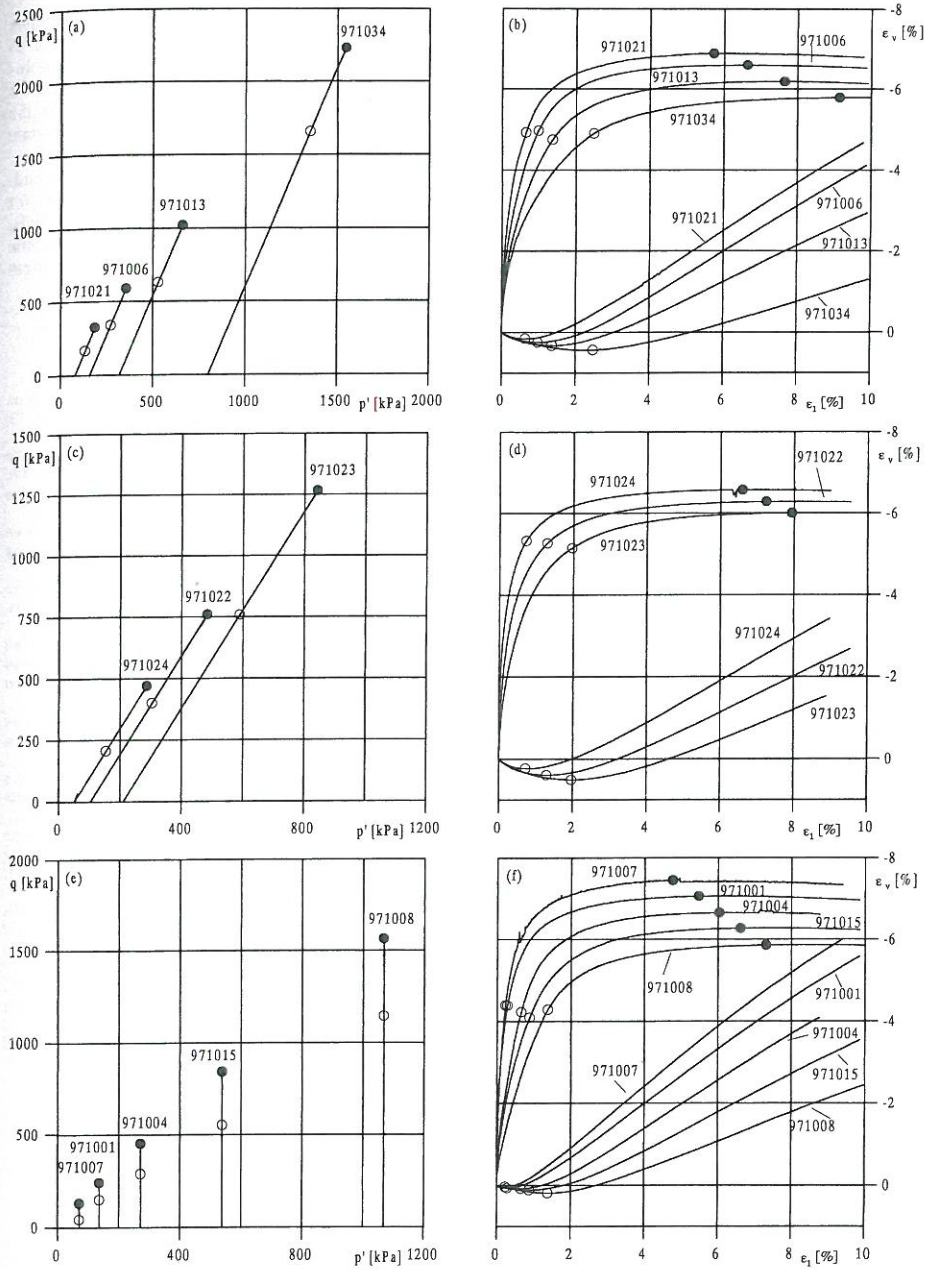

Figure 5. Test results from twelve triaxial tests. (a), (c) and (e) Stress Paths in $p' - q$ diagram, (b), (d) and (f) $\varepsilon_1 - q - \varepsilon_v$ curves.

5.1 Evaluation of tests results

The results appear to be very reliable and exhibit the anticipated development in the stress-strain curves as the stress level increases. The effective friction angles corresponding to the measured characteristic stress state and failure states are shown in Figure 6.

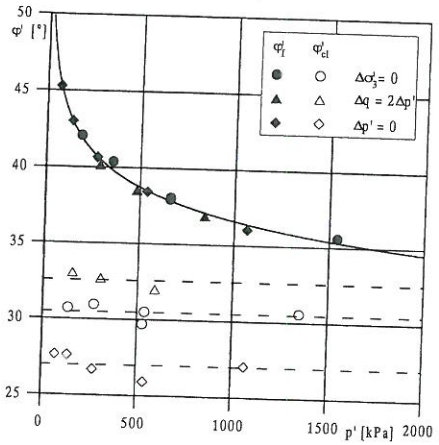

Figure 6. Friction angles at characteristic stress states and failure for various stress paths.

The figure shows the expected effect of stress path as the characteristic angle increases with decreasing slope of the stress path and this confirm the conclusions drawn from the initial tests. The results also indicate that the characteristic angles, and hence the characteristic stress states, are independent of the stress level. It is observed that the determination of the characteristic angles is ambiguous as the volume change curves are relatively flat near the characteristic state, while the stresses vary considerably.

6 CONCLUSION

The characteristic stress state has been studied by means of drained triaxial compression tests. It has been shown that the characteristic line, originally defined by Luong (1982), is not an intrinsic parameter to describe the volumetric behaviour of soils. Thus, results from tests with different stress paths show a significant and consistent variation in the characteristic angles. Thus, the angle decreases as the slope of the stress path increases. In some tests it has, however, been impossible to detect a characteristic state. These findings make the characteristic line concept in its present form incompatible with development of constitutive soil models as correct prediction of the volumetric behaviour becomes doubtful. In consequence it has been proposed to define the characteristic state from the plastic volumetric strain increment. This would give a basis for consistent elasto-plastic constitutive models as the plastic potential surface and the characteristic state thus are mutually connected.

Besides the investigation of stress path dependency additional tests have been performed for evaluation of the dependency of stress level. The results of these tests indicate that the characteristic friction angle is constant for a given type of stress path.

7 REFERENCES

Ibsen, L.B. 1993. The stable state in cyclic triaxial testing on sand. *Soil Dynamics and Earthquake Engineering*, 13, 63-72.

Ibsen, L.B. & Lade, P.V. 1998. The role of the characteristic line in static soil behaviour. *Proceedings of the 4th. International Workshop on Localization and Bifurcation Theory for Soil and Rocks.* Gifu, Japan

Jakobsen, K.P. & Praastrup, U. 1998. Drained triaxial tests on Eastern Scheldt Sand, *AAU Geotechnical Engineering Papers*, ISSN 1398-6465 R9821.

Kim, M.K. & Lade, P.V. 1988. Single hardening constitutive model for frictional materials, I: Plastic potential function. *Computers and Geotechnics*, 5:4, 307-324.

Kirkpatrick, V.M. 1961. Discussion on soil properties and their measurement. *Proceedings of the 5th. International Conference on Soil Mechanics and Foundation Engineering*, Vol. III, 131-133, Paris.

Lade, P.V. & Kim, M.K. 1988a. Single hardening constitutive model for frictional materials, II: Yield criterion and plastic work contours. *Computers and Geotechnics*, 6:1, 13-29.

Lade, P.V. & Kim, M.K. 1988b. Single hardening constitutive model for frictional materials, III: Comparison with experimental data. *Computers and Geotechnics*, 6:1, 30-47.

Lade, P.V. & Nelson, R.B. 1987. Modelling the elastic behaviour of granular materials. *International journal for numerical and analytical methods in geomechanics*, 11, 521-542.

Loung, M.P. 1982. Stress-strain aspects of cohesiveless soils under cyclic and transient loading. *International Symposium on Soils under Cyclic and Transient Loading*, 315-324, Swansea.

Praastrup, U., Jakobsen, K.P. & Ibsen, L.B. 1998. On the choice of strain measures in geomechanics. *12th. Young Geotechnical Engineers Conference.* Tallinn, Estonia.

Wood, D.M. 1994. *Soil behaviour and critical state soil mechanics.* Cambridge University Press.

Title:
Incrementalization of a single hardening constitutive model for frictional materials.

Authors:
Lade, P.V & K.P. Jakobsen.

Year of publication:
2002

Published in:
International Journal for Numerical and Analytical Methods in Geomechanics 26, 647-659.

INTERNATIONAL JOURNAL FOR NUMERICAL AND ANALYTICAL METHODS IN GEOMECHANICS
Int. J. Numer. Anal. Meth. Geomech., 2002; **26**:647–659 (DOI: 10.1002/nag.216)

Incrementalization of a single hardening constitutive model for frictional materials

P. V. Lade[1,*,†] and K. P. Jakobsen[2]

[1] *Department of Civil Engineering, Aalborg University, Sohngaardsholmsvej 57, 9000 Aalborg, Denmark*
[2] *DHI—Water and Environment, Agern Allé 11, 2970 Hørsholm, Denmark*

SUMMARY

The governing equations for an elasto-plastic constitutive model for frictional materials such as soil, rock, and concrete are presented, and the incremental form is indicated in preparation for implementation of the model in a user-defined module for finite element calculations. This isotropic, work-hardening and -softening model employs a single yield surface, it incorporates non-associated plastic flow, and its capability of capturing the behaviour of different types of frictional materials under various three-dimensional conditions has been demonstrated by comparison with measured behaviour, as presented in the literature. The incrementalization procedure is indicated and the resulting equations for the single hardening model are presented together with parameters for a dense sand. Following the implementation of the model, these parameters are used for evaluation of different integration schemes as presented in a companion paper by Jakobsen and Lade (*Int. J. Numer. Anal. Meth. Geomech.* 2002; **26**:661). Copyright © 2002 John Wiley & Sons, Ltd.

KEY WORDS: incrementalization procedure; elasto-plastic constitutive model; frictional materials; yield surface; non-associated flow

1. INTRODUCTION

An elasto-plastic hardening constitutive model with a single yield surface has been developed on the basis of a thorough review and evaluation of data from experiments on frictional materials such as sand, clay, concrete and rock [1–3]. The numerical implementation of this model into a finite element program, such as ABAQUS [4], through a user-defined material module, requires the elasto-plastic model on incremental form. The components of the constitutive model which involve non-associated plastic flow are reviewed, and the incremental form of the model is presented. This form of the model is then used in the numerical implementation presented and evaluated in a companion paper [5].

The model employs a single, isotropic yield surface shaped as an asymmetric tear-drop with the pointed apex at the origin of the principal stress space. This yield surface, expressed in terms of stress invariants, describes the locus at which the total plastic work is constant. The total

*Correspondance to: P. V. Lade, Department of Civil Engineering, Aalborg University, Sohngaardsholmsvej 57, 9000 Aalborg, Denmark
†E-mail: lade@civil.auc.dk

Received 22 April 2001
Revised 15 November 2001

plastic work (due to shear strains as well as volumetric strains) serves as the hardening parameter, and it is used to define the location and shape of the yield surfaces. The use of contours of constant plastic work (or any other measure of hardening) as yield surfaces results in mathematical consistency in the model, because the measure of yielding and the measure of hardening are uniquely related through one monotonic function. In addition, application of a single yield surface produces computational efficiency when used in large computer programs. The non-associated flow rule is derived from a potential function which describes a three-dimensional surface shaped as a cigar with an asymmetric cross-section.

The model is devised such that the transition from hardening to softening occurs abruptly at the peak failure point. Thus, the transition does not involve any points at which the hardening modulus is zero, but the rate of softening may be controlled and the pointed peak is hardly noticeable in actual comparisons with experimental data.

The main principles of the model and the governing equations for each component are reviewed below. The incremental form of the constitutive model is presented as detailed mathematical expressions required for numerical implementation in a finite element program. The model is then implemented in a user-defined module and employed in evaluation of the efficiency of several integration schemes.

2. SINGLE HARDENING STRESS–STRAIN MODEL

The total strain increments observed in a material when loaded are divided into elastic and plastic components such that

$$d\varepsilon = d\varepsilon^e + d\varepsilon^p \tag{1}$$

These strains are then calculated separately, the elastic strains by Hooke's law, and the plastic strains by a plastic stress–strain law. Both are expressed in terms of effective stresses.

Below, is a brief review of the framework and the components of the constitutive model. In order that the presentation follows a logic developmental sequence, the components are presented in the following order: Elastic behaviour, failure criterion, plastic potential and flow rule, yield criterion and work-hardening/softening law.

2.1. Elastic behaviour

The elastic strain increments, which are recoverable upon unloading, are calculated from Hooke's law, using a recently developed model for the non-linear variation of Young's modulus with stress state [6]. The value of Poisson's ratio, ν, being limited between zero and one-half for most materials, is assumed to be constant. The expression for Young's modulus was derived from theoretical considerations based on the principle of conservation of energy. According to this derivation, Young's modulus E can be expressed in terms of a power law involving non-dimensional material constants and stress functions as follows:

$$E = Mp_a\left[\left(\frac{I_1}{p_a}\right)^2 + 6\left(\frac{1+\nu}{1-2\nu}\right)\frac{J_2'}{p_a}\right]^{\lambda} \tag{2}$$

in which I_1 is the first invariant of the stress tensor, and J_2' is the second invariant of the deviatoric stress tensor, given as follows:

$$I_1 = \sigma_{11} + \sigma_{22} + \sigma_{33} \tag{3}$$

$$J_2' = \tfrac{1}{6}[(\sigma_{11}-\sigma_{22})^2 + (\sigma_{22}-\sigma_{33})^2 + (\sigma_{33}-\sigma_{11})^2] + \sigma_{12}^2 + \sigma_{23}^2 + \sigma_{31}^2 \tag{4}$$

The parameter p_a is the atmospheric pressure expressed in the same units as E, I_1 and $\sqrt{J_2'}$, and the modulus number M and the exponent λ are constant, dimensionless numbers. The three material parameter ν, M, and λ may be obtained from simple tests such as triaxial compression tests. The model can be used for materials with effective cohesion.

2.2. Failure criterion

A general, three-dimensional failure criterion has been developed for soils, concrete, and rock [7–11]. The criterion is expressed in terms of the first and third stress invariants of the stress tensor:

$$f_n = \left(\frac{I_1^3}{I_3} - 27\right)\left(\frac{I_1}{p_a}\right)^m \tag{5a}$$

$$f_n = \eta_1 \text{ at failure} \tag{5b}$$

in which I_1 is given in (3) and

$$I_3 = \sigma_{11}\sigma_{22}\sigma_{33} + \sigma_{12}\sigma_{23}\sigma_{31} + \sigma_{21}\sigma_{32}\sigma_{13} - (\sigma_{11}\sigma_{23}\sigma_{32} + \sigma_{22}\sigma_{31}\sigma_{13} + \sigma_{33}\sigma_{12}\sigma_{21}) \tag{6}$$

The parameters η_1 and m are constant dimensionless numbers.

Figure 1 shows that in principal stress space, the failure criterion is shaped like an asymmetric bullet with the pointed apex at the origin of the stress axes, and the cross-sectional shape in the octahedral plane is triangular with smoothly rounded edges in a fashion that conforms to experimental evidence.

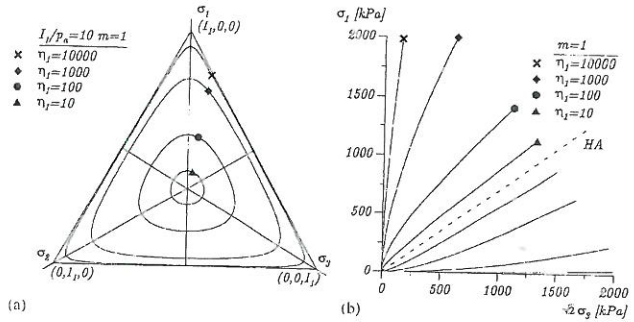

Figure 1. Characteristics of failure criterion in principal stress space: traces shown in (a) octahedral plane, and (b) triaxial plane.

In order to include the effective cohesion and the tension which can be sustained by concrete and rock, a translation of the principal stress space along the hydrostatic axis is performed [8–11]. Thus, a constant stress, ap_a, is added to the normal stresses before substitution in (5)

$$\sigma = \sigma + \delta a p_a \tag{7}$$

in which 'a' is a dimensionless parameter, and δ is Kronecker's delta. The value of ap_a reflects the effect of the tensile strength of the material. The three material parameters, η_1, m, and a, may be determined from results of simple tests such as triaxial compression tests.

2.3. *Plastic potential and flow rule*

The plastic strain increments are calculated from the flow rule

$$d\varepsilon^p = d\lambda_p \frac{\partial g_p}{\partial \sigma} \tag{8}$$

in which g_p is a plastic potential function and $d\lambda_p$ is a scalar factor of proportionality. A suitable plastic potential function for frictional materials was developed and presented by Kim and Lade [1]. This function is different from the yield function and non-associated flow is consequently obtained. The plastic potential function is written in terms of the three invariants of the stress tensor:

$$g_p = \left(\psi_1 \frac{I_1^3}{I_3} - \frac{I_1^2}{I_2} + \psi_2\right)\left(\frac{I_1}{p_a}\right)^{\mu} \tag{9}$$

in which I_1 and I_3 are given in (3) and (6) and the second stress invariant is defined as

$$I_2 = \sigma_{12}\sigma_{21} + \sigma_{23}\sigma_{32} + \sigma_{31}\sigma_{13} - (\sigma_{11}\sigma_{22} + \sigma_{22}\sigma_{33} + \sigma_{33}\sigma_{11}) \tag{10}$$

The material parameters ψ_2 and μ are dimensionless constants that may be determined from triaxial compression tests. The parameter ψ_1 is related to the curvature parameter m of the failure criterion as follows:

$$\psi_1 = 0.00155m^{-1.27} \tag{11}$$

The parameter ψ_1 acts as a weighting factor between the triangular shape (from the I_3 term) and the circular shape (from the I_2 term). The parameter ψ_2 controls the intersection with the hydrostatic axis, and the exponent μ determines the curvature of meridians. The corresponding plastic potential surfaces are shown in Figure 2. They are shaped as asymmetric cigars with smoothly rounded triangular cross-sections similar but not identical to those for the failure surfaces.

2.4. *Yield criterion and work hardening/softening relations*

The yield surfaces are intimately associated with and derived from surfaces of constant plastic work, as explained by Lade and Kim [2]. The isotropic yield function is expressed as follows:

$$f_p = f'_p(\sigma) - f''_p(W_p) = 0 \tag{12}$$

in which

$$f'_p = \left(\psi_1 \frac{I_1^3}{I_3} - \frac{I_1^2}{I_2}\right)\left(\frac{I_1}{p_a}\right)^h e^q \tag{13}$$

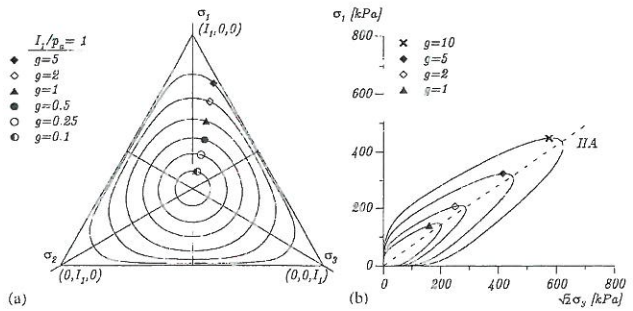

Figure 2. Characteristics of the plastic potential function in principal stress space: traces shown in (a) octahedral plane, and (b) triaxial plane.

where h is constant and q varies from zero at the hydrostatic axis to unity at the failure surface. The expressions for I_1, I_2, and I_3 in (13) are given in (3), (10), and (6), respectively. The parameter ψ_1 acts as a weighting factor between the triangular shape (from the I_3 term) and the circular shape (from the I_2 term), as in the expression for the plastic potential (9). The constant parameter h is determined on the basis that the plastic work is constant along a yield surface.

The value of q varies with stress level S defined as

$$S = \frac{f_n}{\eta_1} = \frac{1}{\eta_1}\left(\frac{I_1^3}{I_3} - 27\right)\left(\frac{I_1}{p_a}\right)^m \tag{14}$$

in which f_n is the expression for the failure criterion in (5a), and η_1 is the value of f_n at failure, given in (5b). The stress level S varies from zero at the hydrostatic axis to unity at the failure surface, and the variation of q with S is expressed as

$$q = \frac{\alpha S}{1 - (1 - \alpha)S} \tag{15}$$

in which α is constant.

For *hardening*, the yield surface inflates isotropically with plastic work according to

$$f''_p = \left(\frac{1}{D}\right)^{1/\rho}\left(\frac{W_p}{p_a}\right)^{1/\rho} \tag{16}$$

In (16) the values of ρ and D are constants for a given material. Thus, f''_p varies with the plastic work only. The values of D and ρ are given by

$$D = \frac{C}{(27\psi_1 + 3)^{\rho}} \tag{17}$$

and

$$\rho = \frac{p}{h} \tag{18}$$

The parameters C and p in (17) are used to model the plastic work during isotropic compression:

$$W_p = C p_a \left(\frac{I_1}{p_a}\right)^p \tag{19}$$

The yield surfaces are shaped as asymmetric tear drops with smoothly rounded triangular cross-sections and traces in the triaxial plane as shown in Figure 3. As the plastic work increases, the isotropic yield surface inflates until the current stress point reaches the failure surface. The relation between f_p'' and W_p is described by a monotonically increasing function whose slope decreases with increasing plastic work, as shown in Figure 4.

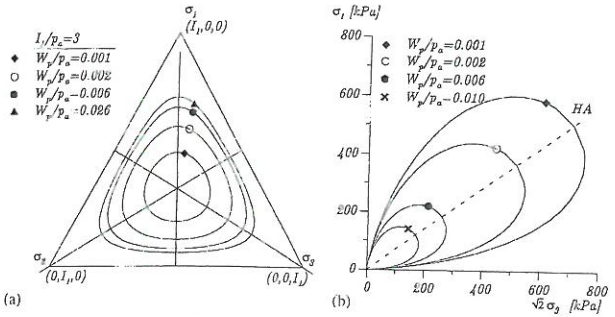

Figure 3. Characteristics of yield function in principal stress space: traces shown in (a) octahedral plane, and (b) triaxial plane.

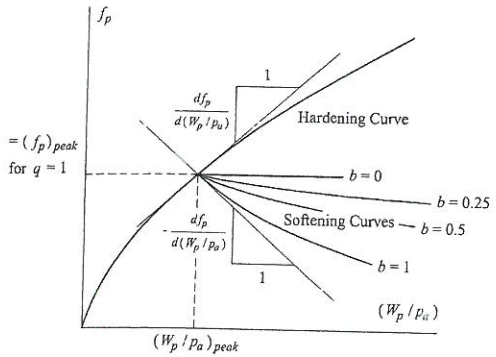

Figure 4. Modelling of work hardening and softening.

For *softening*, the yield surface deflates isotropically according to an exponential decay function:

$$f_p'' = A e^{-BW_p/p_a} \tag{20}$$

in which A and B are positive constants to be determined on the basis of the slope of the hardening curve at the point of peak failure, $S = 1$, as indicated in Figure 4. Thus

$$A = [f_p'' e^{BW_p/p_a}]_{S=1} \tag{21}$$

and

$$B = \left[b \frac{df_p''}{d(\frac{W_p}{p_a})} \frac{1}{f_p''}\right]_{S=1} \tag{22}$$

in which both the size of the yield surface f_p'' and the derivative $df_p''/d(W_p/p_a)$ are obtained from the hardening curve at peak failure, indicated by $S = 1$. The value of df_p'' is negative during softening. The parameter b is greater than or equal to zero, where the lower limit corresponds to that of a perfect plastic material.

Using the expression for the plastic potential in (9), the relation between plastic work increment and the scalar factor of proportionality $d\lambda_p$ in (8) may be expressed as

$$d\lambda_p = \frac{dW_p}{\mu g_p} \tag{23}$$

in which the increment of plastic work can be determined by differentiation of the hardening and softening equations.

Combining (21) and (22) with (23) and substituting this into (8) produces the expression for the incremental plastic strain increments.

2.5. *Materials with effective cohesion*

As explained in connection with the failure criterion, it is possible to include the effective cohesion and the tension which can be sustained by concrete and rock. This is done by translating the principal stress space along the hydrostatic axis, i.e. by adding a constant stress to the normal stress, as in (7), before substitution into the failure criterion in (5).

A similar technique has been shown to work for the elastic modulus variation [6], the plastic potential [1], the yield criterion and the work-hardening/softening law [2]. Inconsistencies in the plastic behaviour of materials with effective cohesion are overcome by assuming that there exists an initial yield surface which goes through the origin of the real stress space, as shown in Figure 5. This implies that only elastic strains occur during major portions of tension type tests in which the main parts of the stress paths are located inside the yield surface. Thus, the stresses applied along the stress paths indicated in Figure 5 do not produce plastic strains until they are close to failure. The existence of an initial yield surface appears to simulate experimental observations with good accuracy.

The technique of performing all calculations in the translated stress space provides a convenient tool for mathematical treatment of cohesive materials. Following all the necessary calculations, the stresses are again modified to hold conventional physical meaning. For cohesionless materials for which 'a' is zero, the calculations are performed in the original stress space.

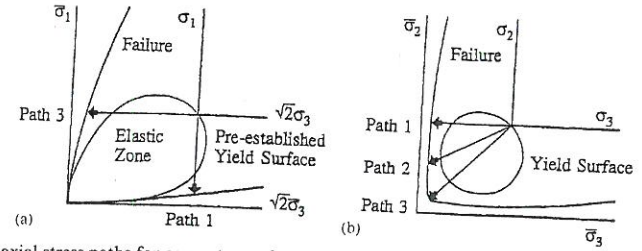

Figure 5. Biaxial stress paths for concrete employed by Kupfer *et al.* [12] and assumed initial yield surface in (a) triaxial plane, and (b) biaxial plane.

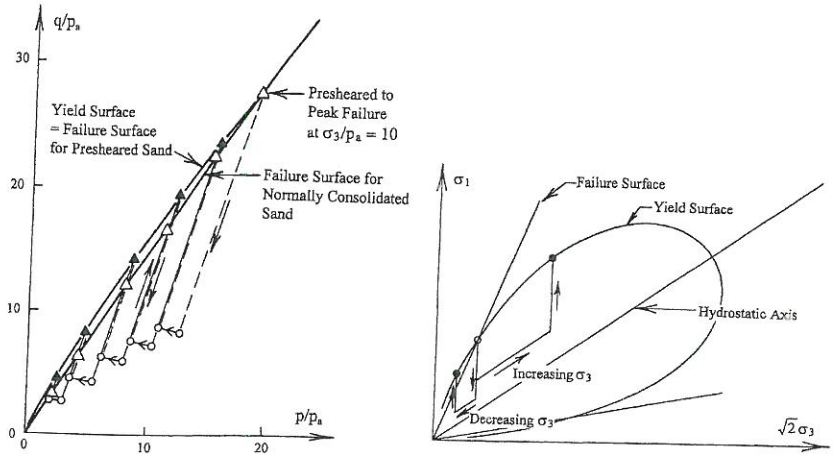

Figure 6. Effects of preshearing and overconsolidation on failure surface for soils.

2.6. *Effects of preshearing and overconsolidation*

An experimental investigation of the behaviour of sand near failure was undertaken by Lade and Prabucki [13] to study the shape, location and movement of the plastic yield surface in the hardening regime and the softening regime near peak failure. This investigation confirmed that the yield surface, defined as a contour of constant plastic work as measured from the origin of stress, captures the behaviour of soil with good accuracy in both the hardening and in the softening regime. It was found that preshearing to peak failure produced effects similar to overconsolidation observed in clays in the region of lower confining pressures, as shown in Figure 6. In this region, the yield surface was found to move out beyond the failure surface for

Table I. Material parameters for dense Eastern Scheldt sand used with the single hardening model

Model component	Parameter names	Parameter values			Equation
Elastic properties	M, λ, ν	458.45	0.4142	0.20	2
Failure criterion	m, η_1, a	0.2879	70.19	0	5, 7
Plastic potential	ψ_2, μ	−3.1540	2.0611		9
Yield criterion	h, α	0.5525	0.6166		13, 15
Hardening/softening law	C, p, b	1.2748×10^{-4}	1.6078	0.5	19, 22

normally consolidated sand, i.e. the sand became stronger. The observed pattern of yielding is captured with good accuracy by the yield criterion employed in the single hardening constitutive model.

2.7. *Summary*

The governing functions of the single hardening model have been presented and the material parameters identified. The material parameters depend on the specific material and must be calibrated to results of isotropic and triaxial compression tests as outlined by Lade [7], Kim and Lade [1], Lade and Kim [2,3]. The components of the constitutive model and the corresponding material parameters are listed in Table I with values indicated for dense Eastern Scheldt sand [14]. These material parameters are employed in the companion paper [5] for an evaluation of the integration schemes used in a user-defined material module employed in a finite element programme.

3. INCREMENTAL FORM OF CONSTITUTIVE MODEL

3.1. *Elasto-plastic stiffness matrix for single hardening model*

Application of an elasto-plastic model in a finite element procedure requires an incremental form in which the stress increments are expressed in terms of the total strain increments, as follows:

$$d\sigma = \mathbf{C}^{ep}\, d\varepsilon = (\mathbf{C}^{e} - \mathbf{C}^{p})\, d\varepsilon \tag{24}$$

in which $\mathbf{C}^{ep}$ is the elasto-plastic stiffness matrix. This is obtained through an incrementalization procedure as described by, e.g. Zienkiewicz and Taylor [15], Smith and Griffiths [16], Chen and Mizuno [17], Lade and Nelson [18]. The incrementalization results in

$$d\sigma = \left[\mathbf{C}^{e} - \frac{\mathbf{C}^{e}\left(\frac{\partial g_p}{\partial \sigma}\right)\left(\frac{\partial f_p}{\partial \sigma}\right)^{T}\mathbf{C}^{e}}{\left(\frac{\partial f_p}{\partial \sigma}\right)^{T}\mathbf{C}^{e}\left(\frac{\partial g_p}{\partial \sigma}\right) + H}\right] d\varepsilon \tag{25}$$

The term in the square brackets is the general expression for the incremental stiffness matrix, $\mathbf{C}^{ep}$, for an elasto-plastic model with a single yield surface.

If the stress point is in the elastic domain, then the plastic stiffness, $\mathbf{C}^{p}$ in (24), vanishes and $\mathbf{C}^{ep}$ and $\mathbf{C}^{e}$ become identical. It is noted that $\mathbf{C}^{p}$ and therefore $\mathbf{C}^{ep}$ is asymmetric for non-associated plastic flow.

It is possible to extract the proportionality factor $d\lambda_p$ from (25)

$$d\lambda_p = \frac{\mathbf{C}^e\left(\frac{\partial f_p}{\partial \sigma}\right)^T}{\left(\frac{\partial f_p}{\partial \sigma}\right)^T \mathbf{C}^e \left(\frac{\partial g_p}{\partial \sigma}\right) + H} d\varepsilon \tag{26}$$

in which $d\lambda_p$ is expressed in terms of the total strain increment, to be used in the integration scheme presented in the companion paper [5].

3.2. Elastic stiffness matrix

In (25) $\mathbf{C}^e$ is the elastic stiffness matrix defined as

$$\mathbf{C}^e = \frac{E}{(1+\nu)(1-2\nu)} \times \begin{bmatrix} 1-\nu & \nu & \nu & 0 & 0 & 0 \\ \nu & 1-\nu & \nu & 0 & 0 & 0 \\ \nu & \nu & 1-\nu & 0 & 0 & 0 \\ 0 & 0 & 0 & \frac{(1-2\nu)}{2} & 0 & 0 \\ 0 & 0 & 0 & 0 & \frac{(1-2\nu)}{2} & 0 \\ 0 & 0 & 0 & 0 & 0 & \frac{(1-2\nu)}{2} \end{bmatrix} \tag{27}$$

where Young's modulus E is given in (2) and Poisson's ratio ν is constant.

3.3. Derivatives of the plastic potential

The plastic potential function, g_p, is given in (9). Since the plastic potential function is expressed in terms of stress invariants, the derivatives of g_p with regard to stresses may be obtained through the chain rule:

$$\frac{\partial g_p}{\partial \sigma} = \frac{\partial g_p}{\partial I_1}\frac{\partial I_1}{\partial \sigma} + \frac{\partial g_p}{\partial I_2}\frac{\partial I_2}{\partial \sigma} + \frac{\partial g_p}{\partial I_3}\frac{\partial I_3}{\partial \sigma} \tag{28}$$

in which

$$\frac{\partial g_p}{\partial I_1} = \left(\psi_1(\mu+3)\frac{I_1^2}{I_3} - (\mu+2)\frac{I_1}{I_2} + \frac{\mu\psi_2}{I_1}\right)\left(\frac{I_1}{p_a}\right)^{\mu} \tag{29}$$

$$\frac{\partial g_p}{\partial I_2} = \frac{I_1^2}{I_2^2}\left(\frac{I_1}{p_a}\right)^{\mu} \tag{30}$$

$$\frac{\partial g_p}{\partial I_3} = -\psi_1\frac{I_1^3}{I_3^2}\left(\frac{I_1}{p_a}\right)^{\mu} \tag{31}$$

and the derivatives of the stress invariants with respect to stresses are

$$\frac{\partial I_1}{\partial \sigma} = \begin{bmatrix} 1 \\ 1 \\ 1 \\ 0 \\ 0 \\ 0 \end{bmatrix} \tag{32}$$

$$\frac{\partial I_2}{\partial \sigma} = \begin{bmatrix} -(\sigma_{22}+\sigma_{33}) \\ -(\sigma_{33}+\sigma_{11}) \\ -(\sigma_{11}+\sigma_{22}) \\ 2\sigma_{23} \\ 2\sigma_{31} \\ 2\sigma_{12} \end{bmatrix} \tag{33}$$

$$\frac{\partial I_3}{\partial \sigma} = \begin{bmatrix} \sigma_{22}\sigma_{33} - \sigma_{23}^2 \\ \sigma_{33}\sigma_{11} - \sigma_{31}^2 \\ \sigma_{11}\sigma_{22} - \sigma_{12}^2 \\ 2(\sigma_{12}\sigma_{31} - \sigma_{11}\sigma_{23}) \\ 2(\sigma_{23}\sigma_{12} - \sigma_{22}\sigma_{31}) \\ 2(\sigma_{31}\sigma_{23} - \sigma_{33}\sigma_{12}) \end{bmatrix} \tag{34}$$

3.4. Derivatives of the yield function

The yield function, f_p', is given in (13). Using the chain rule, the derivatives of the yield function can be written as

$$\frac{\partial f_p'}{\partial \sigma} = \frac{\partial f_p'}{\partial I_1}\frac{\partial I_1}{\partial \sigma} + \frac{\partial f_p'}{\partial I_2}\frac{\partial I_2}{\partial \sigma} + \frac{\partial f_p'}{\partial I_3}\frac{\partial I_3}{\partial \sigma} \tag{35}$$

in which the derivatives of the stress invariants are given in (32)–(34). The derivatives of f_p' with respect to the stress invariants are

$$\frac{\partial f_p'}{\partial I_1} = \left(\frac{3+h}{I_1} + \frac{\partial q}{\partial I_1}\right) f_p' + \frac{I_1}{I_2}\left(\frac{I_1}{p_a}\right)^h e^q \tag{36}$$

$$\frac{\partial f_p'}{\partial I_2} = \frac{I_1^2}{I_2^2}\left(\frac{I_1}{p_a}\right)^h e^q \tag{37}$$

$$\frac{\partial f'_p}{\partial I_3} = f'_p \frac{\partial q}{\partial I_3} - \psi_1 \frac{I_1^3}{I_3^2}\left(\frac{I_1}{p_a}\right)^h e^q \tag{38}$$

It is recalled that the exponent q varies with the actual stress level as defined by (14) and (15). The derivatives of q with respect to the stress invariants are

$$\frac{\partial q}{\partial I_1} = \frac{\alpha}{\eta_1(1-(1-\alpha)S)^2}\left(\frac{mS\eta_1}{I_1} + \frac{3I_1^2}{I_3}\left(\frac{I_1}{p_a}\right)^m\right) \tag{39}$$

$$\frac{\partial q}{\partial I_3} = -\frac{\alpha}{\eta_1(1-(1-\alpha)S)^2}\frac{I_1^3}{I_3^2}\left(\frac{I_1}{p_a}\right)^m \tag{40}$$

3.5. *Hardening modulus*

The last term in the denominator in (25) represents the hardening modulus:

$$H = -\frac{\partial f''_p}{\partial W_p}\sigma\frac{\partial g_p}{\partial \sigma} = -\frac{\partial f''_p}{\partial W_p}\mu g \tag{41}$$

Since the function g_p in (9) is homogeneous and of the order μ, Euler's theorem for homogeneous functions (see, e.g. The International Dictionary of Applied Mathematics, 1960 [19]) produces the last expression for the hardening modulus in (41). The derivative of the yield function with respect to the plastic work depends on the stress history. The derivatives are determined for the hardening and the softening relations in (16) and (20) as follows:

$$\textit{Hardening:}\quad \frac{\partial f_p}{\partial W_p} = \frac{\partial f''_p}{\partial W_p} = \frac{1}{\rho(D p_a)^{1/\rho}} W_p^{\frac{1}{\rho}-1} \tag{42}$$

$$\textit{Softening:}\quad \frac{\partial f_p}{\partial W_p} = \frac{\partial f''_p}{\partial W_p} = -\frac{AB}{p_a} e^{-BW_p/p_a} \tag{43}$$

The above expressions represent the incremental form of the single hardening model. They form the basic expressions used for the implementation in a user-defined material module presented in a companion paper [5].

4. SUMMARY

An elasto-plastic constitutive model developed for frictional materials has been reviewed, and the incremental version of the model has been given in the form of mathematical expressions to be implemented in a user-defined material module for a finite element program. This three-dimensional model for isotropic materials is formulated in terms of stress invariants, it involves hardening and softening, non-associated plastic flow, and it handles volume changes such a contraction and dilation as observed in experiments on frictional material. The model is implemented in a material subroutine and used in a finite element program, as described in a companion paper [5]. Several integration schemes are investigated and evaluated for this elasto-plastic model.

REFERENCES

1. Kim MK, Lade PV. Single hardening constitutive model for frictional materials. I. plastic potential function. *Computers and Geotechnics* 1988; **5**:307–324.
2. Lade PV, Kim MK. Single hardening constitutive model for frictional materials. II. yield criterion and plastic work contours. *Computers and Geotechnics* 1988a; **6**:13–29.
3. Lade PV, Kim MK. Single hardening constitutive model for frictional materials. III. comparisons with experimental data. *Computers and Geotechnics* 1988b; **6**:30–47.
4. ABAQUS *version 5.5—manuals*, Hibbit, Karlson and Sorensen Inc, 1995.
5. Jakobsen KP, Lade PV. Implementation algorithm for a single hardening constitutive model for frictional materials. *International Journal for Numerical and Analytical Methods in Geomechanics* 2002; **26**:661.
6. Lade PV, Nelson RB. Modelling the elastic behavior of granular materials. *International Journal for Numerical and Analytical Methods in Geomechanics* 1987; **11**:521–542.
7. Lade PV. Elasto-plastic stress–strain theory for cohesionless soil with curved yield surfaces. *International Journal of Solids and Structures* 1977; **13**:1019–1035.
8. Lade PV. Three-parameter failure criterion for concrete. *ASCE Journal of Engineering Mechanics Division* 1982; **108**:850–863.
9. Lade PV. Failure criterion for frictional materials. In *Mechanics of Engineering Materials*, Desai CS, Gallagher RH (eds). Wiley: New York, 1984; 385–402.
10. Lade PV. Rock Strength Criteria: The Theories and the Evidence, Vol. I, Chapter 11. In *Comprehensive Rock Engineering, Principles, Practice and Projects*, Hudson JA, et al. (eds). Pergamon Press: Oxford, 1993; 255–284.
11. Kim MK, Lade PV. Modelling rock strength in three dimensions. *International Journal of Rock Mechanics and Mining Sciences & Geomechanics Abstracts* 1984; **21**:21–33.
12. Kupfer H, Hilsdorf HK, Rusch H. Behavior of concrete under biaxial stresses. *Journal of the American Concrete Institute* 1969; **66**:656–666.
13. Lade PV, Prabucki M-J. Softening and preshearing effects in sand. *Soils and Foundations* 1995; **35**(4): 93–104.
14. Jakobsen KP, Praastrup U. Drained triaxial tests on Eastern Scheldt sand. *Aalborg University Geotechnical Engineering Papers*, 1998; ISSN 1398-6465 R9822.
15. Zienkiewicz OC, Taylor RL. *The Finite Element Method—Vol. 2: Solid and Fluid Dynamics and Non-linearity*. McGraw-Hill: London, UK, 1991.
16. Smith IM, Griffiths DV. *Programming the Finite Element Method (2nd Edition)*. Wiley: New York, 1988.
17. Chen WF, Mizuno E. *Non-linear Analysis in Soil Mechanics*. Elsevier: New York, 1990.
18. Lade PV, Nelson RB. Incrementalization procedure for elasto-plastic constitutive model with multiple, intersecting yield surfaces. *International Journal for Numerical and Analytical Methods in Geomechanics* 1984; **8**:311–323.
19. *The International Dictionary of Applied Mathematics*. Van Nostrand Company, Inc: Princeton, NJ, 1960.

Title:
Implementation algorithm for a single hardening constitutive model for frictional materials.

Authors:
Jakobsen, K.P & P.V. Lade.

Year of publication:
2002

Published in:
International Journal for Numerical and Analytical Methods in Geomechanics 26, 661-681.

INTERNATIONAL JOURNAL FOR NUMERICAL AND ANALYTICAL METHODS IN GEOMECHANICS
Int. J. Numer. Anal. Meth. Geomech., 2002; **26**:661–681 (DOI: 10.1002/nag.217)

Implementation algorithm for a single hardening constitutive model for frictional materials

K. P. Jakobsen[1,*,†] and P. V. Lade[2]

[1] *DHI—Water and Environment, Agern Allé 11, 2970 Hørsholm, Denmark*
[2] *Department of Civil Engineering, Aalborg University, Sohngaardsholmsvej 57, 9000 Aalborg, Denmark*

SUMMARY

An advanced elasto-plastic constitutive model for frictional materials, whose incremental version is presented in a companion paper (*Int. J. Numer. Anal. Meth. Geomech.*, 2002; **26**:647), is implemented in a user-defined material module. The general calculation strategy inside this module is presented and discussed, including the initial intersection of the yield surface and the techniques for updating of stresses and hardening modulus. Several integration schemes are implemented in the module and their capabilities in relation to the advanced, three-dimensional constitutive model are evaluated. The forward Euler, modified Euler, and Runge–Kutta–Dormand–Prince integration schemes are explained in detail, compared, and evaluated in view of error tolerances and computational efficiency. Copyright © 2002 John Wiley & Sons, Ltd.

KEY WORDS: implementation algorithm; elasto-plastic constitutive model; frictional materials; yield surface; non-associated flow

1. INTRODUCTION

Implementation of an advanced elasto-plastic constitutive model in a finite element program involves formulation of an incremental version of the model before actual coding of the model for computer application can be performed. A single hardening model for frictional materials and its incremental form are presented in a companion paper by Lade and Jakobsen [1]. The present paper contains the implementation procedures as well as an evaluation of how well several available integration schemes perform for this advanced elasto-plastic model with non-associated flow. Such integration schemes have been developed and used with relatively simple constitutive models and with some advanced models, and their qualities are studied here for the single hardening model.

The employment of more advanced and accurate elasto-plastic constitutive models in finite element codes is occasionally omitted due to a substantial increase in the computational costs. Analyses based on more accurate modelling of the true material behaviour can obviously not be obtained without a loss of efficiency. However, by a critical assessment of the used integration

*Correspondance to: K. P. Jakobsen, DHI—Water and Environment, Agern Allé 11, 2970 Hørsholm, Denmark
†E-mail: kpj@dhi.dk

Received 22 April 2001
Revised 15 November 2001

schemes it is possible to limit the additional computational costs. The problem of selection of suitable integration schemes is two-fold as the analysis implies the use of integration schemes for the computation of updated stresses and hardening parameters by an integration of the constitutive relation, and an integration for establishment of the overall equilibrium of the system. In the latter case, the rate of convergence and therefore the efficiency rely on the determination of the material tangent stiffness (see e.g. References [2,3]). The use of the 'consistent' tangent stiffness may preserve the quadratic convergence inherited from the Newton–Raphson method. However, this implies that the integration scheme used for the overall equilibrium is of the Newton–Raphson type [3, p. 178]. The method of updating stresses and hardening parameters has on the other hand a direct impact on both accuracy and efficiency.

The solution of non-linear finite element problems involving the mechanical behaviour of materials usually consists of a series of load steps, each involving iterations to establish equilibrium between internal and external forces at the new load level. This global iteration process is entirely handled by the finite element program, e.g. Reference [4]. However, the evaluation of the internal forces and displacements, used in the global iterations, is dependent on the applied stress–strain relation. The role of the user material module, which includes the single hardening model, is therefore two-fold. It must provide (1) an update of stresses for evaluation of internal forces, and (2) a material stiffness for establishment of the global stiffness matrix used for equilibrium iterations and estimation of the corresponding displacement field.

Since ABAQUS uses a Gauss integration scheme to establish the tangent stiffness matrix for each element, it is only necessary to consider a single material point within an element. Whenever a new estimate of updated stresses and material stiffness is needed, the user material module is called once for each Gauss point. The determination of the updated quantities will essentially depend on the imposed strain increment, but as the material behaviour is of the path-dependent type, knowledge of the stress and strain history is also required.

The input to each step consists of the material parameters, the current stresses, the current maximum plastic work, and the new strain increments. The subroutine then produces the six new stresses, the plastic work corresponding to the new stress state as well as the updated tangent stiffness matrix, the so-called Jacobian matrix. The following section explains the overall calculation strategy.

2. CALCULATION STRATEGY

The calculation strategy is illustrated schematically in Figure 1 and a flow chart is shown in Figure 2. Based on the current stresses (σ_0, point A in Figure 1), the maximum plastic work, $W_{p,0}$, and the new strain increments ($\Delta\varepsilon$), stress point B is calculated assuming the strain increment to be entirely elastic (step 1 in Figure 2). The stresses at point B are used for calculation of f', being the value of the yield function corresponding to the current state of stress, and compared with the current value of the yield function f'' calculated from the current maximum plastic work (step 2). The expressions for f' and f'' are defined in the companion paper [1], but the subscript p has been omitted here. If the difference is less than or equal to zero $[f = (f' - f'') \leqslant 0]$, then the new stress point (B) is located inside the yield surface and the strain increment is truly elastic. The calculation for this increment have already been performed and the Jacobian matrix is elastic (step 3a).

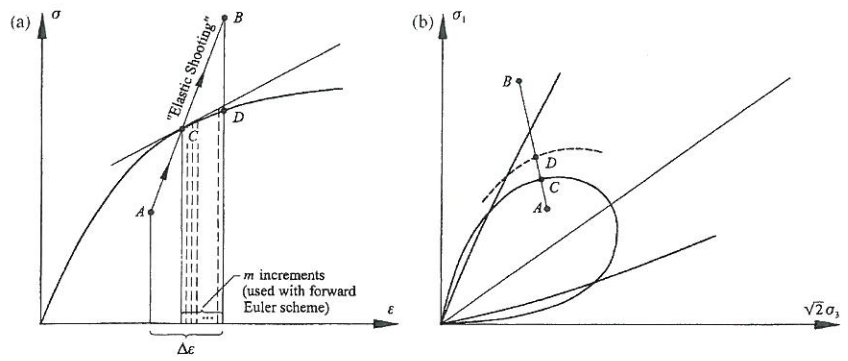

Figure 1. Schematic illustration of (a) stress–strain relation, and (b) triaxial plane with stress states used in explanation of calculation strategy.

If on the other hand $f = (f' - f'') > 0$, then point B is outside the current yield surface and a portion of the strain increment is plastic. In this case it is determined whether the current stress state (point A) is located inside or on the current yield surface. The stresses at point A are used for calculation of f' and compared with the previously calculated f'' (step 3b). If $f = (f' - f'') = 0$, then point A is on the yield surface and coincides with point C in Figure 1, and $\alpha = 0$ (step 4a).

If $f = (f' - f'') < 0$ (step 3b), then point A is inside the yield surface, as shown schematically in Figure 1. In this case it is necessary to determine the portion of the stress-path from A to B that is purely elastic (AC) by determining the ratio $\alpha = AC/AB$ (step 4b). For explicit integration schemes it is required that point C be found, and the technique for finding point C is further discussed below (Section 3).

Having calculated the elastic strains from A to C, the remaining portion of the total strain increment (calculation in step 5) is used to update the stresses and the hardening parameter (steps 6–8). Three integration schemes are implemented: (1) forward Euler scheme with subincrementation, (2) modified Euler scheme with error control, and (3) Runge–Kutta–Dormand–Prince scheme with error control. These techniques are discussed in detail in Sections 4–8. At the end of either one of these schemes, the user material module is exited with the stresses, the Jacobian matrix, and the plastic work at point D (step 8).

3. INITIAL INTERSECTION WITH YIELD SURFACE

If the stress point changes from an elastic to an elasto-plastic state, as it occurs for presheared or overconsolidated materials, then it is necessary to determine the portion of the stress increment that causes purely elastic deformations, as indicated in Figure 1. The technique for finding point C is illustrated in Figure 3, indicated in step 4b in Figure 2, and described mathematically below.

The initial state of stress at point A lies within the yield surface corresponding to:

$$f(\sigma_A, W_{p,A}) = f_A < 0 \tag{1}$$

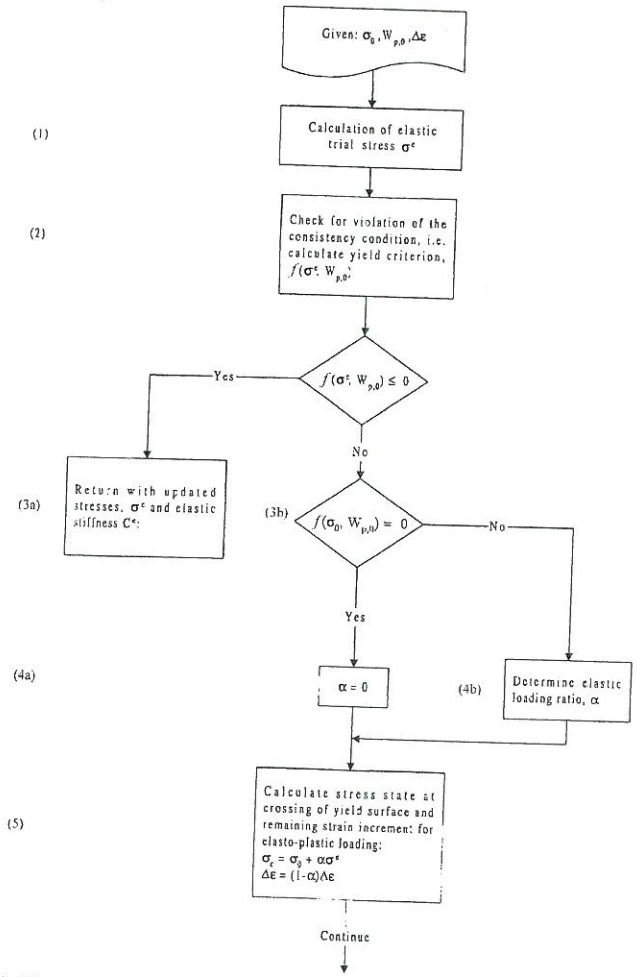

Figure 2. Flow chart for implementation of constitutive model with a single yield surface in user-defined material module.

The 'elastic shooting' from A to B produces an elastic trial stress increment calculated from Hooke's law:

$$\Delta\sigma^e = \mathbf{C}^e(\sigma_A)\Delta\varepsilon \tag{2}$$

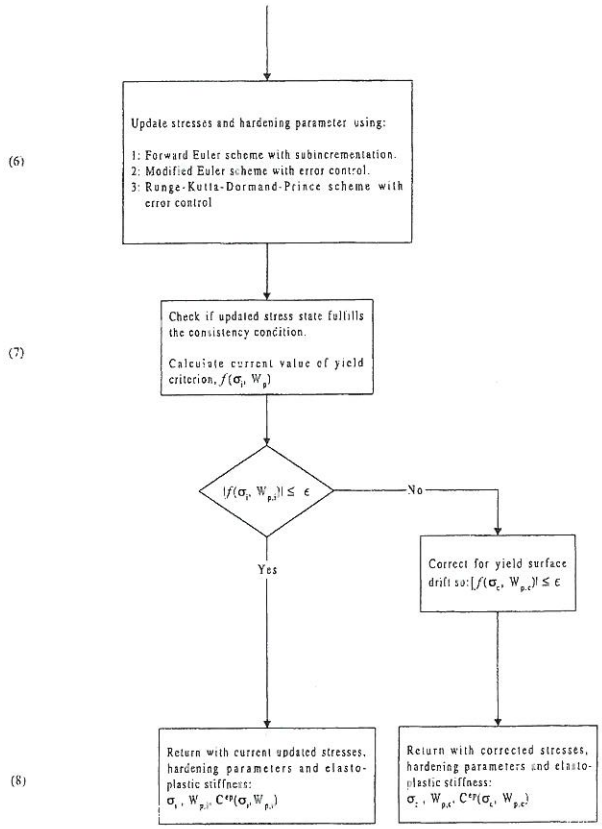

Figure 2. (*Continued*)

Thus, the elastic non-linearity is accounted for in the implementation. Hence, Young's modulus and the elastic stiffness matrix are determined on the basis of (2) and (27) of the companion paper. If the stress point changes from an elastic state (point A) to an elasto-plastic state (point B), then the trial stresses at B may violate the yield criterion:

$$f(\sigma_A + \Delta\sigma^e, W_{p,C}) = f(\sigma_B, W_{p,C}) = f_B > 0 \tag{3}$$

It is therefore necessary to determine a scalar α $(0<\alpha<1)$ corresponding to the portion of the stress increment that lies within the yield surface so that the stress state at point C fulfills the

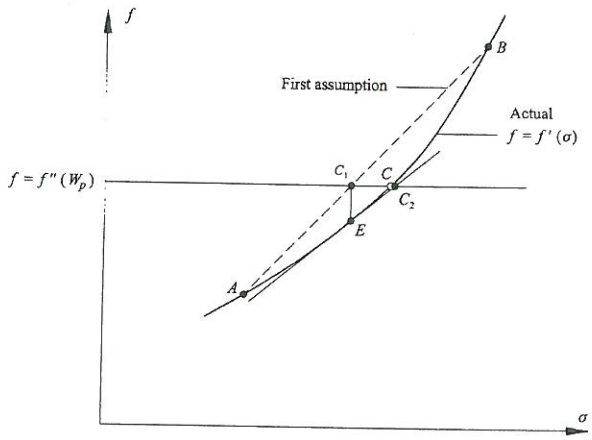

Figure 3. Schematic illustration of technique for finding intersection with yield surface.

yield criterion:

$$f(\sigma_A + \alpha\Delta\sigma^e, W_{p,C}) = f(\sigma_C, W_{p,C}) = f_C = 0 \tag{4}$$

Explicit expressions for the scalar α can be derived only for simple types of yield functions. A first estimate may be determined by a simple linear interpolation in f [5,6]

$$\alpha_0 = -\frac{f_A}{f_B - f_A} \tag{5}$$

The yield function is, however, highly non-linear and the scalar estimate determined by (5) will generally not satisfy the yield criterion:

$$f(\sigma_A + \alpha_0\Delta\sigma^e, W_{p,C}) = f(\sigma_E, W_{p,C}) = f_E \neq 0 \tag{6}$$

A more accurate estimate for α may be obtained by a Taylor series expansion around point E:

$$\alpha = \alpha_0 - \frac{f_E}{(\partial f/\partial(\sigma_A + \alpha_0\Delta\sigma^e)^T\Delta\sigma^e} \tag{7}$$

This approach for the calculation of the stresses on the yield surface at point C will be accurate for small strain increments only. In order to avoid any initial yield surface drift in the integration schemes and enhance the prediction capabilities of the stress–strain relations it is advisable to apply an iterative scheme [5]. Using the Newton–Raphson technique, for example, the stresses and α are updated as outlined in Figure 4. The iterative procedure is started by assuming the initial stresses at point A and using α_0 from (5). The procedure is terminated when the stress norm $\|\sigma_i - \sigma_{i-1}\|/\|\sigma_{i-1}\|$ is less than a specified tolerance. The resulting elastic stress increments $\alpha\Delta\sigma^e$ correspond to an elastic strain increment $\alpha\Delta\varepsilon$ and the strain increment used in the integration of the elasto-plastic stress–strain relation equals $(1-\alpha)\Delta\varepsilon$.

Initial state $\sigma_0, W_{p,0}$

If $f(\sigma_0, W_{p,0}) > 0$

$$\alpha_0 = -\frac{f_A}{f_B - f_A}$$

Iterations $i = 1, 2, \ldots, i_{max}$

$$\sigma_i = \sigma_{i-1} + \alpha_{i-1}\Delta\sigma^e$$

$$\Delta\alpha_i = -\frac{f(\sigma_i, W_p)}{(\frac{\partial f}{\partial\sigma_i})^T\Delta\sigma^e}$$

$$\alpha_i = \alpha_{i-1} + \Delta\alpha_i$$

Stop iteration when $\|\sigma_i - \sigma_{i-1}\|/\|\sigma_{i-1}\| \leq \in$

Final state $\sigma_c = \sigma_i, \alpha_c = \alpha_i$

Figure 4. Algorithm with improved procedure for finding the initial intersection with the yield surface.

3.1. Handling effects of preshearing and overconsolidation on the material strength

The numerical problems that occur for presheared or overconsolidated materials are generally handled by applying the procedure outlined in the previous section. However, in special cases the current yield surface, which indicates the previously experienced highest load level, extends beyond the failure surface and actually strengthens the material, as indicated in Figure 6 of the companion paper. Thus, the material should not reach a state of failure until the yield surface is reached. This is accomplished numerically by calculating the intersection of the yield surface, as presented above, and then performing a check for failure. The stress level relative to failure, as defined by (14) in the companion paper, will in such cases exceed unity, but is for consistency set equal to unity.

3.2. Back-scaling of elastic stresses

The single hardening model is developed for frictional materials, and only stress combinations in the pressure octant of the principal stress space are allowed, even for materials with effective cohesion, as explained in Section 2.5 of the companion paper. This implies that if the elastic trial stresses correspond to one (or more) negative or zero principal stresses, then they must be scaled back into the pressure octant, in order to facilitate the calculation of the elasto-plastic stress–strain response. The problem is most likely to occur for large strain increments and near failure in the extension region.

4. UPDATING STRESSES AND HARDENING PARAMETER

The requirement of an accurate integration of the constitutive law is traditionally accomplished by use of a backward Euler or an explicit subincrementation scheme (see e.g. References [5,7,8]).

Both types of schemes have a number of advantages and disadvantages. The backward Euler scheme is an elastic predictor and plastic corrector type of method and is attractive because it does not require the initial intersection of the yield surface to be computed if the stress point passes from an elastic to an elasto-plastic state. The plastic correction is obtained by solving a small system of non-linear equations [3] by an iterative procedure, which ensures that the consistency condition may be satisfied within a specified tolerance. The approach, however, has some major disadvantages. The establishment of the system of equations becomes laborious for more advanced models and convergence is not necessarily guaranteed. The backward Euler scheme has apparently only been used and documented for simple constitutive models having associated flow rules (e.g. von Mises, Tresca, Mohr–Coulomb and Cam–Clay). Actually, Abbo and Sloan [8] make comparisons between the backward Euler and explicit integration schemes for a non-associated Mohr–Coulomb model. However, the handling of the non-associated flow rule is not described at all and the conclusions are merely based on a table containing the final results. Furthermore many soil models have a separate failure criterion and the numerical handling may be obstructed near failure as the elastic trial stress intersects the failure criterion. Alternatively, integration schemes of the forward Euler and Runge–Kutta types, which use explicit formulations, can be used. These types of schemes have the disadvantage that the initial intersection with the yield surface must be computed if a stress point passes from an elastic to an elasto-plastic state and they do not necessarily ensure that the consistency condition is fulfilled. The validity of these types of methods can, however, be enhanced and the disadvantages are balanced by their robustness.

As already explained, the forward Euler integration scheme is only accurate for small strain increments. By subdividing the strain increment into a fixed number of subincrements, as done in Section 5, the accuracy will be improved. However, this approach turns out to be computationally expensive [5]. Hence, two other schemes for explicit integration have been investigated and implemented. These include a refined subincremental version of the forward Euler scheme with active error control and an enhanced Runge–Kutta scheme. These methods are applicable to non-linear stress–strain relations in general, but the stress–strain relations given by the single hardening model are employed here. The paper is concluded by an example where the capabilities of the different methods are studied.

5. FORWARD EULER INTEGRATION SCHEME WITH SUBINCREMENTATION

Following the determination of the intersection with the yield surface, as described above, the subsequent objective is to determine the updated state of stress and hardening parameter as a total strain increment is imposed. A commonly used integration scheme for elasto-plastic stress–strain relations is the forward Euler scheme. In the following it is presumed that the initial state of stress is located on the yield surface and that the next stress increment causes elasto-plastic strains.

5.1. Procedure

In the forward Euler scheme the stresses are updated by replacing the infinitesimal elasto-plastic stress–strain relation in (25) of the companion paper by a finite incremental relation:

$$\Delta\sigma = \mathbf{C}^{\mathrm{ep}}(\sigma_0, W_{\mathrm{p},0})\Delta\varepsilon \tag{8}$$

where the constitutive matrix is evaluated at the initial state of stress. As the elasto-plastic constitutive matrix depends on the stress and strain history, this linear approximation is only accurate for very small strain increments. The method may be refined by a piece wise linear integration where the strain increment is subdivided into smaller subincrements [3,5,6,9,10]:

$$\delta\varepsilon = \Delta T\Delta\varepsilon = \frac{\Delta\varepsilon}{m} \tag{9}$$

where ΔT is a dimensionless time step of fixed size and the finite stress increment is determined as the sum of the m subincrements, $\delta\sigma_i$, each evaluated as a forward Euler step:

$$\delta\sigma_i = \mathbf{C}^{\mathrm{ep}}(\sigma_0 + \Delta\sigma_{i-1}, W_{\mathrm{p},0} + \Delta W_{\mathrm{p},i-1})\delta\varepsilon \tag{10}$$

$$\delta W_{\mathrm{p},i} = \delta\lambda_{\mathrm{p}}(\sigma_0 + \Delta\sigma_{i-1}, W_{\mathrm{p},0} + \Delta W_{\mathrm{p},i-1}, \delta\varepsilon)(\sigma_0 + \Delta\sigma_{i-1})\frac{\partial g}{\partial(\sigma_0 + \Delta\sigma_{i-1})} \tag{11}$$

where

$$\Delta\sigma_{i-1} = \sum_{j=1}^{i-1}\delta\sigma_j \tag{12}$$

$$\Delta W_{\mathrm{p},i-1} = \sum_{j=1}^{i-1}\delta W_{\mathrm{p},j} \tag{13}$$

The given change to the hardening parameter is valid for work hardening and is computed by use of (26) and (41) of the companion paper, with derivatives evaluated at the stress state $(\sigma_0 + \Delta\sigma_{i-1})$. As illustrated in Figure 5, the forward Euler scheme has the advantage of being straight forward and easy to implement compared to other schemes.

However, the yield criterion is not necessarily fulfilled, and the stress increments tend to drift away from the yield surface, i.e. $f(\sigma_0 + \Delta\sigma, W_{\mathrm{p},0} + \Delta W_{\mathrm{p}}) \neq 0$. Even though the subdivision may

Initial state $\sigma_0, W_{p,0}, \Delta\varepsilon, \delta\varepsilon = \frac{\Delta\varepsilon}{m}$

Strain subincrements $i = 1, 2, \ldots\ldots, m$

$$\delta\sigma_i = C^{ep}(\sigma_{i-1}, W_{p,i-1})\delta\varepsilon$$

$$\delta W_{p,i} = \delta\lambda_p(\sigma_{i-1}, W_{p,i-1}, \delta\varepsilon)\sigma_{i-1}\frac{\partial g}{\partial\sigma_{i-1}}$$

$$\sigma_i = \sigma_{i-1} + \delta\sigma_i$$

$$W_{p,i} = W_{p,i-1} + \delta W_{p,i}$$

Stop strain subincrementation when $i = m$

Final state $\sigma_i, W_{p,i} C^{ep}(\sigma_i, W_{p,i})$

Figure 5. Algorithm for subincremental forward Euler scheme for evaluation of new stress state, plastic work, and Jacobian matrix.

reduce the yield surface drift, the procedure may lead to unacceptable results as the error accumulates during subsequent load steps (e.g. References [3,5,11]). Moreover, the subincremental form has the disadvantage that it uses subincrements of equal size. This turns out to be computationally inefficient as the number of subincrements must be determined by trial-and-error so that the maximum error is within some close tolerance.

5.2. *Correction for yield surface drift*

When using explicit integration schemes such as the forward Euler scheme for updating of stresses, the stress state predicted at the end of the elasto-plastic load increment may not lie on the current yield surface and the consistency condition is violated. The error will essentially depend on the size of the strain increment and number of subdivisions, but as the error is cumulative it is important to ensure that the stresses are corrected back to the yield surface during each increment of loading.

A method proposed by Potts and Gens [11] accounts for the changes in elastic strains that accompany any stress correction. The problem of yield surface drift and correction is illustrated schematically in Figure 6, where the material is subjected to loading that causes elasto-plastic deformation. The initial stress state is initially located on the yield surface $f(\sigma_A, W_{p,A}) = 0$. Further loading involves elasto-plastic deformation and a change in stresses as determined by the integration scheme. This new state σ_B will, due to the tendency for yield surface drift, not necessarily be located on the new yield surface $f(\sigma, W_{p,B}) = 0$, and the objective is therefore to correct the stresses so that the yield criterion is fulfilled. During the correction process the total strain increment will remain constant, and this implies that any elastic strain change must be balanced by an equal and opposite change in plastic strain. These changes will affect the stresses and the hardening parameter, and the new updated elasto-plastic stress state is denoted σ_C and $W_{p,C}$.

The requirement of an unaltered total strain increment throughout the correction process can be formulated as

$$d\varepsilon^p = -d\varepsilon^e = -\mathbf{C}^{e^{-1}}(\sigma_C - \sigma_B) \tag{14}$$

The plastic strain increment is also proportional to the gradient of the plastic potential:

$$d\varepsilon^p = \beta \frac{\partial g}{\partial \sigma} \tag{15}$$

where β is a scalar quantity. The corrected stress state is obtained by substituting (15) into (14) and solving for σ_C:

$$\sigma_C = \sigma_B - \beta \mathbf{C}^e \frac{\partial g}{\partial \sigma_B} \tag{16}$$

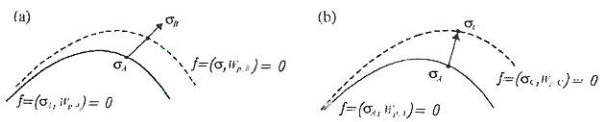

Figure 6. Illustration of correction for yield surface drift: (a) initial estimate of updated hardening parameter and stresses causing yield surface drift, and (b) corrected values of hardening parameter and stresses located on the yield surface.

The change in plastic strains will also affect the hardening parameter:

$$W_{p,C} = W_{p,B} + \Delta W_p \tag{17}$$

where ΔW_p for work-hardening is given by

$$\Delta W_p = \beta \left(\frac{\partial g}{\partial \sigma_B} \right)^T \sigma_B \tag{18}$$

The corrected stress state must satisfy the yield criterion:

$$f(\sigma_C, W_{p,C}) = f\left(\sigma_B - \beta \mathbf{C}^e \frac{\partial g}{\partial \sigma_B}, W_{p,B} + \beta \left(\frac{\partial g}{\partial \sigma_B} \right)^T \sigma_B \right) = 0 \tag{19}$$

A first order estimate of the scalar β can be obtained by a Taylor series expansion around σ_B:

$$\beta = \frac{f(\sigma_B, W_{p,B})}{\left(\frac{\partial f}{\partial \sigma_B}\right)^T \mathbf{C}^e \left(\frac{\partial g}{\partial \sigma_B}\right) - \left(\frac{\partial f}{\partial W_{p,B}}\right)\left(\frac{\partial g}{\partial \sigma_B}\right)^T \sigma_B} \tag{20}$$

The above procedure may be sufficiently accurate if the load increment is small. However, it must in general be checked that the corrected stress state fulfils the yield criterion $f(\sigma_C, W_{p,C}) = 0$ to some close tolerance. Otherwise, an iterative procedure as outlined in Figure 7 must be applied. The iterative procedure is started by assuming $\sigma_0 = \sigma_B$ and $W_{p,0} = W_{p,B}$.

Initial state $\sigma_0, W_{p,0}$

If $|f(\sigma_0, W_{p,0})| > \epsilon$

Iterations $i = 1, 2, \ldots, i_{max}$

$$\beta_{i-1} = \frac{f(\sigma_{i-1}, W_{p,i-1})}{\left(\frac{\partial f}{\partial \sigma_{i-1}}\right) C^e \left(\frac{\partial g}{\partial \sigma_{i-1}}\right) - \left(\frac{\partial f}{\partial W_{p,i-1}}\right)\left(\frac{\partial g}{\partial \sigma_{i-1}}\right)^T \sigma_{i-1}}$$

$$\sigma_i = \sigma_{i-1} - \beta_{i-1} C^e \frac{\partial g}{\partial \sigma_{i-1}}$$

$$\Delta W_{p,i-1} = \beta_{i-1} \sigma_{i-1} \frac{\partial g}{\partial \sigma_{i-1}}$$

$$W_{p,i} = W_{p,i-1} + \Delta W_{p,i-1}$$

Stop iteration when $|f(\sigma_i, W_{p,i})| \leq \epsilon$

Final state $\sigma_c = \sigma_i, W_{p,c} = W_{p,i}$

Figure 7. Algorithm for correction of yield surface drift.

6. MODIFIED FORWARD EULER SCHEME WITH ERROR CONTROL

In order to reduce the yield surface drift and computational costs of the forward Euler scheme, a modified Euler scheme with active control can be used [5,12]. Instead of using a fixed number of subincrements of equal size, the size of the subincrements is varied throughout the integration process. Hence, the size of each subincrement is determined so that the new stress state fulfils the yield criterion within some small tolerance and only the absolutely necessary number of subdivisions are applied.

The modified scheme uses a pair of first- and second-order Euler formulas to estimate the error produced by the standard forward Euler scheme at the end of a strain increment, $\delta\varepsilon = \Delta T\Delta\varepsilon$. The first estimate of the updated stresses and the work hardening parameter at the end of the strain increment is given by

$$\sigma = \sigma_0 + \delta\sigma^{\mathrm{I}} \tag{21}$$

$$W_{\mathrm{p}} = W_{\mathrm{p},0} + \delta W_{\mathrm{p}}^{\mathrm{I}} \tag{22}$$

where

$$\delta\sigma^{\mathrm{I}} = \mathbf{C}^{\mathrm{ep}}(\sigma_0, W_{\mathrm{p},0})\delta\varepsilon \tag{23}$$

$$\delta W_{\mathrm{p}}^{\mathrm{I}} = \delta\lambda_{\mathrm{p}}(\sigma_0, W_{\mathrm{p},0}, \delta\varepsilon)\sigma_0 \frac{\partial g}{\partial \sigma_0} \tag{24}$$

A more accurate estimate of the updated stress state may be found by

$$\hat{\sigma} = \sigma_0 + \tfrac{1}{2}(\delta\sigma^{\mathrm{I}} + \delta\sigma^{\mathrm{II}}) \tag{25}$$

$$\hat{W}_{\mathrm{p}} = W_{\mathrm{p},0} + \tfrac{1}{2}(\delta W_{\mathrm{p}}^{\mathrm{I}} + \delta W_{\mathrm{p}}^{\mathrm{II}}) \tag{26}$$

where

$$\delta\sigma^{\mathrm{II}} = \mathbf{C}^{\mathrm{ep}}(\sigma_0 + \delta\sigma^{\mathrm{I}}, W_{\mathrm{p},0} + \delta W_{\mathrm{p}}^{\mathrm{I}})\delta\varepsilon \tag{27}$$

$$\delta W_{\mathrm{p}}^{\mathrm{II}} = \delta\lambda_{\mathrm{p}}(\sigma_0 + \delta\sigma^{\mathrm{I}}, W_{\mathrm{p},0} + \delta W_{\mathrm{p}}^{\mathrm{I}}, \delta\varepsilon)(\sigma_0 + \delta\sigma^{\mathrm{I}}) \frac{\partial g}{\partial(\sigma_0 + \delta\sigma^{\mathrm{I}})} \tag{28}$$

The method is seen to employ two evaluations of the elasto-plastic constitutive matrix in each subincrement. The difference between the stress states given by (21) and (25) can be seen as an estimate of the local error in σ:

$$\delta\sigma^{\mathrm{I-II}} \approx \hat{\sigma} - \sigma = \tfrac{1}{2}(\delta\sigma^{\mathrm{II}} - \delta\sigma^{\mathrm{I}}) \tag{29}$$

This error estimate serves as a guide for selecting the size of the next time step, ΔT, when integrating over the total strain increment $\Delta\varepsilon$. Thus, the relative error for a subincrement is defined by the norm:

$$\xi = \frac{\|\delta\sigma^{\mathrm{I-II}}\|}{\|\hat{\sigma}\|} \tag{30}$$

and the size of each step is continually adjusted until ξ is less than some specified tolerance, $\in$.

The integration is started by choosing a value of the dimensionless time step ΔT and computing $\delta\varepsilon, \sigma, W_{\mathrm{p}}, \hat{\sigma}, \hat{W}_{\mathrm{p}}, \delta\sigma^{\mathrm{I-II}}$ and ξ using (21)–(30). If $\xi \leqslant \in$, then the new updated stresses and hardening parameters are taken as $\hat{\sigma}$ and $\hat{W}_{\mathrm{p}}$. Otherwise it is necessary to reduce ΔT and

repeat the calculation. The size of the next dimensionless time step is generally given by local extrapolation:

$$\Delta T = q\Delta T \tag{31}$$

where

$$q = 0.9\left(\frac{\in}{\xi}\right)^{1/2} \tag{32}$$

The exponent $\frac{1}{2}$ relates to the local truncation error $O(\Delta T^2)$ of the first-order formulae, whereas the factor of 0.9 is introduced to reduce the number of subincrements that are likely to be rejected during the integration process. The size of the new increment is furthermore constrained as q must lie within the interval:

$$0.01 \leqslant q \leqslant 2 \tag{33}$$

The modified Euler scheme with active error control is summarized in Figure 8.

7. RUNGE–KUTTA–DORMAND–PRINCE SCHEME WITH ERROR CONTROL

Variations of the Runge–Kutta scheme are widely used for integration purposes. The classical Runge–Kutta scheme uses a fourth-order integration scheme with only one strain increment for stress updating. Several higher order schemes with subincrementation have been proposed (e.g. References [12–15]). The Runge–Kutta scheme modified by Dormand and Prince [15] is used in the following. The scheme uses a pair of fourth- and fifth-order formulas to estimate the new updated stresses and work hardening parameter. The coefficients in these formulas have been chosen to control and minimize the error, and to estimate the new updated stresses and work hardening parameter as accurately as possible:

$$\sigma = \sigma_0 + \frac{31}{540}\delta\sigma^{\mathrm{I}} + \frac{190}{297}\delta\sigma^{\mathrm{III}} - \frac{145}{108}\delta\sigma^{\mathrm{IV}} + \frac{351}{220}\delta\sigma^{\mathrm{V}} + \frac{1}{20}\delta\sigma^{\mathrm{VI}} \tag{34}$$

$$W_{\mathrm{p}} = W_{\mathrm{p},0} + \frac{31}{540}\delta W_{\mathrm{p}}^{\mathrm{I}} + \frac{190}{297}\delta W_{\mathrm{p}}^{\mathrm{III}} - \frac{145}{108}\delta W_{\mathrm{p}}^{\mathrm{IV}} + \frac{351}{220}\delta W_{\mathrm{p}}^{\mathrm{V}} + \frac{1}{20}\delta W_{\mathrm{p}}^{\mathrm{VI}} \tag{35}$$

$$\hat{\sigma} = \sigma_0 + \frac{19}{216}\delta\sigma^{\mathrm{I}} + \frac{1000}{2079}\delta\sigma^{\mathrm{III}} - \frac{125}{216}\delta\sigma^{\mathrm{IV}} + \frac{81}{88}\delta\sigma^{\mathrm{V}} + \frac{5}{56}\delta\sigma^{\mathrm{VI}} \tag{36}$$

$$\hat{W}_{\mathrm{p}} = W_{\mathrm{p},0} + \frac{19}{216}\delta W_{\mathrm{p}}^{\mathrm{I}} + \frac{1000}{2079}\delta W_{\mathrm{p}}^{\mathrm{III}} - \frac{125}{216}\delta W_{\mathrm{p}}^{\mathrm{IV}} + \frac{81}{88}\delta W_{\mathrm{p}}^{\mathrm{V}} + \frac{5}{56}\delta W_{\mathrm{p}}^{\mathrm{VI}} \tag{37}$$

where

$$\delta\sigma^{\mathrm{I}} = \mathbf{C}^{\mathrm{ep}}(\sigma_0, W_{\mathrm{p},0})\delta\varepsilon \tag{38}$$

$$\delta W_{\mathrm{p}}^{\mathrm{I}} = \delta\lambda_{\mathrm{p}}(\sigma_0, W_{\mathrm{p},0}, \delta\varepsilon)\sigma_0 \frac{\partial g}{\partial \sigma_0} \tag{39}$$

$$\delta\sigma^{\mathrm{II}} = \mathbf{C}^{\mathrm{ep}}(\sigma^{\mathrm{I}}, W_{\mathrm{p}}^{\mathrm{I}})\delta\varepsilon \tag{40}$$

$$\delta W_{\mathrm{p}}^{\mathrm{II}} = \delta\lambda_{\mathrm{p}}(\sigma^{\mathrm{I}}, W_{\mathrm{p}}^{\mathrm{I}}, \delta\varepsilon)\sigma^{\mathrm{I}} \frac{\partial g}{\partial \sigma^{\mathrm{I}}} \tag{41}$$

Initial state $\sigma_0, W_{p,0}, \Delta\varepsilon, \delta\varepsilon_0 = \Delta\varepsilon, q = 1$

Strain increment $i = 1, 2, \ldots\ldots, n$

$$\delta\varepsilon_i = \min\left[q\delta\varepsilon_{i-1}, 1 - \Sigma_{j=1}^{i-1}\delta\varepsilon_j\right]$$

do

$$\delta\sigma_i^I = \boldsymbol{C}^{ep}(\sigma_{i-1}, W_{p,i-1})\delta\varepsilon_i$$

$$\delta W_{p,i}^I = \delta\lambda_p(\sigma_{i-1}, W_{p,i-1}, \delta\varepsilon_i)\sigma_{i-1}\frac{\partial g}{\partial\sigma}$$

$$\delta\sigma_i^{II} = \boldsymbol{C}^{ep}(\sigma_{i-1} + \delta\sigma_i^I, W_{p,i-1} + \delta W_{p,i}^I)\delta\varepsilon_i$$

$$\delta W_{p,i}^{II} = \delta\lambda_p(\sigma_{i-1} + \delta\sigma_i^I, W_{p,i-1} + \delta W_{p,i}^I, \delta\varepsilon_i)(\sigma_{i-1} + \delta\sigma_i^I)\frac{\partial g}{\partial\sigma}$$

$$\delta\sigma_i^{I-II} = \tfrac{1}{2}(\delta\sigma_i^{II} - \delta\sigma_i^I)$$

$$\hat{\sigma}_i = \sigma_{i-1} + \tfrac{1}{2}(\delta\sigma_i^I + \delta\sigma_i^{II})$$

$$\hat{W}_{p,i} = W_{p,i-1} + \tfrac{1}{2}(\delta W_{p,i}^I + \delta W_{p,i}^{II})$$

$$\xi_i = \frac{\|\delta\sigma_i^{I-II}\|}{\|\hat{\sigma}_i\|}$$

If $\xi_i > \in$ *then* $q = \max\left[0.9(\frac{\in}{\xi})^{\frac{1}{2}}, 0.01\right]; \delta\varepsilon_i = q\delta\varepsilon_i$

Until $\xi_i \leq \in$

$$q = \min\left[0.9(\tfrac{\in}{\xi})^{\frac{1}{2}}, 2\right]$$

Stop strain incrementation when $\Sigma_{i=1}^{n}\delta\varepsilon_i = \Delta\varepsilon$

Final state $\hat{\sigma}_i, \hat{W}_{p,i}, C^{ep}(\hat{\sigma}_i, \hat{W}_{p,i})$

Figure 8. Algorithm for modified Euler scheme with active error control.

in which

$$\sigma^{\mathrm{I}} = \sigma_0 + \tfrac{1}{5}\delta\sigma^{\mathrm{I}}$$

$$W_{\mathrm{p}}^{\mathrm{I}} = W_{\mathrm{p},0} + \tfrac{1}{5}\delta W_{\mathrm{p}}^{\mathrm{I}}$$

and further

$$\delta\sigma^{\mathrm{III}} = \mathbf{C}^{\mathrm{ep}}(\sigma^{\mathrm{II}}, W_{\mathrm{p}}^{\mathrm{II}})\delta\varepsilon \tag{42}$$

$$\delta W_{\mathrm{p}}^{\mathrm{III}} = \delta\lambda_{\mathrm{p}}(\sigma^{\mathrm{II}}, W_{\mathrm{p}}^{\mathrm{II}}, \delta\varepsilon)\sigma^{\mathrm{II}}\frac{\partial g}{\partial\sigma^{\mathrm{II}}} \tag{43}$$

in which

$$\sigma^{\mathrm{II}} = \sigma_0 + \frac{3}{40}\delta\sigma^{\mathrm{I}} + \frac{9}{40}\delta\sigma^{\mathrm{II}}$$

$$W_{\mathrm{p}}^{\mathrm{II}} = W_{\mathrm{p},0} + \frac{3}{40}\delta W_{\mathrm{p}}^{\mathrm{I}} + \frac{9}{40}\delta W_{\mathrm{p}}^{\mathrm{II}}$$

and further

$$\delta\sigma^{\mathrm{IV}} = \mathbf{C}^{\mathrm{ep}}(\sigma^{\mathrm{III}}, W_{\mathrm{p}}^{\mathrm{III}})\delta\varepsilon \tag{44}$$

$$\delta W_{\mathrm{p}}^{\mathrm{IV}} = \delta\lambda_{\mathrm{p}}(\sigma^{\mathrm{III}}, W_{\mathrm{p}}^{\mathrm{III}}, \delta\varepsilon)\delta^{\mathrm{III}}\frac{\partial g}{\partial\sigma^{\mathrm{III}}} \tag{45}$$

in which

$$\sigma^{\mathrm{III}} = \sigma_0 + \frac{3}{10}\delta\sigma^{\mathrm{I}} - \frac{9}{10}\delta\sigma^{\mathrm{II}} + \frac{6}{5}\delta\sigma^{\mathrm{III}}$$

$$W_{\mathrm{p}}^{\mathrm{III}} = W_{\mathrm{p},0} + \frac{3}{10}\delta W_{\mathrm{p}}^{\mathrm{I}} - \frac{9}{10}\delta W_{\mathrm{p}}^{\mathrm{II}} + \frac{6}{5}\delta W_{\mathrm{p}}^{\mathrm{III}}$$

and further

$$\delta\sigma^{\mathrm{V}} = \mathbf{C}^{\mathrm{ep}}(\sigma^{\mathrm{IV}}, W_{\mathrm{p}}^{\mathrm{IV}})\delta\varepsilon \tag{46}$$

$$\delta W_{\mathrm{p}}^{\mathrm{V}} = \delta\lambda_{\mathrm{p}}(\sigma^{\mathrm{IV}}, W_{\mathrm{p}}^{\mathrm{IV}}, \delta\varepsilon)\delta^{\mathrm{IV}}\frac{\partial g}{\partial\sigma^{\mathrm{IV}}} \tag{47}$$

in which

$$\sigma^{\mathrm{IV}} = \sigma_0 + \frac{226}{729}\delta\sigma^{\mathrm{I}} - \frac{25}{27}\delta\sigma^{\mathrm{II}} + \frac{880}{729}\delta\sigma^{\mathrm{III}} + \frac{55}{729}\delta\sigma^{\mathrm{IV}}$$

$$W_{\mathrm{p}}^{\mathrm{IV}} = W_{\mathrm{p},0} + \frac{226}{729}\delta W_{\mathrm{p}}^{\mathrm{I}} - \frac{25}{27}\delta W_{\mathrm{p}}^{\mathrm{II}} + \frac{880}{729}\delta W_{\mathrm{p}}^{\mathrm{III}} + \frac{55}{729}\delta W_{\mathrm{p}}^{\mathrm{IV}}$$

and further

$$\delta\sigma^{\mathrm{VI}} = \mathbf{C}^{\mathrm{ep}}(\sigma^{\mathrm{V}}, W_{\mathrm{p}}^{\mathrm{V}})\delta\varepsilon \tag{48}$$

$$\delta W_{\mathrm{p}}^{\mathrm{VI}} = \delta\lambda_{\mathrm{p}}(\sigma^{\mathrm{V}}, W_{\mathrm{p}}^{\mathrm{V}}, \delta\varepsilon)\sigma^{\mathrm{V}}\frac{\partial g}{\partial\sigma^{\mathrm{V}}} \tag{49}$$

in which

$$\sigma^{\mathrm{V}} = \sigma_0 - \frac{181}{270}\delta\sigma^{\mathrm{I}} + \frac{5}{2}\delta\sigma^{\mathrm{II}} - \frac{266}{297}\delta\sigma^{\mathrm{III}} - \frac{91}{27}\delta\sigma^{\mathrm{IV}} + \frac{189}{55}\delta\sigma^{\mathrm{V}}$$

$$W_{\mathrm{p}}^{\mathrm{V}} = W_{\mathrm{p},0} - \frac{181}{270}\delta W_{\mathrm{p}}^{\mathrm{I}} + \frac{5}{2}\delta W_{\mathrm{p}}^{\mathrm{II}} - \frac{266}{297}\delta W_{\mathrm{p}}^{\mathrm{III}} - \frac{91}{27}\delta W_{\mathrm{p}}^{\mathrm{IV}} + \frac{189}{55}\delta W_{\mathrm{p}}^{\mathrm{V}}$$

Even though the integration process requires six evaluations of the elasto-plastic constitutive matrix, the scheme rapidly becomes competitive with the modified Euler scheme as the error tolerance is tightened. As for the modified Euler scheme, the estimated relative error can be

expressed as

$$\xi = \frac{\|\hat{\sigma} - \sigma\|}{\|\hat{\sigma}\|} \tag{50}$$

As the local truncation error in the fourth-order formulae is $O(\Delta T^5)$ the exponent in (32) is replaced by $\frac{1}{5}$ and the factor that controls the size of the next dimensionless time step is instead given by:

$$q = 0.9\left(\frac{\in}{\xi}\right)^{1/5} \tag{51}$$

But the constraints in (33) still apply. The Runge–Kutta–Dormand–Prince scheme with active error control is summarized in Figure 9.

8. COMPARISON OF INTEGRATION SCHEMES

The effectiveness of the integration schemes presented in Sections 5–7 is examined in the following. For this purpose a single point of Eastern Scheldt sand [16] with the parameters listed in Table I of the companion paper is undergoing triaxial compression under constant volume. The triaxial compression as started from an anisotropic stress state of $\sigma_0^I = [450\ 400\ 400\ 0\ 0\ 0]$, with all stresses in kPa. The resulting stress path is somewhat simple, because it does not involve rotation of principal axes, but even a relatively small strain increment will nevertheless lead to considerable change in principal stresses. The simulation is conducted by imposing a number of strain increments of equal size $\Delta\varepsilon^T = 10^{-4} \times [5\ -2.5\ -2.5\ 0\ 0\ 0]$ and using the three integration schemes for determination of the corresponding change in stresses. The resulting stress path and development in hardening parameter, shown in Figure 10, is composed of 40 sequential strain increments of equal size. All the shown simulations are performed without correction for yield surface drift.

Figure 10 shows a comparison of the calculated effective stress paths for the undrained triaxial compression of the sand element, for which the parameter values are listed in Table I in the companion paper. The modified Euler and Runge–Kutta–Dormand–Prince integration schemes yield similar results, whereas the forward Euler integration scheme produces visibly different results for decreasing values of σ_3. This deviation becomes less distinct on the linear part of the undrained stress path, but the forward Euler scheme generally overestimates the final stress state considerably. The applicability of the forward Euler scheme, however, improves as the number of subincrements in the integration process are increased. Hence, the discrepancy is more or less reduced by a factor of two as the number of subincrements are doubled. Similar observations hold for the development in the hardening parameter W_p, as indicated in Figure 10c.

The observations above illustrate the effect of integration method for rate independent material behaviour. A reduction of the size of the strain increments, $\Delta\varepsilon$, may:

1. Change the appearance of the stress path for all methods and lead to results that are in better agreement with the 'correct' solution.
2. Reduce the discrepancy between the integration schemes.
3. Decrease the computational efficiency.

Initial state $\sigma_0, W_{p,0}, \Delta\varepsilon, \delta\varepsilon_0 = \Delta\varepsilon, q = 1$

Strain increments $i = 1, 2, \ldots\ldots, n$

$$\delta\varepsilon_i = \min\left[q\delta\varepsilon_{i-1}, 1 - \Sigma_{j=1}^{i-1}\delta\varepsilon_j\right]$$

do

Stress increments $m = I, II, \ldots\ldots, VI$

$$\delta\sigma_i^m = C^{ep}(\sigma_i^{m-1}, W_{p,i}^{m-1})\delta\varepsilon_i$$

$$\delta W_{p,i}^m = \delta\lambda_p(\sigma_i^{m-1}, W_{p,i}^{m-1}, \delta\varepsilon_i)\sigma_i^{m-1}\frac{\partial g}{\partial\sigma_i^{m-1}}$$

Stop stress incrementation when $j = VI$

$$\sigma_i = \sigma_{i-1} + \tfrac{31}{540}\delta\sigma_i^I + \tfrac{190}{297}\delta\sigma_i^{III} - \tfrac{145}{108}\delta\sigma_i^{IV} + \tfrac{351}{220}\delta\sigma_i^V + \tfrac{1}{20}\delta\sigma_i^{VI}$$

$$W_{p,i} = W_{p,i-1} + \tfrac{31}{540}\delta W_{p,i}^I + \tfrac{190}{297}\delta W_{p,i}^{III} - \tfrac{145}{108}\delta W_{p,i}^{IV} + \tfrac{351}{220}\delta W_{p,i}^V + \tfrac{1}{20}\delta W_{p,i}^{VI}$$

$$\hat{\sigma}_i = \sigma_{i-1} + \tfrac{19}{216}\delta\sigma_i^I + \tfrac{1000}{2079}\delta\sigma_i^{III} - \tfrac{125}{216}\delta\sigma_i^{IV} + \tfrac{81}{88}\delta\sigma_i^V + \tfrac{5}{56}\delta\sigma_i^{VI}$$

$$\hat{W}_{p,i} = W_{p,i-1} + \tfrac{19}{216}\delta W_{p,i}^I + \tfrac{1000}{2079}\delta W_{p,i}^{III} - \tfrac{125}{216}\delta W_{p,i}^{IV} + \tfrac{81}{88}\delta W_{p,i}^V + \tfrac{5}{56}\delta W_{p,i}^{VI}$$

$$\xi_i = \frac{\|\hat{\sigma}_i - \sigma_i\|}{\|\hat{\sigma}_i\|}$$

If $\xi_i > \in$ *then* $q = \max\left[0.9(\frac{\in}{\xi})^{\frac{1}{5}}, 0.01\right]; \delta\varepsilon_i = q\delta\varepsilon_i$

Until $\xi_i \leq \in$

$$q = \min\left[0.9(\tfrac{\in}{\xi})^{\frac{1}{5}}, 2\right]$$

Stop strain incrementation when $\Sigma_{i=1}^n \delta\varepsilon_i = \Delta\varepsilon$

Final state $\hat{\sigma}_i, \hat{W}_{p,i}, C^{ep}(\hat{\sigma}_i, \hat{W}_{p,i})$

Figure 9. Algorithm for Runge–Kutta–Dormand–Prince scheme with error control.

The choice of the strain increment will therefore essentially depend on the required accuracy of the global solution, and the purpose of the integration schemes is merely to provide an accurate stress update for a given strain increment.

As already seen, it is possible to obtain similar results using the three different schemes, but another consideration involve their computational efficiencies. The computational cost is strongly related to the evaluation of the elasto-plastic constitutive matrix, and as described in

Table I. Comparison of results of integration of the single hardening model using three different schemes.

Method	E_{max}/ϵ			E_{avg}/ϵ		
	$\epsilon = 10^{-3}$	$\epsilon = 10^{-4}$	$\epsilon = 10^{-5}$	$\epsilon = 10^{-3}$	$\epsilon = 10^{-4}$	$\epsilon = 10^{-5}$
FE	1.16	1.16	1.16	0.99	1.00	1.00
	(0.30)	(0.34)	(0.31)	(0.22)	(0.22)	(0.23)
ME	0.26	0.41	0.45	0.15	0.22	0.24
	(0.41)	(0.44)	(0.45)	(0.22)	(0.25)	(0.26)
RKDP	0.04	0.04	0.13	0.02	0.03	0.10
	(0.04)	(0.04)	(0.11)	(0.01)	(0.01)	(0.08)

Method	Maximum number of subincrements			Relative CPU time		
	$\epsilon = 10^{-3}$	$\epsilon = 10^{-4}$	$\epsilon = 10^{-5}$	$\epsilon = 10^{-3}$	$\epsilon = 10^{-4}$	$\epsilon = 10^{-5}$
FE	72	710	7091	9.8	102.9	924.0
ME	10	29	89	0.8	1.6	4.0
RKDP	1	2	3	1.0	1.1	1.1

Notes: Values denoted by ( ) indicate errors in stresses after correction for yield surface drift. Forward Euler (FE). Modified Euler (ME), Runge–Kutta–Dormand–Prince (RKDP)

Sections 5–7, the forward Euler, the modified Euler, and the Runge–Kutta–Dormand–Prince schemes require one, two and six evaluations per subincrement, respectively. The computational costs are evaluated by performing a number of runs, in which the updated stresses must lie within some tolerance, ϵ, of a reference state. Since no analytical solution is available for integrating the relations of the single hardening model exactly, the reference stresses are computed by using the Runge–Kutta–Dormand–Prince scheme with 250 subincrements of equal size. The error in each strain increment for the different schemes can then be expressed as

$$E_i = \frac{\|\sigma_i - \sigma_{ref}\|}{\|\sigma_{ref}\|} \tag{52}$$

and the average and maximum errors along the stress path are given by:

$$E_{avg} = \frac{1}{40}\sum_{i=1}^{40} E_i \tag{53}$$

$$E_{max} = \max E_i \quad \text{for } 1 \leqslant i \leqslant 40 \tag{54}$$

The maximum number of subincrements within a single strain increment and the accumulated relative CPU time required for fulfilment of a given error tolerance along the stress path in Figure 10 are listed in Table I. The simulations have been performed with and without correction for yield surface drift. The CPU time is a measure of the computational cost due to the application of the user defined material module. For the forward Euler scheme the number of subincrements is adjusted until the average error equals the specified tolerance. The modified Euler and Runge–Kutta–Dormand–Prince schemes use the specified tolerance for adjustment of the size of the subincrements. The simulations have been performed both with and without correction for yield surface drift.

As indicated in Table I, the simulations reveal that the two higher order schemes have normalized errors that are substantially less than unity and are largely unaffected by correction

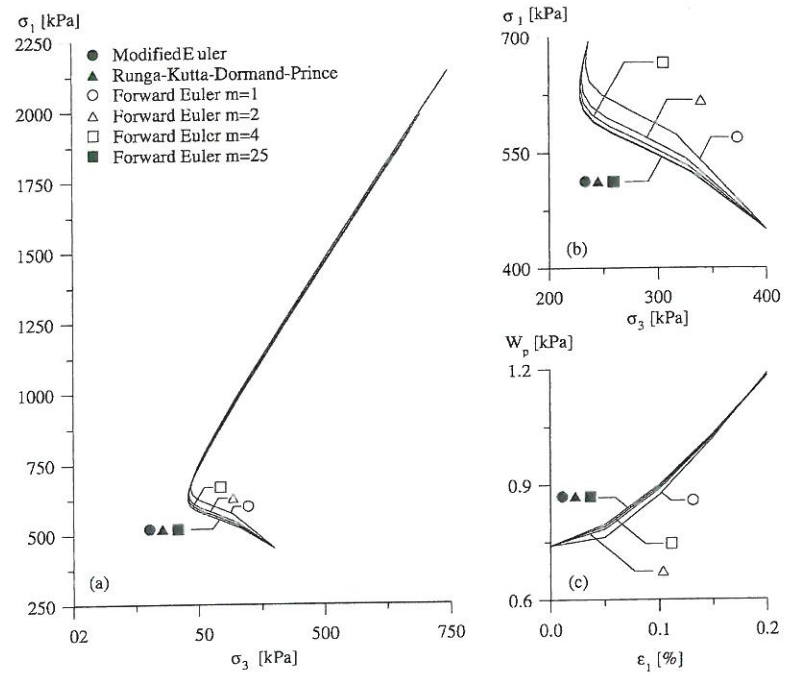

Figure 10. Comparison of various integration schemes used for determination of constant volume stress path: (a) stress path in $\sigma_3 - \sigma_1$ diagram, (b) segment of stress path, and (c) development of the hardening parameter W_p with the major principal strain.

for yield surface drift. However, the correction for yield surface drift becomes very important when using the forward Euler scheme, because it reduces the maximum and average errors in stresses by at least 70%. Moreover, if the subdivision of the strain increment is insufficient the correction for yield surface drift tends to diminish the overestimation of the final stress state shown in Figure 10.

As expected the forward Euler scheme shows a more or less proportional growth in the maximum number of subincrements and relative CPU time with the tightening of the error tolerance. For the modified Euler scheme the maximum number of subincrements and relative CPU time grows slightly with the reduction of the error tolerance, whereas the Runge–Kutta–Dormand–Prince scheme is barely affected. For all the schemes the first few increments (where the stress path is changing direction) are decisive for the maximum number of subincrements needed for fulfilment of a given error tolerance. Thus, for the two higher order schemes only a few of the imposed strain increments are subject to subincrementalization.

The Runge–Kutta–Dormand–Prince integration scheme is in general found to be superior to both the modified Euler and the forward Euler schemes in terms of both accuracy and computational costs as the error tolerance is tightened. Even the modified Euler scheme is only competitive for large error tolerances.

9. CONCLUSIONS

The procedures involved in implementation of a single hardening constitutive model for frictional materials have been employed in creation of a user-defined material module based on the incremental form of the model presented in a companion paper by Lade and Jakobsen [1]. The general calculation strategy inside this module is presented and discussed, including the initial intersection of the yield surface, the techniques for updating of stresses and hardening modulus, and correction for a possible yield surface drift. Several integration schemes are implemented in the module and their capabilities in relation to the three-dimensional constitutive model are evaluated. The forward Euler, modified Euler, and Runge–Kutta–Dormand–Prince integration schemes have been compared in view of error tolerances and computational efficiency. The modified Euler and the Runge–Kutta–Dormand–Prince schemes, which include active error control, posses the advantage of allowing greater strain increments to be imposed as subincrementalization automatically is performed if needed for fulfilment of a specific error tolerance. The traditional forward Euler scheme is, due to the principle of a fixed number of subincrements, not competitive with the higher order schemes, because too many subincrements are needed in order to obtain the required accuracy. However, the capability of the forward Euler scheme can be improved by adopting an iterative scheme correcting for a possible yield surface drift.

The present study shows that the Runge–Kutta–Dormand–Prince scheme is superior in terms of both accuracy and computational costs, and it is conclusively the most advantageous integration scheme for this advanced constitutive model.

REFERENCES

1. Lade PV, Jakobsen KP. Incrementalization of a single hardening constitutive model for frictional materials. *International Journal for Numerical and Analytical Methods in Geomechanics* 2002; **26**:647.
2. Simo JC, Taylor RL. Consistent tangent operator for rate-independent elastoplasticity. *Computer Methods in Applied Mechanics and Engineering* 1985; **48**:101–118.
3. Crisfield MA. *Non-linear Finite Element Analysis of Solids and Structures*. Wiley: Chichester, U.K. 1991.
4. ABAQUS *version 5.5—manuals*. Hibbit, Karlson and Sorensen Inc., 1995.
5. Sloan SW. Substepping schemes for the numerical integration of elasto-plastic stress–strain relations. *International Journal for Numerical Methods in Engineering* 1987; **24**:893–911.
6. Chen WF, Mizuno E. *Non-linear Analysis in Soil Mechanics*. Elsevier: New York, 1990.
7. Ortiz M, Simo JC. An analysis of a new class of integration algorithms for elastoplastic constitutive relations. *International Journal for Numerical Methods in Engineering* 1986; **23**:353–366.
8. Abbo AJ, Sloan SW. Backward Euler and subincrementation schemes in computational plasticity. In *Computational Plasticity*, Valliapan et al. (eds). Balkema: Rotterdam, 1993.
9. Smith IM, Griffiths DV. *Programming the Finite Element Method* (2nd edn). Wiley: New York, 1988.
10. Zienkiewicz OC, Taylor RL. *The Finite Element Method—Volume 2: Solid and Fluid Dynamics and Non-linearity*. McGraw-Hill: London, U.K. 1991.
11. Potts DM, Gens A. A critical assessment of methods of correcting for drift from the yield surface in elasto-plastic finite element analysis. *International Journal for Numerical and Analytical Methods in Geomechanics* 1985; **9**:149–159.
12. Sloan SW, Booker JR. Integration of Tresca and Mohr–Coulomb constitutive relations in plane strain elastoplasticity. *International Journal for Numerical Methods in Engineering* 1992; **33**:163–196.

13. England R. Error estimate for Runge–Kutta type solutions to systems of ordinary differential equations. *Computer Journal* 1969; **12**:166–170.
14. Fehlberg E. Klassiche Runge–Kutta formeln vierter und niedrigerer ordnung mit schrittweiten-kontrole und ihre anwendungen auf wärmleitungs-probleme. *Computing* 1970; **6**:61–71.
15. Dormand JR, Prince PJ. A family of embedded Runge–Kutta formulae. *Journal of Computer Applied Mathematics* 1980; **6**:19–26.
16. Jakobsen KP, Praastrup U. Drained triaxial tests on Eastern Scheldt sand. *Aalborg University Geotechnical Engineering Papers*, 1998; ISSN 1398-6465 R9822.

ISSN 1398-6465 R2002-2